EXCITED STATES OF SILICON CARBIDE CLUSTERS BY TIME DEPENDENT DENSITY FUNCTIONAL THEORY

THESIS

John E. Boyd, First Lieutenant, USAF

AFIT/GNE/ENP/04-02

DEPARTMENT OF THE AIR FORCE

AIR UNIVERSITY

AIR FORCE INSTITUTE OF TECHNOLOGY

Wright Patterson Air Force Base, Ohio

The views expressed in this thesis are those of the author and do not reflect the official policy or position of the United States Air Force, Department of Defense, or the United States Government.

AFIT/GNE/ENP/04-02

EXCITED STATES OF SILICON CARBIDE CLUSTERS BY TIME DEPENDENT DENSITY FUNCTIONAL THEORY

THESIS

Presented to the Faculty
Department of Engineering Physics
Graduate School of Engineering and Management
Air Force Institute of Technology
Air University
Air Education and Training Command
in Partial Fulfillment of the Requirements for the
Degree of Master of Science (Nuclear Science)

John E. Boyd, BS
First Lieutenant, USAF

June, 2004

AFIT/GNE/ENP/04-02

EXCITED STATES OF SILICON CARBIDE CLUSTERS BY TIME DEPENDENT DENSITY FUNCTIONAL THEORY

John E. Boyd, BS
First Lieutenant, USAF

Approved:

Larry W. Burggraf (Chairman)	7 Jun 04 Date
David E. Weeks (Member)	7 Jun 04 Date
Xiaofeng F. Duan (Member)	14 Jun 04 Date

AFIT/GNE/ENP/04-02

Abstract

Previous AFIT research with density functional theory (DFT) has shown itself to be accurate for small Si_mC_n (m,n $\leq$ 5) clusters at a fraction of the cost of other quantum mechanical methods, but it is only a ground state theory. Time dependent density functional theory (TDDFT), however, is able to calculate excited states as well. Evaluating the accuracy of these methods with respect to the excited states of these clusters was the focus of this research, specifically with respect to the excitation energies, geometries, and vibrational frequencies. It is shown that for the excited states that can be expressed as a single electron configuration, energies calculated are generally within .1 eV or better of experimental differences. A possible scheme for correcting multiconfigurational states is also presented, which also brings those energies to within .1 eV of experiment.

This research has demonstrated the ability of TDDFT to give an accurate picture of silicon carbide excitations, placing future calculations with larger clusters on solid ground. Calculations on larger, cage-like structures show excitation energies consistent with spectroscopic measurements of SiC surface defects, suggesting the possibility that the SiC surface forms similar clusters. Calculations on the equilibrium geometries and vibrational frequencies of yet unobserved states of the smaller clusters can aid in their detection in interstellar atmospheres and the laboratory. Most importantly, this research offers further insight into how silicon and carbon interact with one another, which may one day lead to better semiconductors for aerospace applications.

Acknowledgements

I would like to express my sincere appreciation to my faculty advisors, Dr. Burggraf, Dr. Duan, and Dr. Weeks for their guidance and support throughout the course of this thesis effort. The insight and experience was certainly appreciated. I would also like to thank all of the people at AFIT who helped me out when I needed it, and for that matter all the people in high places who have stepped in to help me get to where I am today. And of course, I would also like to thank my family and the rest of my friends for helping me be more like the person God wants me to be. Love you all.

"Whoever is not against us is on our side." - Jesus

John E. Boyd

Table of Contents

List of Figures

List of Tables

EXCITED STATES OF SILICON CARBIDE CLUSTERS BY TIME DEPENDENT DENSITY FUNCTIONAL THEORY

1. Introduction

The Air Force needs wide band gap semiconductors for aerospace applications. One of the most promising materials for these applications is silicon carbide (SiC). Silicon carbide has a wide band gap, high thermal conductivity, high breakdown electric field, high saturated electron drift velocity, and is resistant to radiation. These qualities make it an ideal material for electronic devices in high temperature environments, like the interior of jet engines, and high radiation environments, such as space.[58]

One of these devices is the MOSFET (metal oxide semiconductor field effect transistor), but, lattice defects near the oxide interface and a poor control of the SiC surface make SiC MOSFETs difficult to fabricate. To better understand these defects, efforts have been underway to model semiconductor defects with quantum mechanics. However, it is virtually impossible to model an entire lattice and approximations have to be made. The SIMMOM (Surface Integrated Molecular Orbital/Molecular Mechanics) approach, created by Jim Shoemaker et. al., takes a major step by treating small clusters quantum mechanically and embedding those clusters in a molecular mechanics framework to simulate the rest of lattice.[60] An example of such an embedded cluster can be seen in Figure 1. However, the computational cost of these simulations is still too great if no approximations are made for the embedded cluster. So, before any of this can be accomplished, we must know

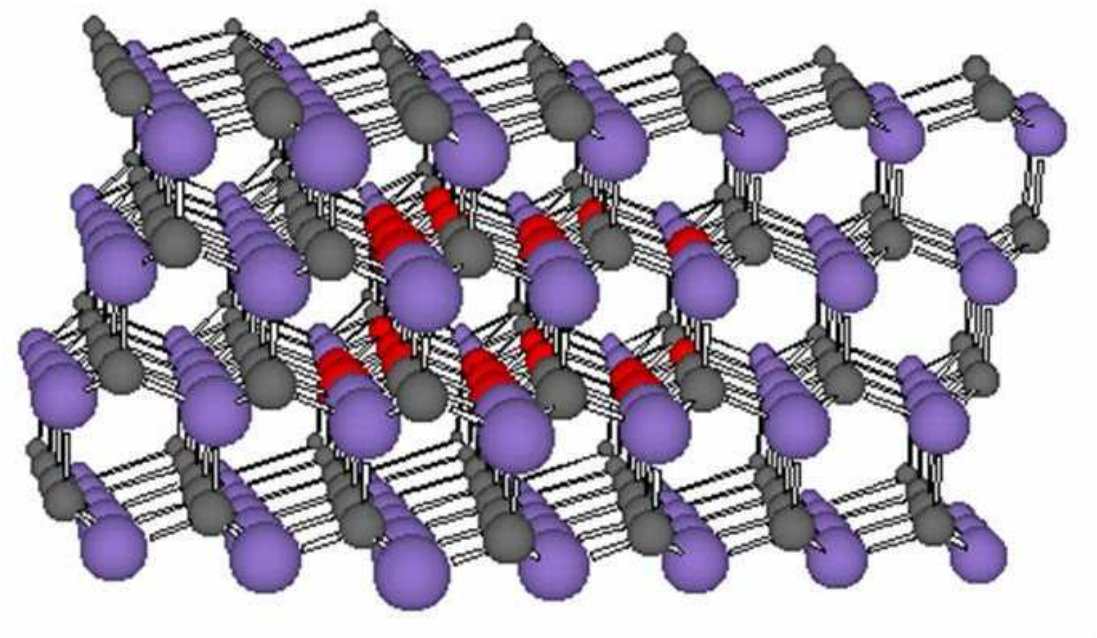

Figure 1 Example of a SIMMOM cluster
In this figure, the darker spheres represent the atoms within a SiC lattice that are treated quantum mechanically, while the larger and smaller spheres represent silicon and carbon atoms, respectively.

what quantum mechanical approximations and computational methods can be used without diminishing accuracy.

Here at the Air Force Institute of Technology, this task has begun by studying the smallest of these clusters using an efficient and reliable method known as density functional theory (DFT). DFT Calculations by Ms. Jean Henry in 2001 [31] were comparable to known experimental values for Si_mC_n m,n ≤ 4 clusters in the neutral and anion states. Further work by Lt. John Roberts on Si_mC_nO clusters has also shown similarly favorable results, and he along with Dr. Xiaofeng Duan extended Ms. Henry's cluster geometry map, shown in Figure 2.[21] However, this work has all been focused on cluster ground states because standard implementations of DFT are only equipped to model ground electronic states.

Ground state calculations alone can not model the relative energies of electronic states near the surface and around defects. Various spectroscopic techniques can

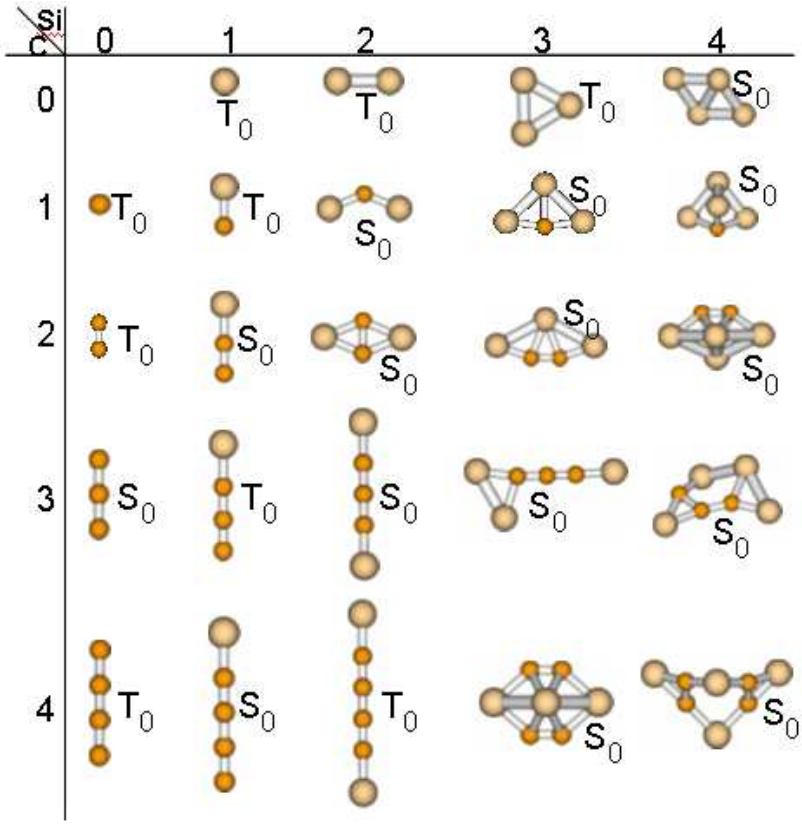

Figure 2 Map of the Ground State Geometries of Si_mC_n Clusters [31, 21] These geometries were generated using B3LYP density functional calculations by researchers at AFIT, showing the lowest energy isomer when calculated with the aug-cc-pVDZ basis set. The aug-cc-pVTZ basis set correctly predicts SiC_2 to be triangular instead of linear as shown above.

detect the the presence of these electronic states, and the energy difference of those states with the ground state. [64] But, without calculations it is impossible to assign the features in various spectra to the structures of defects and surface anomalies. We must be able to compare accurate quantum mechanical models for the ground and excited states of these structures to experiment. Time Dependent DFT (TDDFT) allows DFT methods to give predictions about excited states as well, and the method is also very efficient when compared with other excited state methods. Thus, the next step in AFIT's drive towards semiconductor modeling is to test TDDFT on these clusters, and benchmark the results with the excited states observed in experiments.

There have been a handful of Si_mC_n cluster excited states detected in experiment. The first "discovery" of an excited state cluster was actually in 1926 when blue-green bands were identified in certain stars by Merril and Sanford [42]. It was later shown that these spectral lines came from transitions between the two lowest lying electronic states of SiC_2. Michalopoulos et. al. correctly identified the triangular structure of this molecule and detected these transitions using resonant two photon ionization (R2PI) spectroscopy.[43] After this laboratory detection of SiC_2, a handful of optical transitions in the smallest of these clusters, SiC, were detected using various spectroscopic techniques.[8, 11, 10, 29] As a result, there are at least six electronic states of this molecule that have been observed in experiment: the X $^3\Pi$, A $^3\Sigma^-$, B $^3\Sigma^+$, C $^3\Pi$, b $^1\Pi$, and d $^1\Sigma^+$ states. Later work by Grutter et. al.[29] was able to obtain vibrational frequencies and excitation energies for the A $^2\Pi$ and B $^2\Sigma^+$ excited states of the anion as well.

Numerous experiments have also been performed using anion photoelectron spectroscopy (PES), where peaks that do not correspond to any allowed vibrational transitions appear.[17] This leaves the possibility that they involve other isomers or excited states. A peak in the spectrum of SiC_3 likely corresponds to an excited state. Another peak in the spectrum of Si_2C_3 likely corresponds to a low lying isomer, but may also be from an excited state. There are also two possible excited state peaks in the spectrum produced by Lineberger et. al. of Si_2C_4. The earlier PES work of Nakajima et. al. may also have excited state information available, but only if the contributions of the ground and excited states can be distinguished.[46]

These experiments can thus serve as a testing ground for the effectiveness of various excited state quantum mechanical methods on Si_mC_n clusters, but it is also useful to compare with other computational methods. However, there are not many calculations to compare with. There were a few theoretical studies of the excited states of SiC, the smallest cluster I examined, in the 1980's.[8, 38] There was also a theoretical study of the excited states of Si_2C. Finally, there was a study by

Rintelman and Gordan where two low lying states of the linear isomers of SiC_3 and Si_2C_2 were calculated.

1.1 Objective

In this thesis work, TDDFT and DFT were used to investigate the excited states of Si_mC_n clusters, using Gaussian 03 and similar quantum chemistry packages. Predictions are made about the electronic spectrum and the character of the excited states. Spectroscopic simulations are used in conjuction with various experimental spectra to distinguish between ground and excited state information and assess the accuracy of geometries and vibrational frequencies. The performance of any relevant approximation schemes and levels of theory was determined and recommendations for future calculations are be given.

1.2 Research Objectives/Questions/Hypotheses

In this research, I answer the following questions:

1) Can we expect many more excited states of these clusters in Photoelectron spectra?

2) What will the spectrum look like of these excited states?

3) Can any inferences be made about the excited states of larger clusters?

4) How accurate is DFT/TDDFT with respect to experimental results for excitation energies?

5) Are there any major shortfalls of TDDFT? Can these shortfalls be corrected?

1.3 Scope

This study is concerned with the excited electronic states using the ground state geometries determined by Ms. Henry, Lt. Roberts, and Dr. Duan[31, 21] as starting points, as well as the geometries of low lying isomers. I determine the equilibrium

geometries, vibrational frequencies, and excitation energies of the selected clusters for the first four excited states in hopes of aiding experimental detection. I also present insights into the bonding of silicon and carbon by examining the orbital interactions, and suggest ties between the work that has been done with clusters to the silicon carbide surface.

2. Theory

2.1 Chapter Overview

The purpose of this chapter is to provide the preliminaries needed to understand the results of the calculations I have completed. The quantum mechanics of nuclei moving within these clusters is the easiest place to start. From there I will move to the quantum mechanics of the electrons which ultimately drives the motion of the nuclei. After that, I will talk about density functional theory and time dependant density functional theory, which are the specific theoretical models used in this work. Finally, I will put everything together in the context of photoelectron spectroscopy and other experiments which will serve as an ample foundation to understand the results I have generated.

2.2 Quantum Mechanics [16]

Quantum mechanics has been the most influential theory in physics and chemistry for the past century. It postulates that all physical systems can be described by a wave function, Ψ. For a molecule like SiC, the wavefunction is a product of parts that specify the locations of each particle in the whole molecule, e.g.:

$$\Psi_{SiC} = \Psi_{carbon-nucleus}\Psi_{silicon-nucleus}\Psi_{electrons}$$

The wavefunction can be used to calculate a a probability density function, $\rho(\vec{r}, t)$ for locating the particles in the system at a given position $\vec{r}$ and time t. This is given by the absolute value squared of the wavefunction:

$$\rho(\vec{r}) = \langle \Psi(\vec{r}) \mid \Psi(\vec{r}) \rangle = |\Psi(\vec{r})|^2$$

When integrated over all space, this probability cannot exceed one, and this constraint is known as the normalization condition:

$$\int |\Psi(\vec{r})|^2 \, dr = 1$$

The wavefunction for a system changes in time according to the time dependent Schrodinger equation. In Cartesian coordinates, this is:

$$i\hbar/dt\Psi(\vec{r},t) = \hat{H}(\vec{r},t)\Psi(\vec{r},t) = -\frac{p^2}{2m}\Psi(\vec{r},t) + V(\vec{r},t)\Psi(\vec{r},t)$$

$$-\frac{p^2}{2m}\Psi(\vec{r},t) = \hbar^2\nabla^2\Psi(\vec{r},t)$$

The Hamiltonian, $\hat{H}$, relates the state of the particles to the total energy of the system. This energy can be divided into kinetic energy, $\nabla^2\Psi(\vec{r},t)$, and potential energy, $V(\vec{r},t)\Psi(\vec{r},t)$.

The Hamiltonian is the an important example of what is known as an operator. If we operate on the wavefunction by the Hamiltonian, we get an expression for the energy of the system. In fact, for any measurement taken of a quantum mechanical system, the quantity being measured can be expressed with an operator. For the sake of generality let us consider an arbitrary operator, $\hat{O}$. Since the probability distribution is normalized, the average or expectation value of the operator is given by:

$$\int \Psi^*(\vec{r},t)\hat{O}(\vec{r},t)\Psi(\vec{r},t)dr = \left\langle \hat{O}(\vec{r},t) \right\rangle$$

Thus, the total energy of a quantum mechanical system is given by:

$$\int \Psi^*(\vec{r},t)\hat{H}(\vec{r},t)\Psi(\vec{r},t)dr = \left\langle \hat{H}(\vec{r},t) \right\rangle$$

The wavefunction Ψ can be expressed as a normalized vector with values for every point in space and time. When this is done, the products and integrals above become matrix multiplication with the operator O being left and right multiplied by the two vectors to give a single value. To express this in "bra-ket" notation, the most common notation used in quantum mechanics, we have:

$$\int \Psi^*(\vec{r},t)O(\vec{r},t)\Psi(\vec{r},t)dr = \langle\Psi| O |\Psi\rangle$$

The vectors are known respectively as the "bra," $\langle\Psi^*|$, and the "ket," $|\Psi\rangle$. Using this compact notation, the overlap of two different wavefunctions is:

$$\int \Psi_1^*(\vec{r},t)\Psi_2(\vec{r},t)dr = \langle\Psi_1|\ \Psi_2\rangle$$

It is also useful to note that what we normally think of as a function of space, $\Psi(\vec{r})$ can also be thought of as the overlap integral of the vector $|\Psi\rangle$ and a dirac delta function centered at the coordinate r, which can be expressed by:

$$\langle r\ |\Psi\rangle = \Psi(r)$$

Normally, we do not already know the solution for the wavefunction for a system. In some problems the solution for the wavefunction can be as simple as quick boundary value problems, while solutions for the molecules in this research can require days to evaluate on supercomputers.

Because the operators can be expressed as matrices, linear algebraic methods are used to get answers. We can express the wave function vector in terms of a convenient basis, such as Cartesian coordinates, plane waves, spherical harmonics or any other set of functions that can represent the wavefunction accurately. Once this is done, a solution is found by finding the eigenvectors that diagonalize the Hamil-

tonian. Thus the time independent Schrodinger equation becomes an eigenvalue problem and the solution becomes:

$$\hat{H} \left| m \right\rangle = \varepsilon_m \left| m \right\rangle$$

where the $|m\rangle$ and ε_m are the respective eigenstates and eigenvalues of the Hamiltonian operator. The wavefunction is then expressed as a linear combination of these eigenvectors.

$$\Psi = \sum_{m=0}^{\infty} c_m \left| m \right\rangle$$

If the original basis was infinite and complete, the lowest eigenvalue would be the ground state. The time dependence of the each eigenstate can then be expressed in terms of the original Schrodinger equation in matrix form:

$$i\frac{d}{dt} c_m(t) \left| m \right\rangle = c_m(t) \hat{H} \left| m \right\rangle = \varepsilon_m c_m(t) \left| m \right\rangle$$

This has the solution:

$$c_m(t) = c_m(0) \exp(\pm i \varepsilon_m t / \hbar)$$

This solution shows that for a system described by a single eigenstate, the probability density does not change over time, and the system will not radiate energy away electromagnetically. However, a system described by a mixture of two or more non-degenerate eigenstates will have a changing probability density that will emit energy via electromagnetic radiation until it settles at a lower energy eigenstate. As a result, quantum mechanical systems can only stop at these eigenstates, which means that the energy they radiate or absorb can only come in discrete amounts. A spectroscopist can measure these discrete amounts of energy and to know what state the system was in before and after these transitions, but only if there are theoretical results for the relative energies of these states.

The Schrodinger equation mentioned above has an analytic solution for only a few systems. In the case that the potential energy does not vary with time, the equation is separable between time and space. The time dependent part of the wavefunction can then be expressed as:

$$\langle t \,|\Psi\rangle = e^{iEt/\hbar}\,|m\rangle$$

In the absence of a potential, the spatial solution of the Schrodinger equation becomes a linear combination of plane waves. The center of mass for any molecule could be described by such linear combinations, but this does not help us to understand the interaction between the particles that make up the molecule.

2.2.1 Computation of Molecular Systems [62]. The solution for a molecular problem is a coupled differential equation of too many variables to handle all at once, so chemists simplify the picture and work up to every last detail. Approximations are made based on reasonable chemical and physical arguments to allow the computer to reach a solution, and then these approximations are corrected with subsequently higher level calculations. These approximations allow the computer to converge to a solution, but they also give a framework for people to understand the results and (if they are talented enough) make predictions without turning on the computer.

The first approximation that is traditionally made is called the Born-Oppenheimer approximation. The mass of a proton (and thus any nucleus) is over 900 times the mass of an electron. Thus the kinetic energies of the nuclei are small compared to the rest of the system. The Born-Oppenheimer approximation assumes that the nuclei barely move when compared with the electrons, so that the electrons adjusts before the nuclei can. At every nuclear arrangement there is an electronic configuration that minimizes the total electron energy, and the energies of these electron configurations can can be used to generate a potential energy surface. The low point of the

valleys of that potential energy surface determines the most stable positions of the nuclei.

At first glance, we have 3M (M being the number of nuclei) total degrees of freedom and therefore, 3M is the dimension for this potential energy surface, but this is quickly reduced. However, I have already mentioned that the center of mass can be used to describe the translation of the molecule as a whole, and this reduces the total degrees of freedom by three. The coordinates can also be rotated without changing the locations of the nuclei with respect to one another, further reducing the degrees of freedom. Thus, for a diatomic molecule we only need to specify the interatomic distance. For a triatomic molecule we only need two more coordinates, and for every atom greater than three we need an additional three coordinates. If a molecule is symmetric, like Si_4C_4, even fewer coordinates need to be specified.

A gradient in the potential energy surface exerts a force on the nuclei that causes the molecule to change shape. Thus the low points of the potential energy surface are stable geometries, known as isomers, that may or may not occur in nature. The relative proportions of each isomer can be described by a Boltzman distribution or a similar distribution from statistical mechanics, and except at very high temperatures the the lowest energy isomer will often be the one that is most likely found. Finding these low lying isomers computationally is a process known as a geometry optimization. A quantum chemistry program like Gaussian, NWChem, or Turbomole takes a small sample of the potential energy surface at a geometry given by the user, to see what direction the forces are pointing and how curved the surface is. Based on that sample, the program guesses what the minimum energy nuclear configuration will be. The process is repeated in steps until the guesses converge and the forces are essentially zero.

2.2.2 Vibration Frequencies and Normal Modes. Although the first derivative of the potential energy surface is zero when the geometry is minimized, the

second derivative of the potential energy surface is not. The interaction between the nuclei can be treated as a system of coupled harmonic oscillators where the non-zero second derivatives are the spring constants. This approximation helps because the harmonic oscillator has a relatively simple analytic solution, which I will only summarize here because the full solution can be found in any introductory quantum mechanics textbook[16]. The total energy of a particle in a quadratic potential well is given by the sum of the kinetic and potential energies:

$$E = T + V = \frac{p^2}{2m} + \frac{1}{2}m\omega^2 x^2$$

Here, ω is the characteristic frequency of the oscillator, and m is the mass of the particle in the harmonic well. The ground state of the system is a Gaussian function centered at the bottom of the well:

$$\langle x \,|\varphi_0\rangle = \left(\frac{m\omega}{\pi\hbar}\right)^{1/4} e^{-\frac{1}{2}\frac{m\omega}{\hbar}x^2}$$

Furthermore, the excited states are given by:

$$\langle x \,|\varphi_n\rangle = \frac{1}{\sqrt{n}}\frac{1}{\sqrt{2^n}}\left[\sqrt{\frac{m\omega}{\hbar}}x - \sqrt{\frac{\hbar}{m\omega}}\frac{d}{dx}\right]^n \varphi_0(x)$$

Finally, energy eigenvalue for the nth state is $\hbar\omega$ (n+1/2).

The one dimensional harmonic oscillator can quickly be generalized to multiple dimensions, and it is easy to show that the resulting multidimensional wavefunctions are the product of one dimensional harmonic oscillator wavefunctions.

With this approximation in mind, a quantum chemistry program starts with the ground state geometry and calculates the energy and gradient for slight shifts of each of the M nuclei in all three directions. With this information the second derivatives, $\hat{k}$, with respect to nuclear coordinates are obtained, and an equation for

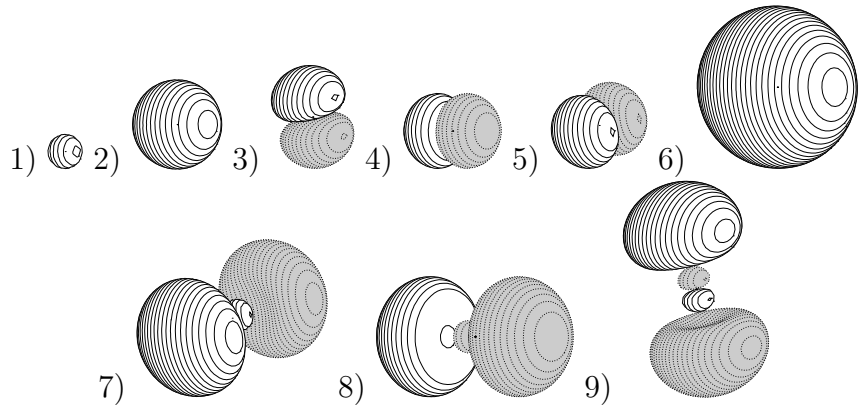

Figure 3 Atomic Orbitals for Atomic Silicon
These contour plots show the 1s (1), 2s (2), 2p (3,4,5), 3s (6) and 3p (7,8,9) orbitals of atomic silicon.

the system's vibrational behavior can be expressed in matrix form:

$$\hat{m}\ddot{\vec{X}} = \hat{k}\vec{X}$$

Here, $\hat{m}$ is a diagonal matrix containing the nuclear masses, and the matrix $\hat{k}$ is known as a "Hessian". The eigenvalues of this system are the vibrational frequencies, and the eigenvectors are known as the normal modes. While the geometries of many systems can not be directly measured, the vibrational frequencies can be measured in many different ways. Furthermore, the normal mode wavefunctions can be used to approximate the nuclear wavefunctions as solutions to multidimensional quantum mechanical harmonic oscillators. This gives an analytic expression for the overlap integral between two nuclear wavefunctions, which is proportional to the intensity of transitions from one vibrational state to the next.[14] The height of vibrational peaks should then be proportional to the overlap integral of the respective transitions, and the accuracy of a given geometry is can be supported or refuted by vibrational spectroscopy.

2.2.3 The Hydrogen Atom and Atomic Orbitals [16]. Another analytic solution to the Schrodinger equation is for the hydrogen atom and other single electron

ions. It is very important because it is the foundation for understanding electronic state models. The potential energy has a simple -1/r dependence, so separation of variables can be used to obtain radial and angular components to the eigenstates of the wavefunction.

$$\langle r, \theta, \varphi \, | \Psi \rangle = R_n(r) Y_m^l(\theta, \varphi)$$

The $Y_m^l(\theta, \varphi)$ are spherical harmonics, while the radial dependence $R_n(r)$ has the form:

$$R_n(r) = L_n(r) e^{-r/a_0}$$

where L_n is the n^{th} Laguerre polynomial, a class of orthogonal polynomials that are the solution to the radial equation.

The eigenvalues of the spatial Hamiltonian are specified by n, l, and m, and these three are known as quantum numbers. The number n denotes the total electron energy, the number l denotes the angular momentum, and m denotes the z component of the angular momentum. There is a fourth quantum number, s, which accounts for the spin (a relativistic effect [5]) of the electron, either α (spin up) or β (spin down). The eigenfunctions that these quantum numbers specify are known as orbitals, and they form the foundation for understanding the way electrons behave in other atoms. The Pauli exclusion principle prevents any two electrons from occupying the same quantum state, so instead of all the electrons dropping to the lowest energy orbital, each orbital is filled by at most one α and one β electron. These orbitals distort radially as the electrons fill these shells, but much of the same spherical symmetry remains. They can be classified by the number and location of nodal planes, places where the wavefunction goes from positive to negative.

As a visual aid, the atomic orbitals for silicon can be seen in Figure 3, and the atomic orbitals for carbon are qualitatively just like the first five silicon atomic orbitals in the same figure. These pictures are contour plots of each orbital, where the positive and negative contours are differentiated by the grey shading. Because

the contour value is non-zero (typically .01 throughout this paper), the location of the nodal planes may not be immediately evident, but they can be found by looking for the midway point between the positive and negative contours shown.

The spherical functions are known as "s" functions and the polarized functions are known as "p" functions. An s function has no nodal plane, while a p function has one. Functions with more nodal planes exist as well, where the angular dependance changes a great deal. For example, a function with two nodal planes, the xz and yz planes, can be designated a "d_{xz}" function. The number of nodal planes increases the kinetic energy of an orbital, and as a result the atomic d orbitals are not occupied in silicon or carbon, although they sometimes participate in silicon bonding.

Table 1 Conversion of Atomic Units to SI Units [62]

Physical Quantity	Conversion Factor X	Value of X (SI)
Length	a_o	5.2918 x 10^{-11} m
Mass	m_e	9.1095 x 10^{-31} kg
Charge	e	1.6022 x 10^{-19} C
Energy	E_a	4.3598 x 10^{-18} J
Angular Momentum	$\hbar$	1.0546 x 10^{-34} J s
Wave function	$a_o^{-3/2}$	2.5978 x 10^{15} $m^{-3/2}$

Also, the useful "atomic units" system is based on the hydrogen atom, and it greatly reduces the number of physical constants in the equation for the Hamiltonian of any molecular system. Mass, charge, energy, and distance are all expressed in terms of the electron mass, electron charge, Planck's constant, and the Bohr radius of the hydrogen atom. The final unit for energy is called the hartree. One hartree is equal to 27.211 eV, which is twice the binding energy of a hydrogen atom. The atomic units system is summarized in Table 1.

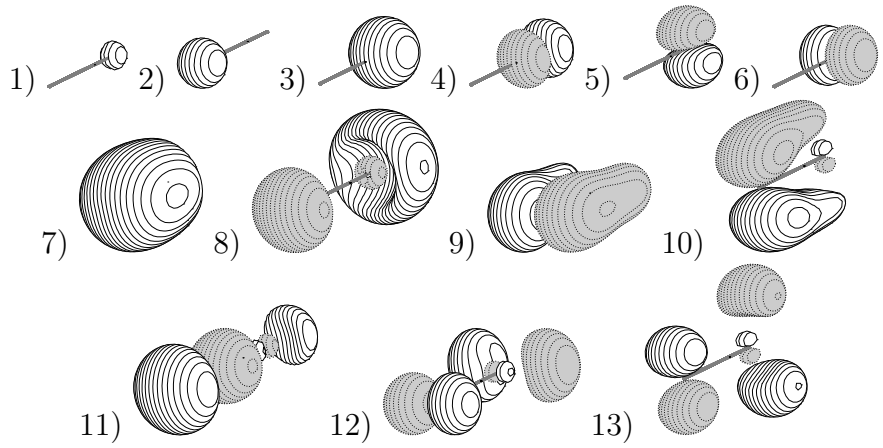

Figure 4 Molecular Orbitals for a $^1\Sigma$ SiC

2.3 Basic Molecular Orbital Theory [50, 2]

While there are many qualitative lessons that can be learned from the hydrogenic atom, the move to molecules adds more complexity. To understand much of my research, the reader must understand some simple molecular orbital theory. The approach that I have found quite helpful when describing the orbitals of Si_mC_n clusters is known as LCAO, or linear combination of atomic orbitals. As its name implies, it takes the approach that the molecular orbitals can be described as combinations of the atomic orbitals.

When two atoms come close together their atomic orbitals start to overlap, either constructively (in phase) or destructively (out of phase). When the orbitals add constructively, they form "bonding orbitals", where electron density collects between the two atoms. When they add destructively, the resulting orbital is known as an "anti-bonding orbital". An anti-bonding orbital will form a nodal plane somewhere between the two atoms, so that the wavefunction will be shaded on one and unshaded on the other in a contour plot. To help illustrate this, the orbitals calculated for SiC can be seen in Figure 4.

As the observant person can tell, the first six orbitals look just like atomic orbitals. This is because much of the orbital interaction in many molecular systems

is largely restricted to the valence electrons. This is also true with carbon and silicon, where each have four valence electrons and the rest of the electrons are not greatly affected by chemical processes. In the rest of my orbital plots, I won't include these "core" orbitals because they don't change much at all.

But starting with orbital 7, we can see the LCAO theory in action. This orbital is the result of adding the valence s functions in phase from carbon and silicon, and is a bonding orbital. Orbital 8 is an antibonding orbital, formed mostly from the subtraction of the same two atomic s orbitals. In a linear molecule, the axis along the chain of the molecules is designated the z-axis, and the molecular orbitals that are symmetric around this axis are designated as σ orbitals. Clearly, orbitals 7 and 8 are σ orbitals.

In a similar manner, orbitals that transform like the functions x or y upon rotation are known as π orbitals. These designations come from the same idea as the atomic orbitals, but using greek versions of s and p to distinguish molecular orbitals from atomic orbitals. Thus, it is easy to see that orbitals 9 and 10 of SiC are bonding π orbitals. Finally, we can understand orbital 11 as a linear combination of the p_z orbitals of carbon and sillicon. It is a bonding σ orbital because the atomic orbitals are in phase and we can see the density between the two atoms.

2.3.1 Symmetry and Group Theory. In other molecules, the symmetry of each orbital is designated by the symmetry group irreducible representation (known as "irreps") of the highest symmetry that the molecules has. Most of my molecules could be grouped into what is known as the C_{2v} symmetry group, and there is an analogy between this group and the linear molecules (members of the $C_{\infty v}$ symmetry group). To see this analogy, first select the axis with the highest symmetry as the z axis. If the molecule is planar, select the y axis so that all the atoms are in the yz plane, but otherwise select a yz plane that gives the molecule reflective symmetry. Once this is done, there are four symmetry irreps. The irrep A_1 is like the sigma

orbitals, if you reflect the wavefunction about the y or x axes, it does not change. The irreps B_1 and B_2 behave like π_x and π_y functions with respect to reflection. The final irrep of this symmetry group, A_2, behaves like the simple function xy upon reflection about the xz or yz planes. Each orbital is then designated with the lowercase version of the irrep, just as atomic orbitals use lowercase designations. Since these irreps transform like functions of x and y, they can also be multiplied together in simple ways that are tabulated in group tables and coded into quantum chemistry programs.

As mentioned before, the atomic orbitals and the orbitals of linear molecules can also be described by the $C_{\infty v}$ symmetry group. However, the rules of multiplication for this groups are also the rules for the addition of angular momentum. Those rules can be summarized as adding the z component of the angular momentum. Any σ and s orbitals have angular momentum z-component values of 0. The complex linear combination of π orbitals, $\pi_x + i\pi_y$, has an angular momentum z-component of +1, and π_x - iπ_y has an angular momentum z-component value of -1.

$$\pi_+ = \frac{1}{\sqrt{2}}(\pi_x + i\pi_y)$$

$$\pi_- = \frac{1}{\sqrt{2}}(\pi_x - i\pi_y)$$

For example, a doubly occupied π_+ orbital has a total angular momentum of 2, while a singly occupied pair of π_+ and π_- orbitals will have a total angular momentum of 0. The resulting two electron wavefunction will have the same axial symmetry as an atomic or molecular orbital with the same total angular momentum.

2.3.2 Spin and Term Symbols. Once we know some basic information about the orbitals that are occupied by a molecule in a certain electronic state, we have to be able to express that information succinctly. This is done by term symbols. A term symbols has three parts, the spin multiplicity, the symmetry or

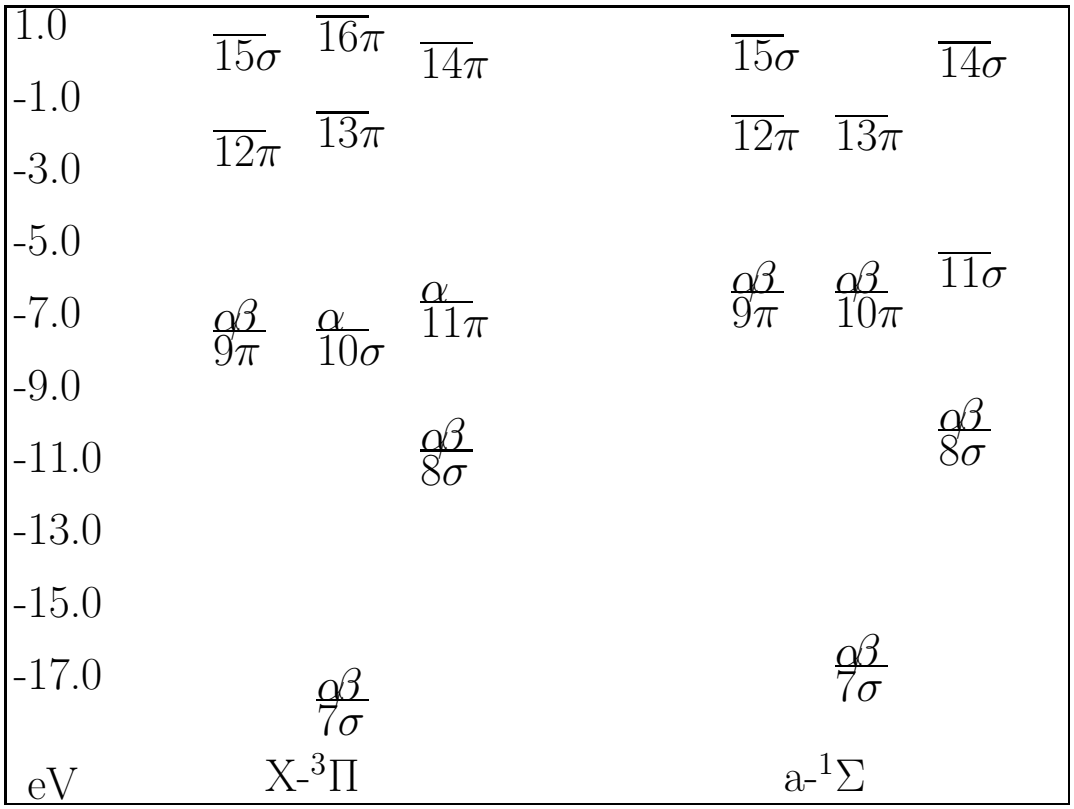

Figure 5 Orbital Occupation Diagram For Two States of SiC

angular momentum of the electronic state, and a letter to distinguish it from all the other electronic states. I have provided Figure 5 as a visual aid to illustrate the following process in the context of identifying two states of SiC.

The spin multiplicity of a state gives us information about how the α and β electrons occupy orbitals. In this research, all the neutral molecule spin multiplicities are either triplet or singlet. In a singlet state, every α electron is paired with a β electron. But, in a triplet state there are two more α electrons than β electrons, so by the Pauli exclusion principle these extra two electrons can not occupy the same orbital.

The next part of the term symbol is the result of group multiplication of the occupied orbital symmetry irreps. This part is written using uppercase instead of

lowercase symbols. So for the simple two electron case mentioned above, if the total angular momentum was 2, the symbol would be "Δ". If the total angular momentum was 0, the symbol would be "Σ."

The letter used to differentiate between states is a capital "X" if the state is the ground state. If the state is of the same spin multiplicity as the ground state, this letter is also capitalized, and the letters of the alphabet are used starting with "A". If the state has a different spin multiplicity, lowercase letters are used instead, yet still starting with "a".

Putting everything together, we can take the example of the ground state of SiC. This molecule has two α electrons occupying different orbitals alone, so we know it is a triplet molecule. If we add the angular momentum we get a total of 1, leading to a Π state. Since it is the ground state, we can now designate it as X $^3\Pi$. The other term symbol in Figure 5 can be found using the same methodology. So how do we do calculations on this and other molecules?

2.4 Many Electron Quantum Mechanics

For a molecular system in atomic units, The Hamiltonian has the form:

$$\hat{H} = -\frac{1}{2}\sum_{i=1}^{N}\nabla^2 - \frac{1}{2}\sum_{A=1}^{M}\frac{1}{M_A}\nabla^2 - \sum_{i=1}^{N}\sum_{A=1}^{M}\frac{Z_A}{r_{iA}} + \sum_{i=1}^{N}\sum_{j<i}^{N}\frac{1}{r_{ij}} + \sum_{A=1}^{M}\sum_{B>A}^{M}\frac{Z_A Z_B}{R_{AB}}$$

The terms on the right hand side are, from left to right, the kinetic energy of the electrons, kinetic energy of the nuclei, nuclear-electron attraction, electron-electron repulsion, and nuclear-nuclear repulsion. The M_A are the masses of each nucleus expressed in atomic units, Z_A are the atomic numbers of each nucleus. The distance between an electron and a nucleus is denoted by r_{iA}, between electrons by r_{ij}, and between nuclei by R_{AB}. These contributions to the energy are obviously summed over all of the electrons and nuclei in the system. Because the interaction between multiple electrons is an inseparable term in the Hamiltonian, methods used to arrive

at analytical solutions break down and we are forced to make approximations and solve the problem numerically.

Even after the Born Oppenheimer approximation is made we are left with an electronic Hamiltonian of the form:

$$\hat{H}_{elec} = -\frac{1}{2}\sum_{i=1}^{N}\nabla^2 - \sum_{i=1}^{N}\sum_{A=1}^{M}\frac{Z_A}{r_{iA}} + \sum_{i=1}^{N}\sum_{j<i}^{N}\frac{1}{r_{ij}} = \hat{T} + \hat{V}_{Ne} + \hat{V}_{ee}$$

The wave function for the electrons is a product of individual electron wavefunctions, known as a Hartree product.

$$\Psi = \psi_1\psi_2...\psi_n$$

However, that product alone is not enough to describe the system. Elementary particles like electrons are indistinguishable from other like particles, but the Hartree product mentioned above would allow us to examine each electron as if we could tell them apart. The probability of finding an electron has to be the same for any electron at any location, and this means that the wavefunction must be either symmetric or antisymmetric with respect to exchanging particles, but not a mixture of both.

$$\Psi = \psi_1\psi_2...\psi_n = \psi_2\psi_1...\psi_n \quad Symmetric$$

$$\Psi = \psi_1\psi_2...\psi_n = -\psi_2\psi_1...\psi_n \quad Antisymmetric$$

By definition, bosons have a symmetric wavefunction that will be exactly the same if you switch two particles. Fermions, which include all electrons, have an anti-symmetric wavefunction that will be exactly negative after a switch. If we pretended for a moment that two electrons of the same spin did somehow occupy the same spatial orbital, we would find that switching them would not make the wavefunction negative, and the wavefunction would not be antisymmetric. Thus the requirement that the multi-particle wavefunction be antisymmetric limits the number of like-spin

electrons in an orbital to one. Since there are two types of electron spin, α or β, the highest number of electrons permitted in a spatial orbital is two. This is the source of the Pauli Exclusion Principle and the shell structure that gives the periodic table it's shape.

2.4.1 The Hartree Fock Approximation. To meet the antisymmetry requirement, a Slater determinant can be used to represent the wavefunction:

$$|\Psi\rangle = \frac{1}{\sqrt{N}} \begin{vmatrix} |1:\psi_1\rangle & |1:\psi_2\rangle & ... & |1:\psi_N\rangle \\ |2:\psi_1\rangle & |2:\psi_2\rangle & ... & |2:\psi_N\rangle \\ ... & ... & ... & ... \\ |N:\psi_1\rangle & |N:\psi_2\rangle & ... & |N:\psi_N\rangle \end{vmatrix}$$

You can think of a Slater determinant as one orbital occupation diagram, like the one shown previously for SiC in Figure 5. All the Slater determinant does is sum up all the possible combinations of a pattern of electrons occupying the same orbitals so that you can no longer tell them apart. It can be shown mathematically that any antisymmetric wavefunction can be expressed as a linear combination of determinants, but the number of determinants we need is unknown. The Hartree Fock approximation simply finds the lowest energy single determinant by the following procedure. Recall that the Hamiltonian for only the electronic energy is:

$$\hat{H}_{elec} = -\frac{1}{2}\sum_{i=1}^{N}\nabla^2 - \sum_{i=1}^{N}\sum_{A=1}^{M}\frac{Z_A}{r_{iA}} + \sum_{i=1}^{N}\sum_{j<i}^{N}\frac{1}{r_{ij}} = \hat{T} + \hat{V}_{Ne} + \hat{V}_{ee}$$

The summations over i can be removed and approximated by N one-electron Fock operators, defined by:

$$\hat{f}_i = -\frac{1}{2}\nabla^2 - \sum_{A=1}^{M}\frac{Z_A}{r_{iA}} + V_{HF}(i)$$

Here V_{HF} is is the average potential felt by electron i from the other N-1 electrons. Solving the eigenvalue equation leads to the Hartree Fock ground state energy of the system. Because both of these equations invoke one another, they have to iterate back and forth until they agree. This procedure in general is known as Self-Consistent Field or SCF, and it is the back bone of any quantum chemical calculation.

In truth, although the Hartree Forck theory is foundational to understanding much of what happens in quantum chemistry, it doesn't give very good answers as far as we are concerned. The energy difference between the Hartree Fock energy and the real answer is called the correlation energy, and other determinants are needed to capture it. Procedures such as Multiconfigurational SCF (MCSCF), Complete Active Space SCF (CASSCF), and Configuration Interaction (CI) have been created to capture the correlation energy, by using more and more determinants. However, each additional determinant makes the calculation more and more expensive, and one of the goals of this research is to find a cheap way to get good results. My research took another route to solve for the electronic energy.

2.5 Density Functional Theory

Another approach to the solution of these molecular systems is known as density functional theory, where the electron density, ρ(r), is used as the principle variable instead of the many-body wavefunction. I will present some of the first attempts to do this for historical reasons, and eventually present the methods used in this research.

2.5.1 The Thomas Fermi Model. The 1927 Thomas-Fermi Model was the first attempt to use the electron density as the principal variable in atomic calculations. Based on statistical mechanics instead of quantum mechanics, it used

the same electron kinetic energy as that of a uniform electron gas.

$$E_{TF}[\rho(\vec{r})] = \frac{3}{10}(3\pi^2)^{2/3}\int \rho^{5/3}(\vec{r})dr - Z\int \frac{\rho(\vec{r})}{r}d\vec{r} + \frac{1}{2}\iint \rho(\vec{r}_1)\rho(\vec{r}_2)/_{r_{12}}d\vec{r}_1 d\vec{r}_2$$

This result was not very accurate at all, but it was the first example of a real density functional theory that did not bother with the wave function at all. At the time however, there was no proof that this was physically justified. Rather, the Thomas Fermi approach was based on assumptions and intuition. It took a little over 30 years for the general approach of using the density as the primary variable to be mathematically validated.

2.5.2 The Hohenburg – Kohn Theorems. It was proven by Hohenburg and Kohn that "the full many particle ground state is a unique functional of the density."[36] This can be proven in the context of molecules by contradiction. Assume two different isomers or molecules somehow led to the same ground state electron density.

$$V_{Ne} \Rightarrow \hat{H} \Rightarrow \Psi \Rightarrow \rho(r) \Leftarrow \Psi' \Leftarrow \hat{H}' \Leftarrow V'_{Ne}$$

The difference between the nuclear-electron attraction causes differences in the Hamiltonian and also the ground state wavefunction for the primed and unprimed cases above. By the variational principle, we know that the lowest energy for the unprimed Hamiltonian will come from the unprimed wavefunction.

$$E_0 = \langle\Psi|\,\hat{H}\,|\Psi\rangle < \langle\Psi|\,\hat{H}\,|\Psi'\rangle$$

$$= \langle\Psi|\,\hat{H}'\,|\Psi'\rangle + \langle\Psi'|\,\hat{H} - \hat{H}'\,|\Psi'\rangle = E'_0 + \langle\Psi'|\,\hat{H} - \hat{H}'\,|\Psi'\rangle$$

The same, however, can be said of the primed variables:

$$E'_0 < E_0 + \langle\Psi|\,\hat{H}' - \hat{H}\,|\Psi\rangle$$

Because the only difference between the two Hamiltonians is the external potential which is integrated over the same density for both primed and unprimed variables, addition of these two equations leaves a contradiction.

$$E_0 + E_0' < E_0 + E_0' \rightarrow 0 < 0$$

Thus, for the same ground state density to appear in two molecules, those two molecules can not be different. A solution for the ground state density determines the ground state wave-function and thus all the energetic properties of the system, and by definition the ground state density (and any other density for that matter) is determined by the wavefunction.

This means a one to one mapping exists between ground state densities and wavefunctions. In the second Hohenburg Kohn theorem, this one to one functional is used to show that the variational methods that are so crucial to finding the ground state of a system by wavefunction methods can be used on the density as well. However, the form of the unique functional that maps the density to the wave-functions is unknown, and a great amount of effort has been expended in trying to find approximate functionals that can give accurate results.

2.6 The Kohn Sham Approach

The first strides toward a chemically relevant density functional theory were undertaken by Kohn and Sham in 1965. The contribution of the coulomb repulsion energy of an arbitrary charge density has a well known form from classical physics. The problem however, is that the classical equation assumes all the electron density interacts with all of the rest of the electron density, when in fact the density from one electron does not interact with the rest of the density from that same electron. This self interaction demands that a non classical term is added that must also be

approximated, E_{ncl}.

$$E_{ee}[\rho] = \frac{1}{2}\iint \frac{\rho(r_1)\rho(r_2)}{r_{12}} dr_1 dr_2 + E_{ncl}$$

Next, in the switch from the wavefunction to the density, we have lost important information about the kinetic energy of the system. The ∇^2 operator for the kinetic energy operates on the wave function before the wavefunction is multiplied by itself to find the probability density. In the form of an equation:

$$\text{Kinetic Energy} = \langle \Psi \left| \nabla^2 \right| \Psi \rangle \neq \nabla^2 \rho$$

The relatively simple act of taking the second spatial derivative of the wavefunction cannot be applied to the electron density, and this creates problems because the shell structure comes from the second spatial derivative of the wavefunction. The electronic shell structure is the foundation of chemistry, and if this shell structure is not reproduced, as was the case with many of the earliest density functional theories, chemical bonding cannot be modeled.

Kohn and Sham reproduced this shell structure by using orbitals similar to the Hartree Fock method described above. However these Kohn-Sham orbitals are the solutions of a density functional theory based one electron operator instead of the Fock operator. In fact, the Hartree Fock equations are a special case of the Kohn Sham equations. The form of the Kohn Sham equations are:

$$f^{KS}\varphi_m = \varepsilon_m \varphi_m$$

$$\left[-\frac{1}{2}\nabla^2 + V_{eff}(r_1)\right]\varphi_m = \varepsilon_m \varphi_m$$

$$V_{eff}(r_1) = \int \frac{\rho(r_2)}{r_{12}} dr_2 + V_{XC} - \sum_A^M \frac{Z_A}{r_{1A}}$$

The non-classical contributions of the coulomb and kinetic energies mentioned above are combined into what is known as the exchange-correlation functional, V_{XC}. The exchange correlation energy is the only approximation that has been made, everything else is in principle exact. So, instead of paying the computational price for multiple determinants, the answer is improved by finding better approximations for the exchange-correlation functional.

2.6.1 Local Density and Local Spin Density Approximations. The simplest method to treat the exchange correlation term is known as the Local Density Approximation (LDA). This method is based on what the exchange correlation energy would be in a uniform electron gas of the same density. The Local Spin Density Approximation (LSDA) is similar, dealing with the respective densities of α and β electrons instead of both at once. The exchange term for this approximation has an analytic form, which is

$$\varepsilon_X = -\frac{3}{4}\sqrt[3]{\frac{3\rho(r)}{\pi}}$$

The correlation term however, does not have a known analytic form. However Monte Carlo simulations done by Ceperly and Alder in 1980 have been fit by various interpolation schemes, so that an analytic expression can be used in calculation. The most commonly used fits are known as those presented by Vosko, Wilk, and Nusair (VWN) in 1980. Of course, these approximations are no longer valid in situations where the electron density changes over space, which includes every molecule.

2.6.2 Generalized Gradient Approximations. To compensate for changing densities, generalized gradient approximations were introduced. Treating the exchange correlation energy as a Taylor expansion about the density at every point gives the form

$$E_{XC}^{GEA}[\rho_\alpha, \rho_\beta] = \int \rho\varepsilon_{XC}(\rho_\alpha, \rho_\beta)dr + \sum_\sigma \int C_{XC}^{\sigma,\sigma'}(\rho_\alpha, \rho_\beta)\frac{\nabla\rho_\sigma}{\rho_\sigma^{2/3}}\frac{\nabla\rho_{\sigma'}}{\rho_{\sigma'}^{2/3}}dr.$$

This is known as the gradient expansion approximation (GEA), but it also fails when applied to molecular systems. A more successful approach has been generalized gradient approximations (GGA) of the form

$$E_{XC}^{GGA}[\rho_\alpha, \rho_\beta] = \int f(\rho_\alpha, \rho_\beta, \nabla\rho_\beta, \nabla\rho_\beta)dr$$

There have been many choices for the functional f, but one in particular should be mentioned here since it is used in this research. In 1988 Lee, Yang, and Parr developed a correlation functional (LYP) based on a highly accurate wavefunction approach to the helium atom containing only one parameter.

2.6.3 Hybrid Functionals. Hybrid functionals combine the good qualities of the LDA and the GGA's by offering exchange correlation functionals that may be mixtures of the two and some amount of exact (HF) exchange. There are many of these functionals, and the way to know what will work in a given situation is based on what has proved successful in the past.

For this research, the B3LYP functional was used for most calculations because of it's proven success in previous work with these clusters. The form of this functional is

$$E_{XC}^{B3LYP} = (1-a)E_X^{LSD} + aE_{XC}^{\lambda=0} + bE_X^{B88} + cE_C^{LYP} + (1-c)E_C^{LSD}$$

The B stands for Becke, the originator of both this functional and the B88 functional for the exchange. The 3 stands for the three empircally determined parameters, a, b, and c, used in the functional, and the LYP means that the LYP correlation mentioned above is used as well. The functional performs surprisingly well even with situations that weren't included in the original experimental set.

2.7 Time Dependent Density Functional Theory

As noted before, the external potential inside the Hamiltonian determines the time evolution of the wavefunction via the Schrodinger equation.

$$i\partial/\partial t\Psi = \hat{H}\Psi$$

But we also know that the density at any point in space is determined by the wavefunction. Although the Hohenburg-Kohn theorem proved that there is a mapping from the ground state density to the external potential, a system evolving in time is not in the ground state. Runge and Gross[28] formalized time dependent density functional theory and extended the Hohenburg-Kohn theorem's into the time domain, by proving that two spatially different external potentials cannot induce the same time dependent densities. To sketch the proof, which is done by contradiction, suppose there were two different potentials that induced the same densities. Because the gradient of a potential is force, which is the time derivative of current, these two differing potentials will lead to different current densities. But since the divergence of current density is the time derivative of density, the two differing potentials must induce different densities.

Because of this extension of the Hohenburg-Kohn theorems into the time domain, we can then know that the wavefunction of a system is a unique functional of the time dependent density, where the following set of hydrodynamical equations governs the time evolution of the system:

$$\partial/\partial t\rho(r,t) = -\nabla \cdot j(r,t)$$

$$\partial/\partial t j(r,t) = \mathrm{P}[\rho](r,t)$$

$$\mathrm{P}[\rho](r,t) \equiv -i \left\langle \Psi[\rho](t) \right| [\hat{j}(r), \hat{H}(t)] \left| \Psi[\rho](t) \right\rangle$$

While this is a formally exact way to find the solution to any time dependent system and a useful way to visualize the relationship between DFT and many macroscopic systems, it has the same problems that early DFT methods had in that it does not represent the orbital structure of molecular systems. Instead, many applications of TDDFT, to include this proposed research, build off of the Kohn-Sham ground state theory of DFT by considering the first order response of the ground state density in a time dependent electric field.

2.7.1 TD Density Functional Response Theory. A time dependent Kohn-Sham scheme can be constructed from the principle of least action. Given a time dependant Hamiltonian, the action is:

$$A = \int \left\langle \Psi(t) | i\frac{\partial}{\partial t} - \hat{H} - v(r,t) | \Psi(t) \right\rangle dt = A[\rho] + const.$$

It is known from elementary quantum mechanics that minimizing the action leads to the time dependent Schrodinger equation, but we are interested in finding the analog in terms of the Kohn-Sham wavefunction. In theory, the expected value of the Hamiltonian is no different than the energy given by the Kohn-Sham scheme. Furthermore, the expected value of the time derivative operator simply becomes half the time derivative of the density, which is precisely what the time derivative operating on the Kohn Sham orbitals produces. Thus the wavefunction and Hamiltonian inside the action integral can be replaced entirely by their counterparts in the Kohn Sham scheme. The time dependent Kohn-Sham equations quickly follow.

$$\left[-\frac{1}{2}\nabla^2 + v_{eff}(r,t) \right] \psi_i = i\frac{\partial}{\partial t}\psi_i$$

$$v_{eff}(r,t) = v(r,t) + \int \frac{\rho(r,t)}{r - r'} dr' + v_{xc}(r,t)$$

The time dependent exchange correlation potential is handled by assuming the exchange correlation contribution to the energy changes slowly with time. If the action due to exchange correlation, A_{xc} is Taylor expanded with respect to time and only the first term is kept, the result is that the exchange correlation potential at a given time is approximated by the exchange correlation of the density at that time. This is known as the the adiabatic approximation.

$$v_{xc}(r,t) = \frac{\delta A_{xc}}{\delta \rho(r,t)} \cong \frac{\delta E_{xc}}{\delta \rho_t(r)} = v_{xc}[\rho_t](r)$$

Once the adiabatic approximation is made, it is possible to derive the first order response, $\delta\rho$, of the Kohn-Sham wavefunction to a perturbing potential, $w(\omega)$, with frequency ω. We first assume a form for the response in the basis of the Kohn-Sham orbitals, δP_{ij}:

$$\delta\rho(r,\omega) = \sum_{i,j} \psi_i \delta P_{ij}(w) \psi_j$$

Solving for the response of a multi-body system, we then have:

$$\delta P_{ij} = \frac{f_j - f_i}{\omega - (\varepsilon_i - \varepsilon_j)} \left[w_{ij}(\omega) + \sum_{kl} K_{ij,kl} \delta P_{kl}(\omega) \right]$$

The matrix K is known as the coupling matrix because it couples the shift in charge density with the resulting change in potential. This term in the response equation is known as v^{SCF}.

$$\delta v_{ij}^{SCF}(\omega) = \sum_{kl} K_{ij,kl} P_{kl}$$

The elements of the matrix K require the evaluation of four center integrals for potential and exchange correlation potential, because the potential felt by electrons in orbitals i and j will change if the electrons in orbitals k and l have moved:

$$K_{ij,kl} = \frac{\partial v_{ij}^{SCF}}{\partial P_{kl}} = \int\int \psi_i \psi_j \frac{1}{r_{12}} \psi_k \psi_l + \int\int \psi_i \psi_j \frac{\partial^2 E_{xc}[\rho]}{\partial \rho_\alpha \partial \rho_\beta} \psi_k \psi_l$$

Because this coupling matrix multiplies the response matrix as part of the solution to the response matrix, the response matrix requires a self consistent calculation. Once a solution has converged, this calculation yields the dynamic polarizabilities of the system. The implementation of this process involves casting the process above into an eigenvalue problem.

$$\Omega\vec{F}_I = \omega^2\vec{F}_I$$

The matrix is then block diagonalized to give the number of eigenvalues for Ω that a user requests. These eigenvalues correspond to the excitation frequencies and the eigenvectors F_I can can be related to the oscillator strengths f_I.

$$f_I = \frac{2}{3}(E_I - E_0)\left(|\langle\Psi_0|\,\hat{x}\,|\Psi_I\rangle|^2 + |\langle\Psi_0|\,\hat{y}\,|\Psi_I\rangle|^2 + |\langle\Psi_0|\,\hat{z}\,|\Psi_I\rangle|^2\right)$$

As mentioned, TDDFT has performed extraordinarily well with respect to other methods for determining excited states, especially when the computational cost of the method is considered.

2.8 Experiments and Other Calculations

In this section I will summarize the experiments from which excited state data was extracted and used to compare with my calculations. I also present a breif review of other calculations that have been performed that have been useful for comparisons.

2.8.1 Photoelectron Spectroscopy. Anion photoelectron spectroscopy has become one of the most powerful tools for confirming the accuracy of quantum mechanics calculations. It gives a great deal of information about the electronic structure and vibrational states of the neutral and anionic species, and it allows the species of interest to be isolated. The experiment by Dr. Lineberger et. al. uses a photoelectron spectrometer, whose setup is shown in 6. The details of its operation

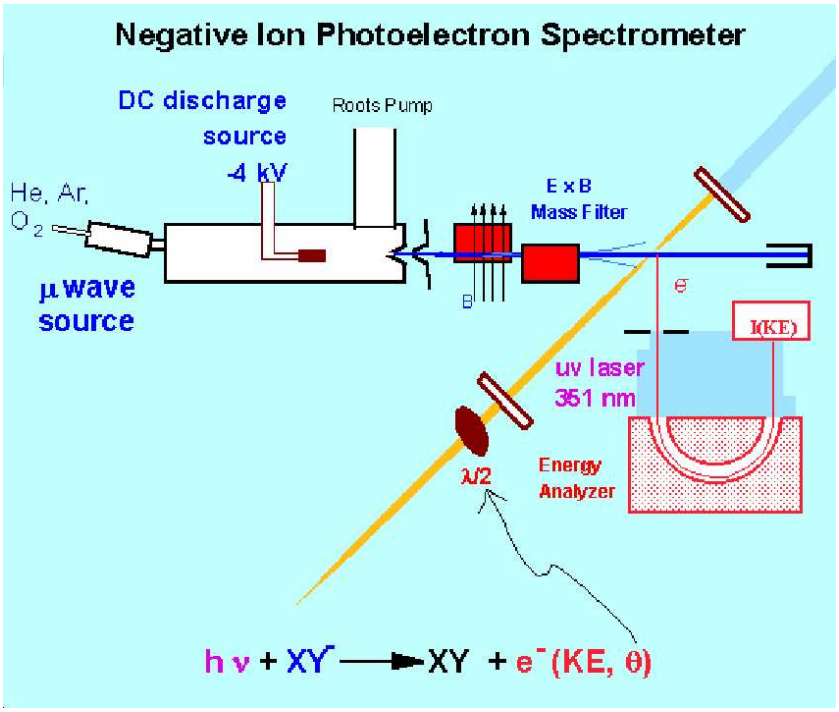

Figure 6 The experimental setup of a photoelectron spectrometer

are only summarized here because further detail has been published elsewhere.[24] A cold cathode discharge is used to form Si_mC_n anions when Ar^+ ions are accelerated towards a SiC rod. The anions are accelerated towards a mass spectrometer and then the desired species are selected using a Wien filter. The beam of anions is made to intersect a 364 nm laser, which photodetaches the extra electron on the anions. This leaves a neutral species and a free electron. The kinetic energy of the photodetached electrons are then measured and recorded in a spectrum. The spectrum of electron kinetic energy is related to the binding energy felt by each electron by conservation of energy:

$$E_{photon} - E_{electron} = E_{binding} + E_{electronic} + E_{vibrational} + E_{rotational}$$

This means that the relative energy of the resulting state of the neutral molecule can be calculated from the location of the electron peaks recorded in the spectrum, but more information can be obtained as well. The geometry of the anion is slightly different from the ground state geometry of the neutral molecule. When the laser detaches the extra electron in the anion, the electrons quickly readjust before the nuclei can move at all, and the nuclei suddenly feel the potential energy surface of the neutral state. Thus we have the wave function of a harmonic oscillator displaced slightly from the center of the potential well, which is a mixture of the ground state and the vibrationally excited states. The greater the displacement from the ground state, the higher the probability of being in a higher vibrationally excited state. Thus, the intensity of each peak gives information about the geometries of the anion and neutral state, and the location of each peak give information about the vibrational frequencies.

Of particular interest and illustrative value is the spectrum of Si_2C_4, shown in Figure 7. Neutral Si_2C_4 is a ground state triplet molecule. The large peak A is from electrons ejected with the vertical detachment energy, the energy difference between the anion and neutral molecule at the anion geometry. The hundreds of anions that made up this peak left the electron with all of the binding energy, and the molecule had no energy left over for a higher electronic state or vibrational state. Peaks C, E, G, and H have all been identified as transitions to vibrational modes of the ground state triplet. These identifications are confirmed by the results of a Franck-Condon simulation that can be seen in the dashed lines underneath the solid line spectrum. This type of simulation takes the calculated vibrational modes and geometries and finds the overlap integrals between the initial (in this case the anion) and final (in this case the possible electronic and vibrational states of the neutral) states. The overlap integrals are usually proportional to the heights of each peak, and since the simulation fails to perfectly match the spectrum it likely means that the calculated geometries are slightly off. However, the simulation does demonstrate that the peaks

C, E, G, and H can all be explained by transitions to vibrational mode.That leaves peaks B and D. From low level Hartree-Fock calculations it is known that two singlet states lie close in energy to the triplet state, and it logically makes sense that peaks B and D correspond to those singlet states. Beyond that however, it is difficult to know which singlet state is really the lower in energy. Excited state theories like TDDFT have the potential to tell the difference.

Similarly, the first unidentified peak in the SiC_3 anion spectrum, peak I in Figure 9, likely corresponds to an excited state in the neutral atom. The smaller peaks, J, K, and L are indicative of vibrational modes for the excited state of peak I, showing similar low frequency vibrations to the main peak A and its corresponding vibrations B-F. Peak AA likely corresponds to transitions involving the nonlinear isomers of SiC_3.

In another work[20], the spectrum for Si_2C_3 was analyzed. However, it was suggested that the unidentified peak H in the spectrum corresponds to transitions involving a nonlinear isomer and not an excited electronic state. TDDFT has the potential to strengthen this assignment by showing that no excited states align with this energy.

A summary of the unidentified photoelectron spectroscopy peaks and the corresponding energy differences from the ground state anion to neutral are listed in Table 2.

2.8.2 Other Forms of Spectroscopy. The fundamental physics of other forms of spectroscopy relevant to this research are not all that different from the essentials of photoelectron spectroscopy. The biggest difference is that instead of measuring the kinetic energy of an electron as in photoelectron spectroscopy, most of these experiments measure the absorption or emission photons.

High resolution Fourier transform emission spectroscopy was used quite a bit in the study of SiC. P.F. Bernath et. al used it to detect the first known transition of

Table 2 Binding Energies of Unidentified Peaks and the Difference From the Main Peak.[20, 17]

	Binding Energies (eV)				
Molecule	Ground	Unidentified Peaks		Differences (eV)	
C_3Si	2.827	3.101	2.629	0.274	-0.198
C_4Si_2	2.543	2.652	2.738	0.109	0.195
Si_2C_3	1.766	2.245	2.297	0.479	0.531

SiC, the $d^1\Sigma^+$-$b^1\Pi$ band. [8] Their technique involves heating a SiC cathode to cause the molecule to emit photons, which they then detected using a Fourier transform spectrometer. Similar experiments were used to detect the $A^3\Sigma^-$-$X^3\Pi$ band. [10] The method does allow rotational transitions to be measured, giving the geometries of each state involved in the transition as well.

Laser Induced Fluorescence (LIF) spectroscopy involves electronically exciting the molecules with a tunable laser, and this was the method used to detect the $C^3\Pi^-$-$X^3\Pi$ band of SiC.[11] Once excited, the molecules emit photons as they return to the ground electronic state, and additional hot bands reveal more information about the rotational and vibrational states of the molecule.

Grutter et. al.[29] used a slightly different technique that was not named. They trapped SiC anions in a Neon matrix by cooling the mixture to 5K. Then they slowly neutralized the anions with a mercury lamp over the course of the two

hours in which they grew the Neon matrix. During this time the absorption spectra were measured of the SiC anion and neutral species. This technique was effective in detecting vibrational bands of four states of neutral SiC and three states of its anion. However, unlike the other methods, the Neon matrix left virtually no rotational freedom, and they inferred no geometric data.

Resonant Two Photon Ionization (R2PI) was the technique that Michalpoulos [43] et. al. used to prove that SiC_2 was a triangular molecule. They used a Nd-YAG laser to electronically excite the molecules, then further excited them with a 1570 $\mathring{A}$ excimer laser. Because the technique gives a very high resolution, they were able to measure the rotational peaks around the 0-0 band. From that information they were able to calculate the geometry of the molecule.

Low energy cathodoluminescences spectroscopy is the final spectroscopic method that gave data about electronic state transitions in SiC, but it is unique from the other methods I mentioned in that it does not treat clusters in the gas phases. Instead, electrons are accelerated towards a clean SiC surface through potentials from .5 to 2 kV. Lower energy electrons do not penetrate as deep into the SiC crystal, which means they will deposit their energy on the surface, and this will cause transitions related to the electronic states of different surface structures. Young, Jones, and Brillson [64] successfully demonstrated the presence of such transitions in the neighborhood of 1 to 2 eV. There is a possibility that some of these surface structures may correspond to the ground state geometries generated by researchers here at AFIT.

2.8.3 Previous Calculations. In addition to experimental data, there have been some useful calculations that should be mentioned. There is of course the AFIT produced Si_mC_n map from which I have all of the B3LYP/aug-cc-pVDZ geometric data needed to start calculations of the excited states. This level of theory has proven its success with the ground states of chains as long as SiC_9 [19], and has appeared

in many other calculations of other chains.[27] There are other density functional calculations available in the literature [33], as well as MP2 and HF calculations [46], but these use smaller basis sets and/or less successful exchange correlation functionals. There are also MP2 and HF calculations Furthermore, they do not mention excited states. Therefore, I will not refer to this work.

For the simplest molecule, SiC, a variety of MCSCF calculations are available for the neutral and anionic species, including some excited states. The earliest of this work was completed in the 1980's. [52, 3, 38] Most recently, Z.-L. Cai and J.P. Francois calculated the $X^2\Sigma^+$, $A^2\Pi$, and $B^2\Sigma^+$ states of the anion using a variety of methods, particularly coupled cluster and multireference configuration interaction techniques. [12] Such calculations have been in good agreement with experimental values for SiC. Therefore, I will cite the experimental results instead of the theoretical results when assessing the accuracy of my answers for this molecule.

Another paper on the electronic states of Si_2C was written in 1996 by A. Splielfiedel et. al.[61] They used coupled cluster and configuratio interaction methods to calculate slices of the potential energy surfaces for multiple singlet and triplet states, along with vertical excitation energies at various geometries. However, they did not give equilibrium geometries for the excited states or vibrational frequencies, so I cannot make a one to one comparison with my calculations and their work.

Finally, for SiC_3 and Si_2C_2, a very useful paper by Rintelman and Gordon [53] uses second order multiconfigurational quasi-degenerate perturbation theory (MC-QDPT) to calculate the relative energies of the lowest singlet and triplet states. They also use other ab-initio methods to calculate the geometries and vibrational frequencies for the isomers of these two clusters that I consider. This is the last theoretical paper I have seen with information about excited states of these clusters. Therefore, most calculations beyond the states mentioned in these papers will be the first of their kind.

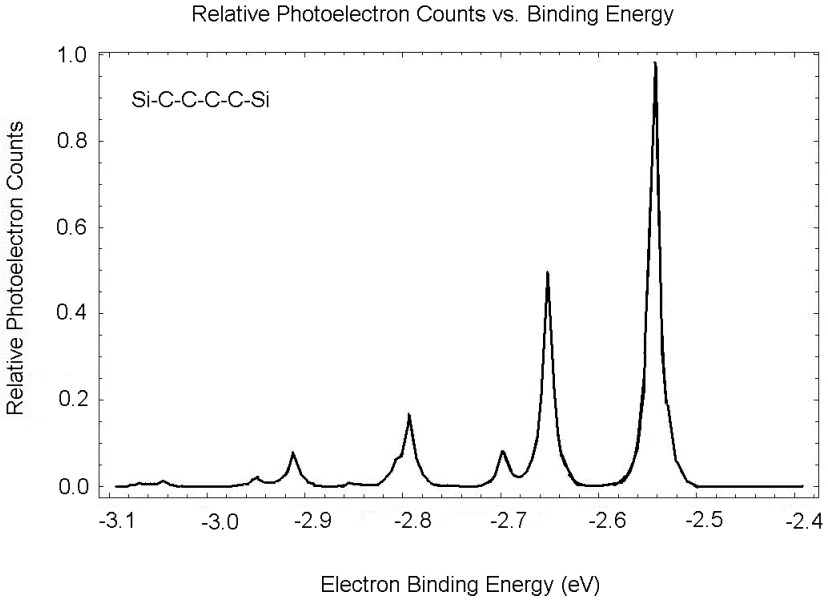

a)

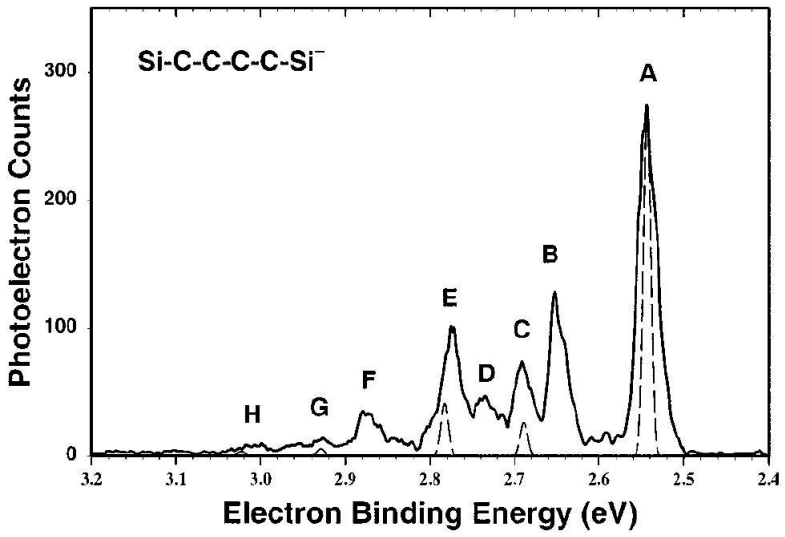

b)

Figure 7 Photoelectron spectroscopy of the Si_2C_4 anion.
Simulated (a) and actual (b) photoelectron spectrum of Si_2C_4 anion. The simulation was created in Mathematica using B3LYP-aug-cc-pVDZ values of geometry and vibration frequencies, and the experimental values for the locations of peaks A and B. The simulation demonstrates that peak D is not a vibrational state of the linear isomer.

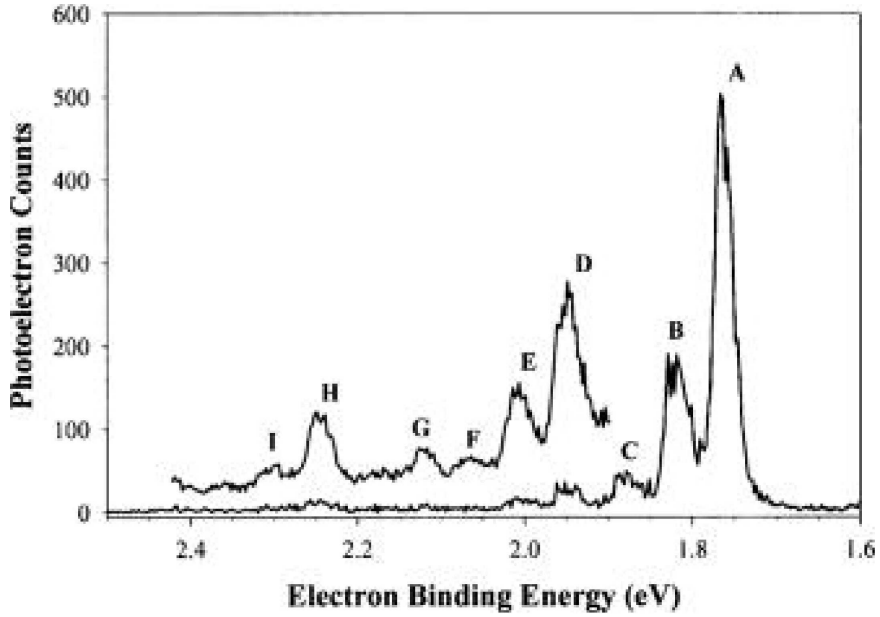

Figure 8 Photoelectron Spectroscopy of the Si_2C_3 anion.[20]
Actual photoelectron spectrum of Si_2C_3 showing the unidentified peak H.

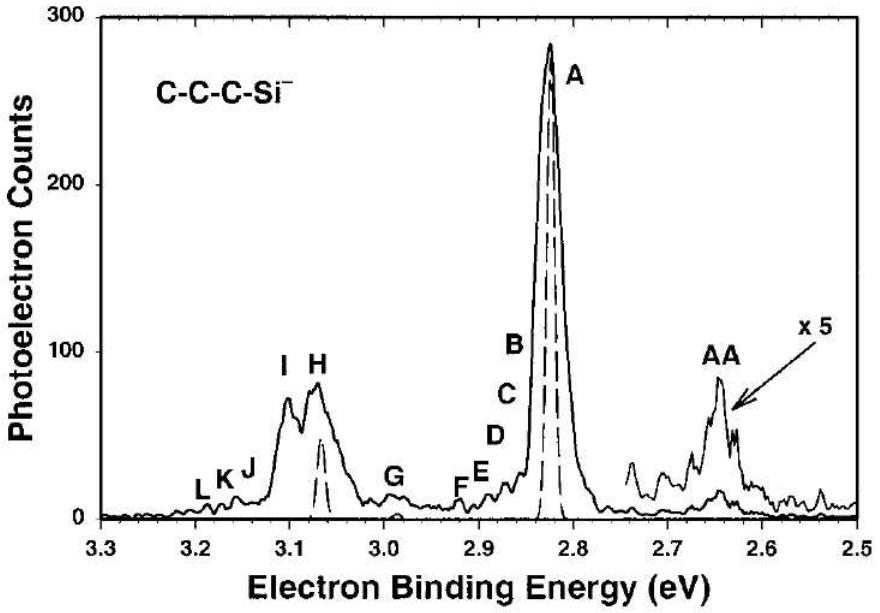

Figure 9 Photoelectron Spectroscopy of the SiC_3 anion.
Actual photoelectron spectrum of SiC_3 showing that peak I is from a transition to an excited state.

3. Methodology

3.1 Chapter Overview

The purpose of this chapter is to present the method I used in this research. My first goal was to get as many calculations done and processed as I could for the purposes of spectroscopic and astronomical detection of these clusters. When this was accomplished, I worked on consolidating the data into formats which could be used as efficient tools for the analysis of the excited states. Thus, I will first go into some of the technical issues of the various quantum chemistry packages I used, and then on to some of the tools I used or wrote to complete these tasks.

3.1.1 Gaussian Input. Although I used NWChem and Turbomole for some calculations, the bulk of this work was completed using the Gaussian 03 [26] computational chemistry package at the ASC MSRC[1] supercomputing center. I will walk through some of the basics of using Gaussian 03 with the example shown in Figure 10. The Gaussian website, www.gaussian.com, can be consulted for information on other types of calculations as well.

This particular input file is meant to optimize and calculate the vibrational frequencies of an excited state of what is believed [56] to be the ground state isomer of SiC_3. Line 1 of this file requests 3 processors using the "Linda" parallelization environment. Line 2 specifies the checkpoint file where results of the calculation will be stored in binary. Line 3 is the route section, and it contains the computational method Gaussian will use. I am requesting a geometry optimization (opt) with the B3LYP/aug-cc-pVTZ level of theory, using TDDFT (td). The TDDFT root to optimize will be the fourth of seven singlet roots requested. The blank fourth line terminates the route section. Line 5 is the job title, and this section is also terminated by a blank line. Line 7 gives the charge and multiplicity of the molecule. Lines 8 through 15 specify the geometry using a symbolic z-matrix, where the first

```
%nprocl= 3
%chk=ns4tzr13r1.chk
#p  b3lyp td=(singlets  nstates=7 root=4 fc) /aug-cc-pvtz opt

TDDFT Optimization

0 1
Si  0     0.0     0.0     zSi
C   0     0.0     yC     0.0
C   0     0.0    -yC     0.0
C   0     0.0     0.0     zC
Variables:
zSi  1.69218
zC  -1.22678
yC   0.734263

--Link1--
%Chk=ns4tzr13r1.chk
#p  b3lyp td=(singlets nstates=7 root=4 fc)
aug-cc-pvtz Geom=Check Guess=Read Freq

TDDFT Vibrations Job

0 1
```

Figure 10 Example of Gaussian Input For Rhomboidal SiC_3

```
 SCF Done:  E(RB+HF-LYP) =  -403.517381532     A.U. after   16 cycles
             Convg  =    0.7810D-09             -V/T =  2.0033
             S**2   =   0.0000
 KE= 4.021730551536D+02 PE=-1.155710805153D+03 EE= 2.488651749742D+02
```

Figure 11 Gaussian SCF Iteration Output

```
 Excited State   3:   Singlet-B2     1.0714 eV 1157.22 nm  f=0.0009
      16 -> 19         0.63818
 This state for optimization and/or second-order correction.
 Total Energy, E(RPA) =  -403.476172188
```

Figure 12 Gaussian TDDFT Output

```
                         ----------------------------
                         !   Optimized Parameters   !
                         ! (Angstroms and Degrees)  !
----------------------                              ----------------------
!      Name          Value   Derivative information (Atomic Units)     !
---------------------------------------------------------------------------
!       zSi         1.5919   -DE/DX =   -0.0002                         !
!       zC         -1.1834   -DE/DX =   -0.0002                         !
!       yC          0.8828   -DE/DX =    0.0                           !
---------------------------------------------------------------------------
```

Figure 13 Gaussian Optimized Geometry Output

integer zero after each atomic symbol tells Gaussian to use cartesian coordinates instead of traditional z-matrix coordinates. Line 17 starts another job, and much is the same except that a hessian is being calculated with the "Freq" keyword to obtain vibrational frequencies. The "Geom=Check" and "Guess=Read" keywords tell Gaussian to get the geometry and the initial guess of the wavefunction from the checkpoint file.

3.1.2 Select Low Lying Isomers for Analysis. Thanks to previous work, [31, 21] the ground state geometries of each of the molecules are known at the B3LYP/aug-cc-pVDZ level of theory using the quantum chemistry programs GAMESS and Gaussian 98. However, certain isomers are close enough in energy to the ground state that they may also appear in nature. As a result, I have included them in my analysis as well since their excited states may also be of interest. All of the isomers I chose to analyze are referenced in the results chapter.

3.1.3 Optimize and Calculate Hessians with DFT. For useful comparisons with the excited states, I performed geometry optimizations and Hessians of the ground states with DFT at the B3LYP/aug-cc-pVDZ and B3LYP/aug-cc-pVTZ levels of theory. This was simplified in many cases by the previous work of Ms. Henry, Lt. Roberts, and Dr. Duan, and the availability of some experimental ge-

ometries in other published literature. However, this step was necessary because of integration grid differences between the various quantum chemistry packages.

3.1.4 TDDFT Optimizations and Hessians. Once I had completed the ground state geometries in Gaussian 03, I ran excited state optimizations using the ground state geometry as the starting point. I generally selected the first four TDDFT roots to optimize, while requesting at least two more roots to ensure the important ones were not skipped by the numerical algorithm. Because of time constraints, not every optimization was fully converged by the end of this research. However, if the optimization did converge I also attempted to calculate Hessians.

3.1.5 Gaussian Output. Once the calculations were completed, the information had to be extracted from the output files. The output file from an Gaussian run is very long. It lists all the calculated information about the molecule in question in the order it was calculated. But it also includes basis functions, SCF convergence information, memory statistics, geometrical steps and a host of other bits and pieces of information that have no spectroscopic signifigance whatsoever. However, there are some key parts of the output that are very important that can be seen in the figures in this chapter. For example, the frequency output gives the vibrational frequency, normal modes, and reduced masses, all of which are needed to do a Franck-Condon simulation. The end of an SCF iteration gives the total DFT or HF energy of the molecule. All of this data may be important to someone in spectroscopy.

3.1.6 Unix Scripting. To complete the process outlined above for as many isomers as I did in the relatively short amount of time available, I had to write many scripts in Unix. I needed a way to submit and resubmit optimization jobs automatically, and I also needed to process the data and condense it into a form that was useful for spectroscopy. To aid in these processes, I learned the powerful

```
                      1                      2                      3
                     B1                     B2                     A1
Frequencies --    258.3403               527.9079               554.7329
Red. masses --     12.6197                13.0347                14.2658
Frc consts  --      0.4962                 2.1403                 2.5865
IR Inten    --      0.0000                 0.0000                 0.0000
Atom AN      X      Y      Z        X      Y      Z        X      Y      Z
  1  14     0.20   0.00   0.00     0.00   0.25   0.00     0.00   0.00   0.38
  2   6    -0.54   0.00   0.00     0.00  -0.55   0.20     0.00  -0.52  -0.19
  3   6    -0.54   0.00   0.00     0.00  -0.55  -0.20     0.00   0.52  -0.19
  4   6     0.62   0.00   0.00     0.00   0.50   0.00     0.00   0.00  -0.49
                      4                      5                      6
                     A1                     A1                     B2
Frequencies --    884.1597              1061.9425              2382.0084
Red. masses --     14.1344                12.1397                12.3085
Frc consts  --      6.5101                 8.0661                41.1472
IR Inten    --      0.0000                 0.0000                 0.0000
Atom AN      X      Y      Z        X      Y      Z        X      Y      Z
  1  14     0.00   0.00   0.37     0.00   0.00   0.09     0.00   0.14   0.00
  2   6     0.00   0.56  -0.27     0.00  -0.09  -0.47     0.00   0.08   0.61
  3   6     0.00  -0.56  -0.27     0.00   0.09  -0.47     0.00   0.08  -0.61
  4   6     0.00   0.00  -0.32     0.00   0.00   0.73     0.00  -0.47   0.00
```

Figure 14 Gaussian Frequency Output

text processing language known as "awk," and used it to write scripts that could read all of my output files for the important information. That information was put into tables or used to write new Gaussian input files to resubmit a geometry optimization where it left off. I highly recommend this language to anyone working in any kind of Unix environment, because it let me replace hours of repeating the same editing keystrokes literally hundreds of times over with calls of a handful of a few shell scripts. It took some extra time to make those scripts work, but the scripts allowed me to resubmit jobs to the MSRC more rapidly and get a higher priority in the work queue than if I had to restart each job manually. This was the only reason I was able to get as many excited state optimizations completed as I did. Figure 15 shows the type of useful information that was extracted using a script in awk.

3.1.7 Mathematica Analyses. For some of the molecules, I also calculated the Franck-Condon factors using a routine I wrote in Mathematica following an algorithm laid out by Dr. Peter Chen[14]. The differences between the anion and neutral state geometries are expressed as a linear combination of the normal mode vectors of the neutral state, and the coefficients of that linear combination are known as the Franck–Condon factors. When the Franck-Condon factors have been calculated, everything needed to perform a spectroscopy simulation is available.

3.1.8 Molden Visualization. When calculations were completed, I needed to view the orbitals to gain an understanding of what was happening electronically in the states of each molecule. This was completed by using the Molden application. [57] This can be downloaded free of charge at:
http://www.cmbi.kun.nl/ schaft/molden/molden.html

Figure 15 Example Of Script Output for C $^1A_2$ SiC_3

```
 Basis: Aug-CC-pVDZ S**2:
 Molecule: C3Si
 Charge: 0 Multiplicity: 1
 Route: #p b3lyp td=(singlets nstates=6 root=3 fc) /aug-cc-pvdz opt
   #p b3lyp td=(singlets nstates=6 root=3 fc) /aug-cc-pvdz
   Geom=Check Guess=Read Freq
 Energy(Hartree): -403.525164940 ZPE corrected: -403.461618
 Root Followed: 3
 Excitation[Bounds]: 1.1284 [-0.4802, 3.3406 ] eV
 Term Symbol: Singlet -A2
 Oscillator Strength: 0.0011, between -0.0000 and 0.0011
 Transition Moments: X: 0.0000 Y: 0.0000 Z: 0.0000
 Orbitals Involved:
  16 -> 17 = 0.81879
 Spatial Extent: 235.2910 [ 232.8642 , 239.5384 ]
 Spin Density:
 Dipole Moments: X: 0.0000 Y: 0.0000 Z: 4.1767 Tot: 4.1767
 Highest Memory Req': 326.3 Geometry Iterations: 15
 Start and End Times: 16:32:06 - 22:25:54
 Processor Hours Used: 17.69 Hours
 Valence Orbitals:
  Occupied 13   A:(B1) -0.39169   B:(B1) -0.39169
  Occupied 14   A:(A1) -0.34055   B:(A1) -0.34055
  Occupied 15   A:(A1) -0.30963   B:(A1) -0.30963
  Occupied 16   A:(A1) -0.24286   B:(A1) -0.24286
  Virtual  1   a:(A2) -0.15139   b:(A2) -0.15139
  Virtual  2   a:(B1) -0.06917   b:(B1) -0.06917
  Virtual  3   a:(B2) -0.05705   b:(B2) -0.05705
 Geometric Parameters (Angstroms or Degrees):
  Conv  1
  R(1,2)    1.8968    R(1,3)    1.8968     R(1,4)    2.5928
  R(2,3)    1.9590    R(2,4)    1.3775     R(3,4)    1.3775
 Frequencies (cm**-1):
  142.5326   636.2960   827.5450  870.1262   1400.6915   2511.4986

---- End of Data ----
```

4. Analysis and Results

In the interest of space and readability, I will not present the numerical results of every calculation in this chapter. The interested reader can consult the appendix if there are spectroscopic quantities or orbital energy diagrams of interest for a particular electronic state. What I present here are the trends in the data that I was able to recognize, and if there are exceptions to those trends make those known to the reader. This section will be broken into my findings for the chains (linear), cyclic (two dimensional, planar), and cage (three dimensional) structures, with subdivisions where useful. At the end of each section I will present my calculations alongside any experimental results. I will refer to the number of silicon atoms with the letter m, and the letter n for the number of carbons. Finally, unless otherwise indicated, all numerical results in this section are from B3LYP/aug-cc-pVDZ calculations or the TDDFT equivalent for excited states.

4.1 Linear molecules

As found in most previous work[21, 31, 33], most clusters with two or less silicon atoms have a stable, silicon-terminated chain structures. Rotational and vibrational spectroscopy has confirmed that B3LYP is effective at describing the ground states of these chains.[19, 21, 17, 20] In these molecules, double bonds link the members of each chain, and as previous work and experiments have shown, even membered chains have triplet ground states and odd membered chains have singlet ground states. As I will discuss, the excited states of these molecules can be best subdivided along these same lines. Because they are all terminated by at least one silicon, when comparing like membered chains I will refer to the carbon terminated chain or the silicon terminated chain to differentiate between the singly and doubly Si terminated chains.

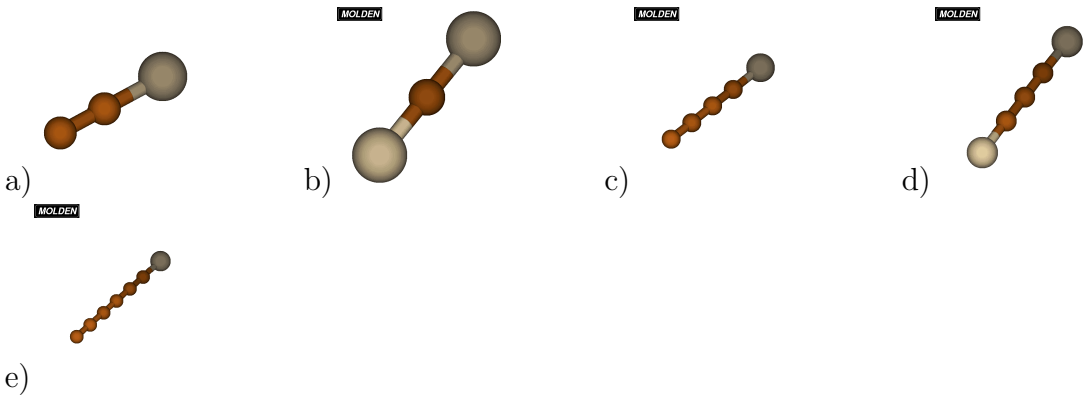

Figure 16 Geometries of Odd Membered Chains
a) Linear SiC_2 b) Si_2C, c) SiC_4, d) Si_2C_3, and e) SiC_6.
Experiments have shown that SiC_2 is not a linear molecule, and neither the B3LYP/aug-cc-pVDZ or the B3LYP/aug-cc-pVTZ levels of theory predict a stable linear geometry. However it is included here because it is informative.

4.1.1 Odd Membered Chains. The orbitals in the linear chains can be understood using simple symmetry arguments. The number of occupied valence σ orbitals in all of the linear chains, even or odd, is always m+n+1, or simply the number of atoms in the chain plus one. If we align a coordinate system so that each atom is on the z-axis, these σ orbitals can all be qualitatively obtained by drawing a series of orbitals, starting with a fully bonding orbital and incrementing the number of nodal xy planes. This procedure hybridizes the valence s and p_z atomic orbitals in each member of the chain, where the lowest orbitals will be of mostly s character and the higher orbitals will be mostly p_z character. The π orbitals have a similar pattern. After counting the total number of electrons and the number of occupied σ orbitals, the number of electron pairs remaining to occupy π orbitals must then be m+n-1. In odd membered chains, this means each molecule will have a closed shell. Similar to the σ orbitals, the lowest pair of π orbitals will have no nodal xy planes, and each successive orbital will have an additional nodal plane. The nodes appear between the atoms where possible, so that no d functions are needed in the atomic

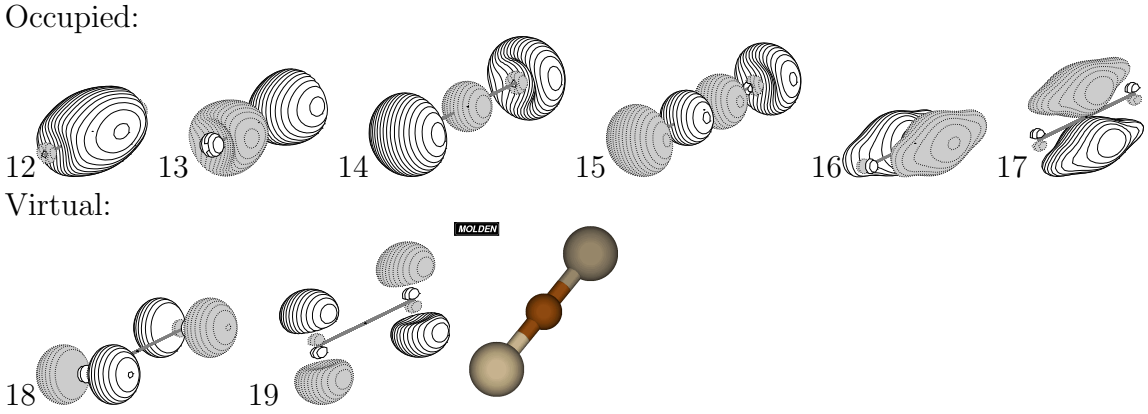

Figure 17 Valence Orbitals for Linear X $^1\Sigma$ Si_2C

Si_2C is the best starting point for grasping the procedure of creating symmetry orbitals in these chains. The creation of σ orbitals by increasing the nodes by one is unambiguously depicted in orbitals 12 through 15. These can be alternatively labeled as the σ_0, σ_1, σ_2, and σ_3 orbitals. The first two steps of the same process with the π orbitals is shown in orbitals 16 through 19, the π_0 and π_1 orbitals of this cluster.

orbitals. All of this can be seen with the simple examples of linear Si_2C and SiC_2 in Figures 18 and 17.

There is a trend in the orbitals with respect to the contribution of silicon and carbon atomic orbitals. The first thing to note is that the prominence of the silicon atomic orbitals in each molecular orbital decreases as orbital energy gets lower. This can be seen just by comparing the orbitals of the two clusters SiC_4 with Si_2C_3, seen in Figures 19 and 20. This becomes important in the excited states, because eventually the terminal silicon atomic orbitals contribute significantly to a virtual orbital. In particular, it is the silicon p_x and p_y atomic orbitals that make the strongest contribution to the first few virtual π orbitals. Because the virtual orbitals have a heavier atomic silicon character than the occupied orbitals, excitations into these orbitals cause the terminal silicon atoms to relax away from the rest of the chain by a few hundredths of an angstrom.

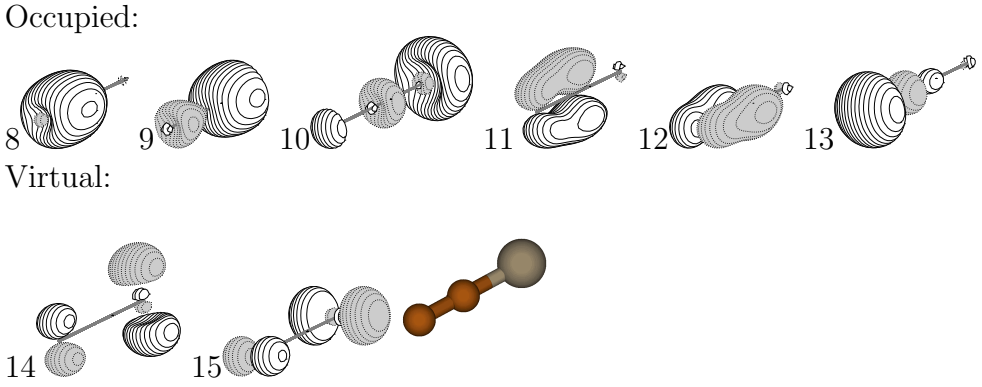

Figure 18 Valence Orbitals for Linear X $^1\Sigma$ SiC_2

SiC_2 differs from Si_2C in that it is no longer symmetric about the center of the chain. As a result, the σ and π orbitals will have larger contributions from the atomic orbitals of the silicon or carbon terminated end. This preference to one side or the other tends to alternate from one symmetry orbital to the next, beginning with a preference for the carbon terminated end.

A trend can also be recognized with the orbital energies of each of these clusters, and examples can be seen in Figures 22 through 24. These diagrams show that the energy gap between the π orbitals decreases if we replace the terminal carbon with a terminal silicon. This is because the overlap integral between the p functions of silicon is much less than that of carbon, so the orbital energy levels do not split as much. This splitting increases as we add more carbon atoms to the chain because the ratio of silicon to carbon p orbitals drops, and the total amount of overlap between the atomic orbitals increases.

And while carbon terminated chains have greater splitting than the silicon terminated chains, the exact opposite trend happens with the two highest occupied σ orbitals in longer chains. The σ orbitals in the SiC_n case are preferentially towards the carbon or silicon terminated end, making them split. However, having both sides equally terminated by a silicon atom makes the situation symmetric, and as the chains get longer these orbitals start to become nearly degenerate. Increasing the length of the chain also has the same effect for the carbon terminated chains,

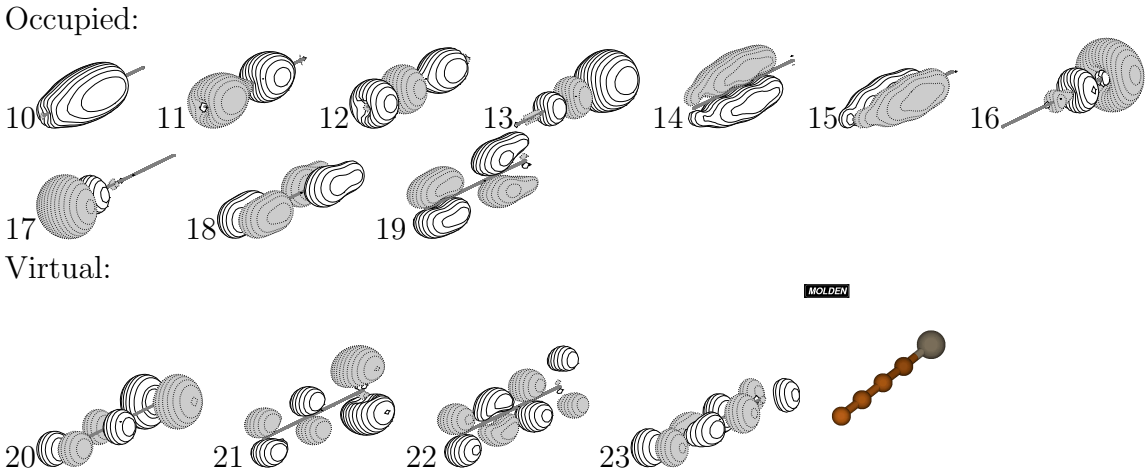

Figure 19 Valence Orbitals for Linear X $^1\Sigma$ SiC_4

The orbitals of SiC_4 can be quickly understood by the same procedure used for SiC_2. However, the preference the σ orbitals have for alternating sides becomes so pronounced that the rest of the nodes are not visible in the plots of orbitals 16 and 17 because the contributions from the unpreferred side are too small.

but this does not happen with shorter chains like SiC_2 because the silicon atom has to be far from the center of the chain for the electrons to treat it like another carbon atom.

Putting these two orbital energy trends together, we can explain why the HOMO orbital of linear SiC_2 and SiC_4 is of σ symmetry, but it is a pair of degenerate π orbitals in Si_2C and Si_2C_3. The improved bonding of the π orbitals and the lack of symmetry in the σ orbitals lets the π orbitals slip beneath the σ orbital. This type of trend is almost counterintuitive, because it suggests that for the low lying excited states of the shorter chains, it may be more useful to group the chains by the terminal atoms instead of by the chain length.

However, an analysis of the HOMO-LUMO gap and first excitation energies in Table 3 takes the side of intuition. The HOMO-LUMO gap decreases by approximately .5 eV when two more carbon atoms are added. This keep the gap in carbon terminate chains .2 eV higher than the equally membered silicon terminated chains.

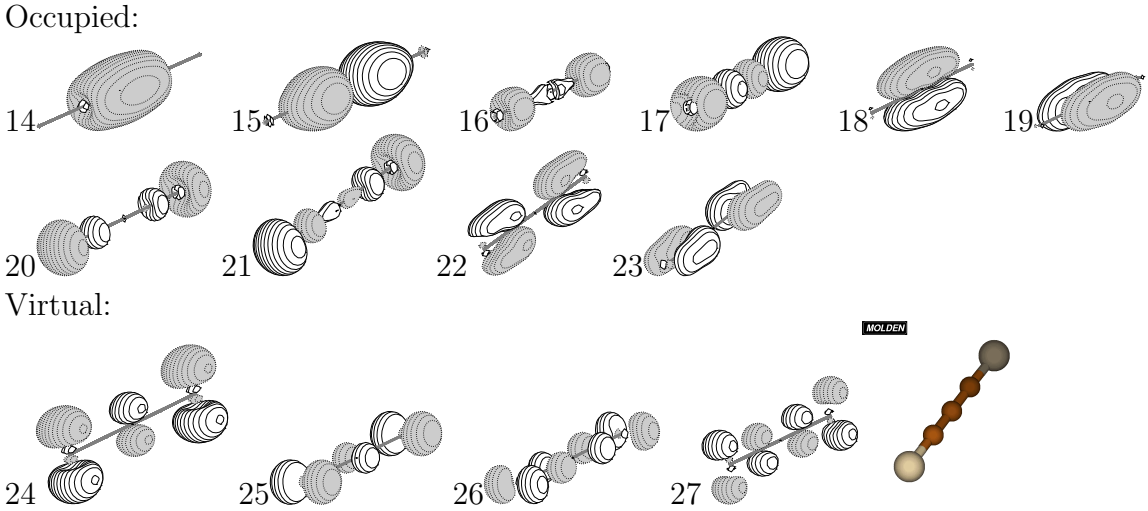

Figure 20 Valence Orbitals for Linear X $^1\Sigma$ Si_2C_3

The orbitals for Si_2C_3 can again be understood by the symmetry orbitals procedures previously mentioned. Furthermore, orbitals 20 and 21 are the first clear examples of σ orbitals becoming nearly degenerate. The orbital plots show that they involve nearly the exact same atomic orbitals, but orbital 21 has an extra node in the center. Linear combinations of these two would give orbitals similar to orbitals 16 and 17 in SiC_4.

Thus, it is in fact more informative to classify these chains by length, recognizing that the terminal atom shifts the relative energies in a predictable manner.

To my knowledge, there have been no detections of the excited states of these particular clusters. Lineberger et. al. detected a non-vibrational peak in the photoelectron spectrum of Si_2C_3, but based on my calculations it was too close energetically to the ground state to be a singlet or triplet excited state of the linear isomer. Thus their tentative conclusion that the peak was from a non-linear isomer is supported.

Thermodynamics can explain why excited states of these clusters are so elusive. First, the excitation energies in the neighborhood of 2 eV are quite high. The excitation energy goes down with increasing cluster size, but so does the chance of creating a longer chain. Second, these linear clusters, while they are stable, are probably not favored by increased entropy, likely losing their linearity upon collisions.

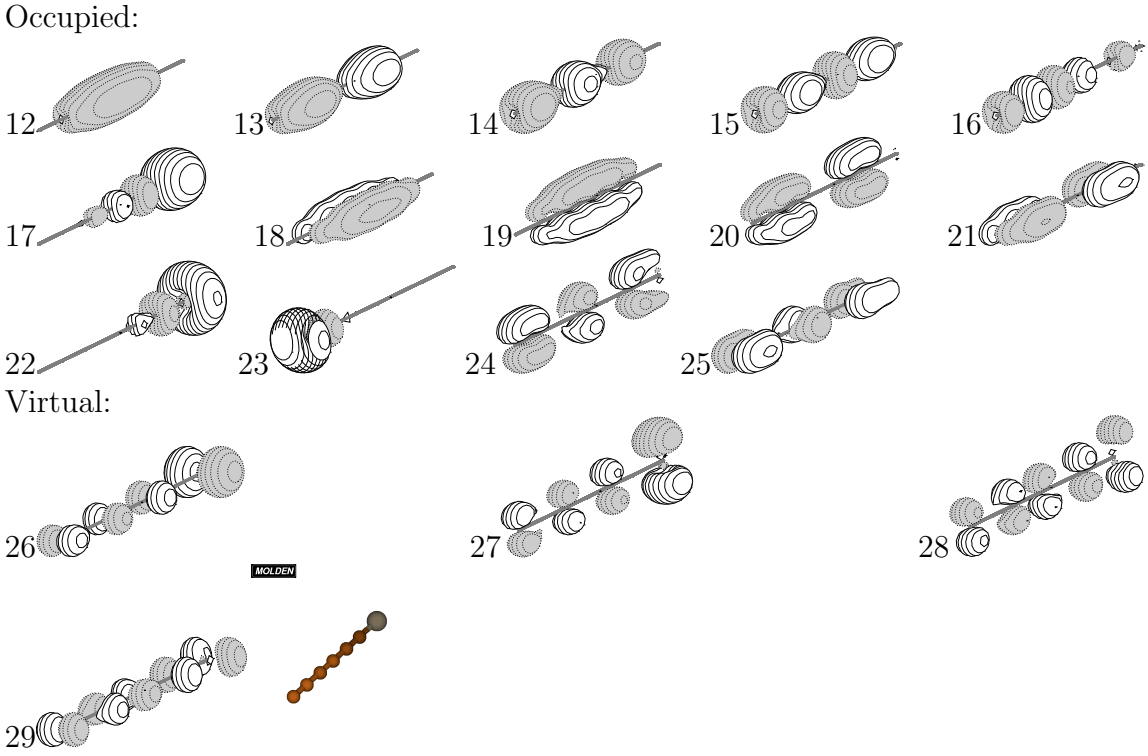

Figure 21 Valence Orbitals for Linear X $^1\Sigma$ SiC_6

Although SiC_6 was not a part of the original SiC map produced at AFIT, I offer it here as useful evidence that the procedures and trends described here likely apply to all Si_mC_n chains.

4.1.2 Even Membered Chains. And while excited states of the odd membered chains have proved elusive, that is not completely the case with the excited states of the even membered chains. The orbitals actually exhibit the same symmetry and energetic trends as the odd membered chains. For example, the orbitals of Si_2C_4, shown in Figure 26, can be understood by the same arguments used for the odd membered chains. The difference in the even membered chains has to do with the orbital occupation patterns, so I will begin there. As mentioned previously, each of these molecules has a triplet ground state, and the reason for this can be seen in terms of the same arguments made in the previous section. As mentioned, there

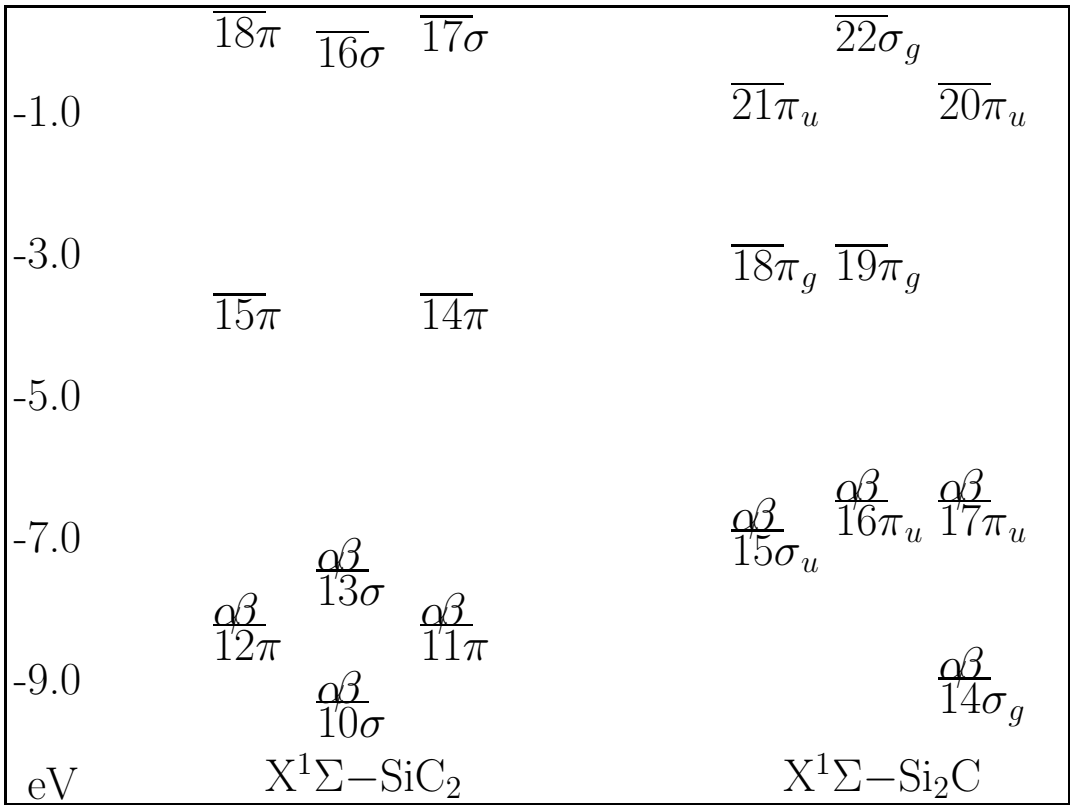

Figure 22 Orbital Energies of Linear Three Membered Chains
This orbital energy diagram shows that the π splitting (difference between orbitals 12 and 15) in the carbon terminated chain SiC_2 is much greater than the like membered chain Si_2C (orbitals 16 and 18). This trend continues for longer chains as well.

are still m+n+1 occupied σ orbitals, and that leaves 2(m+n-1) electrons to fill the π shells, just as in the odd membered chains. This is the source of the difference.

In the change from an odd to an even membered cluster, the number of σ orbitals changes by one, and this leaves four valence electrons with three nearly degenerate orbitals. Even if, as we have seen happen in longer chains, the highest σ orbital drops in energy so that it is no longer nearly degenerate with the partially filled π shell, we are still left with two electrons to fill two π shells. Either way, we are left with open shell systems. Orbital energy diagrams for these open shell systems can be seen in Figures 27 and 28.

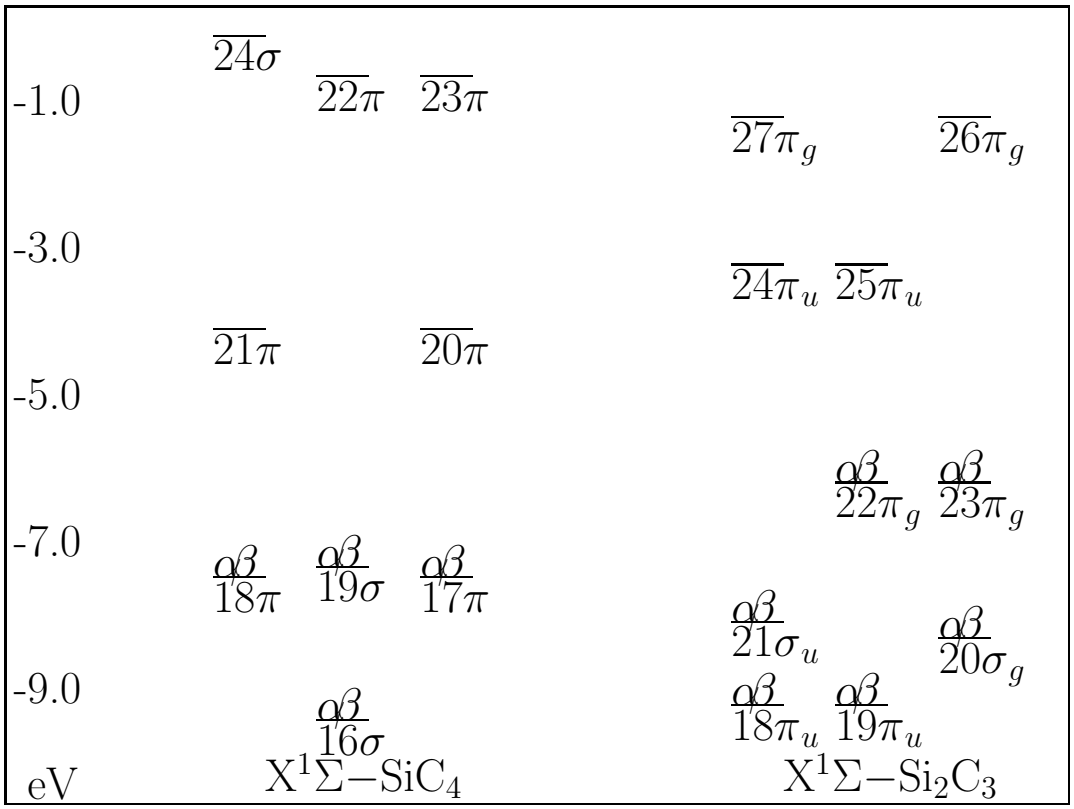

Figure 23 Orbital Energies of Linear Five Membered Chains
As mentioned in the text, it is easy to see that orbitals 20 and 21 of Si_2C_3 become nearly degenerate, an effect that can be justified by comparing these two orbitals. As the chains get longer, the orbitals analogous to these will have less contribution from the central atoms that make these two orbitals different. Thus this energy difference will only get smaller.

These open shells can generate handful of low lying singlet and triplet states simply by populating the space of these three orbitals, leading to the triplet ground state. These low lying excited states that can be produced by various occupations of this partially filled π-σ tier are: $^1\Sigma^+$, $^1\Pi$, $^1\Delta$, $^3\Sigma^-$, $^3\Pi$, and $^3\Delta$.

Because of these open shell configurations, the orbital energy behaviors observed in the odd membered chains become crucially important. Since the larger carbon terminated clusters continue to have a larger π orbital splitting and the longer silicon terminated clusters continue to push the highest σ orbitals together,

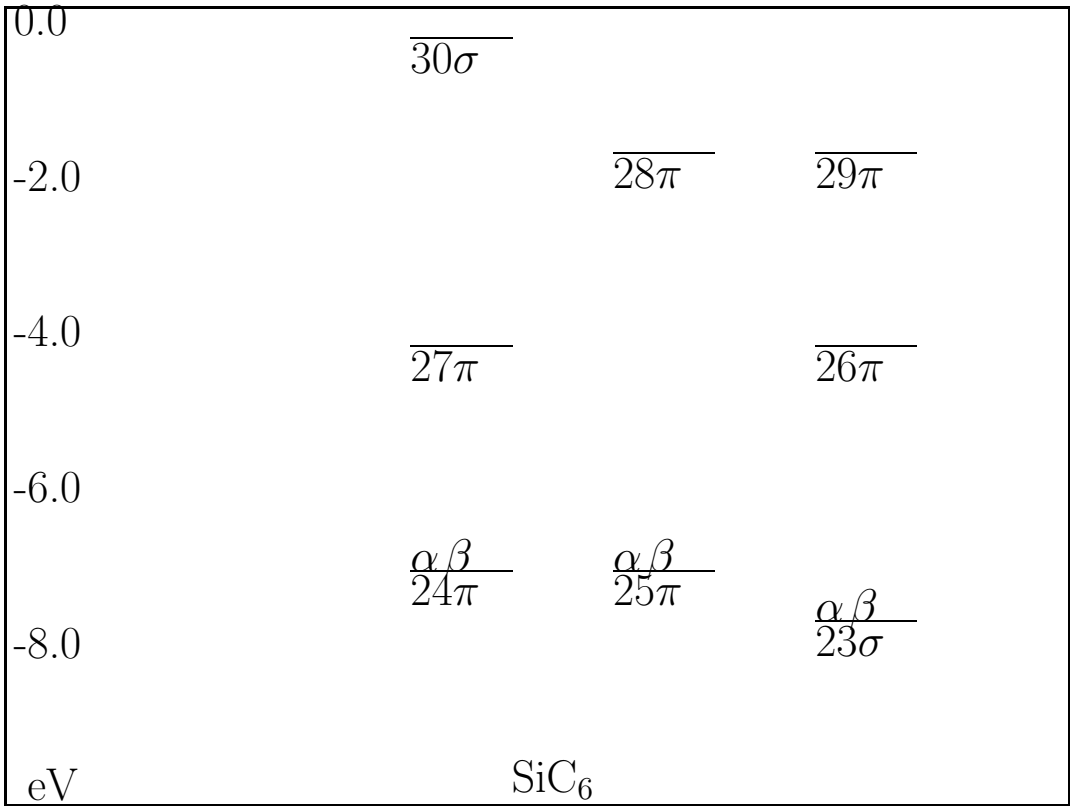

Figure 24 Orbital Energies of Linear Seven Membered Chains
This plot of the orbital energies of SiC_6 shows that, as carbon terminated chains get longer, the highest occupied σ orbital does drop beneath the highest occupied π orbitals.

it will only be in the smaller carbon terminated clusters that the highest occupied σ orbital will play an important role in the low lying states.

This is exemplified of course, by the X-$^3\Pi$ state of SiC, where the highest occupied σ orbital becomes nearly degenerate with the highest occupied π orbitals. In this molecule, the chain is no where near long enough to treat the silicon like another carbon atom, and the splitting between the π orbitals is relatively low. The result is that these top three molecular orbitals are close enough energetically that populating them with electrons can change their relative order. To minimize the

Table 3 Excitations and HOMO-LUMO Gap of Odd Membered Chains

Cluster	H-L Gap	Δ E
SiC_2	3.87	2.573
Si_2C	3.60	2.555
SiC_4	3.24	2.092
Si_2C_3	2.97	1.835
SiC_6	2.88	1.781

This table simply shows the HOMO-LUMO gap in each chain. This gap decreases if the chain is longer or if both ends are terminated by silicon atoms.

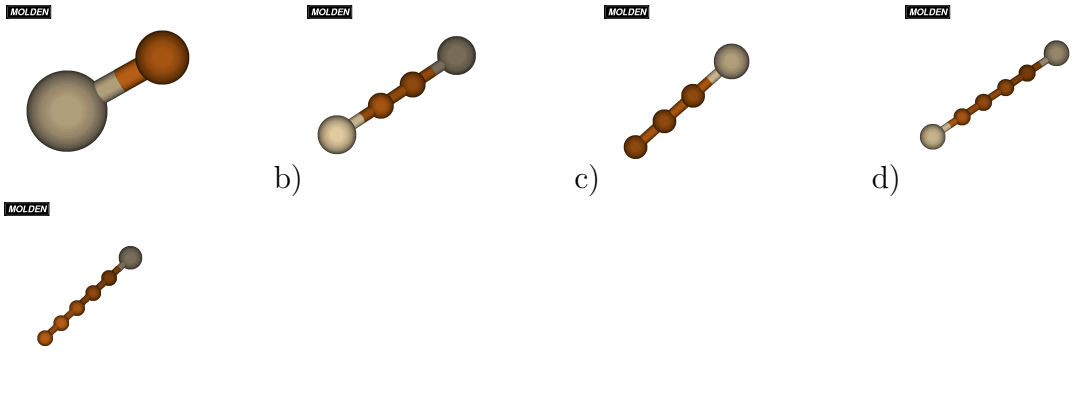

Figure 25 Geometries of Even Membered Chains
a) SiC b) Si_2C_2 c) SiC_3 d) Si_2C_4 e) SiC_5

Occupied:

Partially Occupied:

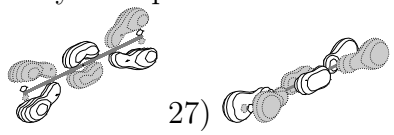

Virtual:

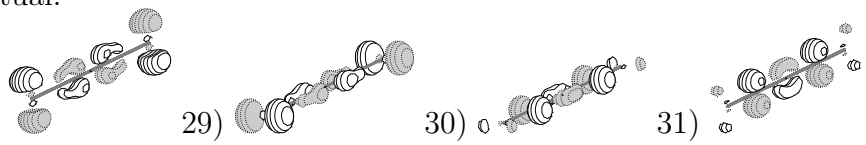

Figure 26 Valence Orbitals for Linear X $^1\Sigma$ Si_2C_4

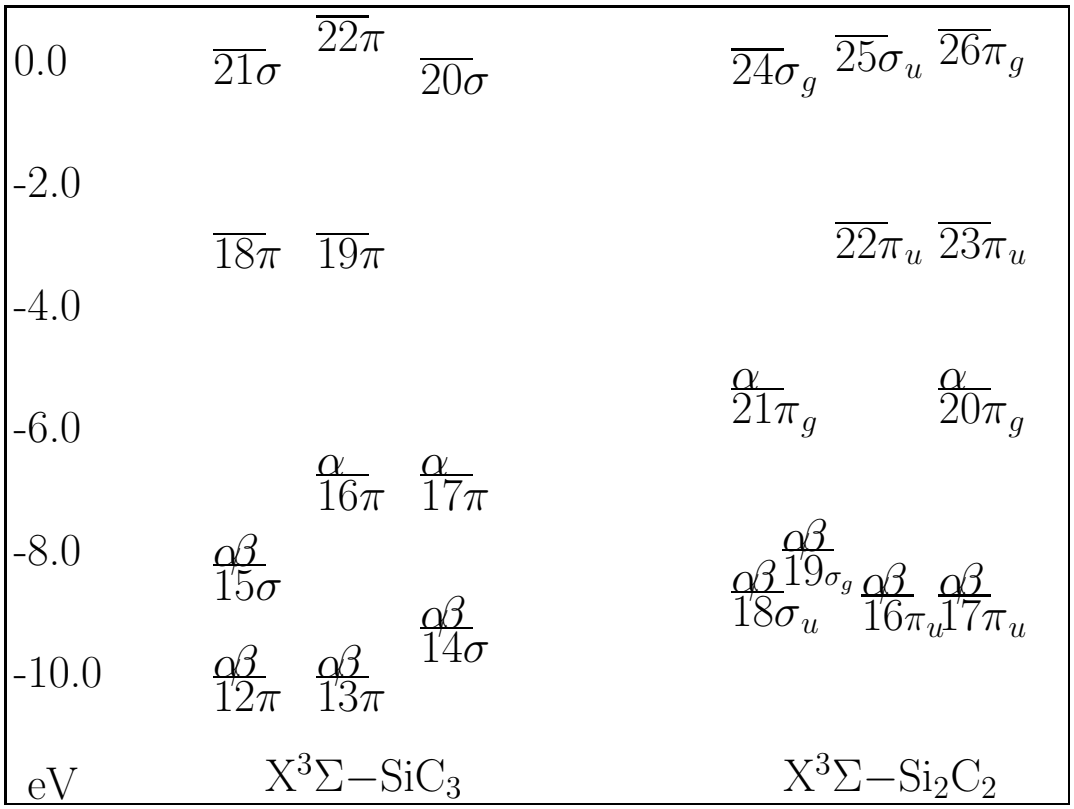

Figure 27 Orbital Energy Comparison of Linear Four Membered Chains
In this diagram and in Figure 28, the same trends of orbital energies as in odd membered chains is observed. Carbon terminated π splitting is greater, as is the difference between the highest occupied σ orbitals. As mentioned in the text, the difference between this and the odd membered chains is the partial occupation of the π orbitals.

repulsion between them, three electrons occupy the π shell and one occupies the σ orbital, leading to the X-$^3\Pi$ ground state.

Beyond the open π shell there are additional π orbitals that behave analogously to the π structures of the odd membered chains. Thus, excitations to these orbitals can be expected to behave similarly to the singlet excited states of the odd membered chains. However, I requested the same number of excited states for all clusters, and this excluded these higher excited states. Furthermore, most of my time with these

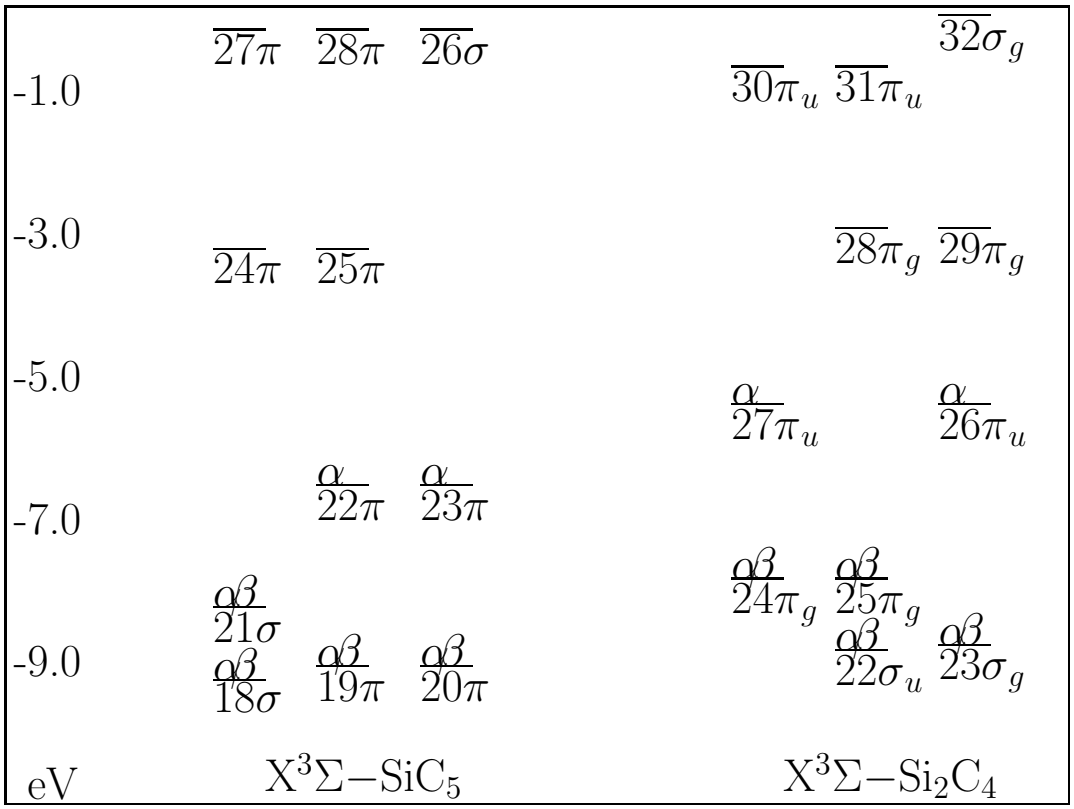

Figure 28 Orbital Energy Comparison of Linear Six Membered Chains
In Si_2C_4, we can see the highest occupied σ orbitals become nearly degenerate, while the highest occupied σ orbitals of SiC_5 also come closer in energy than those of SiC_3. This suggests that as the chains gets longer the carbon-terminated ones may also have the σ degeneracy associated with the silicon-terminated chains.

clusters was spent trying to capture the behavoir of the low lying states because there are some major difficulties involved with using DFT to model open shell systems.

Standard density functional theory implementations do not handle open shell systems very well because certain open shell states cannot be represented as a single Slater determinant.[36] In the case of triplet states, linear combinations of the degenerate triplet states can lead to an accurate single determinant picture, so a single determinant is adequate. The quantum chemistry packages I used were able to take advantage of this approach for the triplet ground states and obtain results

in good agreement with experiment. However, this approach will not work for $^1\Sigma$ states because these are not degenerate states.

The ground singlet states were consistently too high in energy above values from recent experimental work for SiC_3 and Si_2C_4, [17, 20] but even more alarming was the fact that the first singlet TDDFT root would often be another singlet state of lower energy. The energy of that lower state was also too high, while a triplet root would give exactly the same result as the DFT triplet calculation would lie. I could see that the ground state DFT singlet wavefunction was not the real ground state, and this problem made it impossible to match these low lying singlet roots to calculations or experiment.

However, even with the ground triplet states there were certain problems that deserve to be noted. Particularly, if one π orbital was occupied differently from the other, as was the case with X-$^3\Pi$ SiC, the orbitals would no longer be degenerate as they should be. While I do not believe this hurt the accuracy of the energies calculated, it raised a flag as to how realistic the wavefunction was. In truth we know exactly how to fix the problem, simply by taking a linear combination of the two major determinants involved. However, this is not integrated smoothly into the Gaussian 03 implementations of DFT that I used, or for that matter any other quantum chemistry program that I could use. Furthermore, changing the computational method whenever something seemed wrong seemed like a slippery slope down the path of individually adjusting each calculation to fit experiment. I wanted a more objective justification for any corrections to my calculations.

After some research, I found that the problem with the singlet states and the triplet degeneracy splitting involved the fact that quantum chemistry packages restrict orbitals to the space of the real numbers when a full quantum mechanical solution would use complex orbitals. This can be seen simply from recognizing that true π orbitals of a perfectly linear molecule are not designated as π_x or π_y, but a

complex linear combinations of the two.

$$\pi_+ = \frac{1}{\sqrt{2}}(\pi_x + i\pi_y)$$

$$\pi_- = \frac{1}{\sqrt{2}}(\pi_x - i\pi_y)$$

These linear combinations have equal charge density around the z-axis instead of the unphysical picture of an electron avoiding the xz or yz planes of a linear molecule for no apparent reason, and they are the true eigenfunctions of the Hamiltonian. Recalling that the product of these two linear combinations, expressed compactly as (x+iy)(x-iy), actually turns out to be of Σ symmetry, i.e. x^2+y^2, and the product of either with itself, e.g. (x+iy)(x+iy), is of Δ symmetry, the glaring difference with real orbitals is clear. Following the logic of Dr. Masunov and his new theoretical method for dealing with this type of problem, known as spin-balanced unrestricted Kohn Sham formalism (SB-UKS),[39] I found that the use of an additional determinant was fully justified in the case of open shell degenerate π orbitals. In his complex orbital scheme, the real spatial part of any α orbital is set equal to the imaginary part of the corresponding spatial β orbital, and vice versa. In the case of non-degenerate orbitals, this doesn't change anything. But, degenerate π orbitals immediately are given the character of angular momentum eigenfunctions, and if this is done all of my problems, from broken symmetry to poor singlet energies, would disappear.

I am unaware of any implementation of complex orbital DFT, and Dr. Masunov has not yet implemented SB-UKS. However Gaussian 03[26] has an implementation of Hartree Fock theory that uses complex orbitals which may be used to calibrate the non-dynamic correlation experienced by a single determinant. For example, the $^1\Sigma$ state of SiC_3 is .28 eV lower in energy when calculated with complex HF instead of real orbitals. This may be a good approximate measure of the amount of non-

Table 4 Singlet Energies Before and After Corrections

Cluster	ΔE (eV)	S_o-D_o Real	Comp.	Exp.	S_o-T_o Real	Comp.	Exp.
$a^1\Sigma$ SiC_3	.2805	3.300	3.020	3.101	.648	.3675	.274
$b^1\Delta$ SiC_3	N/A	3.313	N/A	N/A	.661	N/A	.460
$a^1\Sigma$ Si_2C_4	.186	2.750	2.564	2.652	.433	.247	.109
$b^1\Delta$ Si_2C_4	N/A	2.764	N/A	2.738	.447	N/A	.195

The ΔE column shows the non-dynamic correlation correction from comparing SCF real and complex orbitals. The calculation for SiC_3 was performed with the aug-cc-pVTZ basis set and the calculation for Si_2C_4 was performed with the aug-cc-pVDZ basis set. The rest of the columns compare experimental values with the computed values before and after the complex orbital correction. The $b^1\Delta$ state is estimated using TDDFT instead of a complex orbital correction. Finally, the experimental value for the $b^1\Delta$ state of SiC_3 is actually an estimate from a MCQDPT/aug-cc-pVDZ calculation.

dynamic correlation that an implementation of complex orbital DFT would provide, and the results of this correction can be seen in Table 4. Because the experiments measured the vertical transition energies from the anion ground state, these numbers would move in the direction of experiment upon optimization.

Of course, this was not the only method I used to make up for the problems associated with a single determinant, but it was the only one that gave good agreement with the energy. I changed the initial guess by populating different orbitals, allowed spatial symmetry between α and β orbitals to be broken, and a number of other things, but only the complex orbital correction seemed to work well. Furthermore, a complex orbital scheme would automatically generate the second determinant where needed, but behave just like regular DFT in the absence of degeneracy, so it is a correction than could be applied universally without affecting systems that do not require it. To be sure of this, I even tested the procedure with the ground state of SiC_2 and found that the real and complex SCF answers are equivalent.

An additional peak in the photoelectron spectrum of Si_2C_4 was detected by Lineberger et. al.[17], and this state may correspond to a $^1\Delta$ state that was generated by my TDDFT calculations. Due to the multideterminant character of this state as

Table 5 Results for X $^3\Pi$ SiC

Source	Bond Length ($\mathring{A}$)	Frequency (cm^{-1})
B3LYP/aug-cc-pVDZ	1.7347	954.53
B3LYP/aug-cc-pVTZ	1.7197	976.58
Brazier (FTIR)	1.72	965
Butenhoff (LIF)	1.718	965.2

Table 6 Results for A $^3\Sigma^-$ SiC

Source	ΔE (eV)	Bond Length ($\mathring{A}$)	Frequency (cm^{-1})
B3LYP/aug-cc-pVDZ	0.292	1.8186	866.76
B3LYP/aug-cc-pVTZ	0.353	1.8054	892.14
Brazier (FTIR)	.461	1.8136	861
Grutter (Neon)	.469	N/A	N/A

well, I cannot be totally sure of the assignments. There is no linear combination of degenerate $^1\Delta$ determinants that reduces to a single real determinant that I am aware of, and this may mean that TDDFT must also be extended to complex orbitals to accurately model this state. If that is the case, further work may improve the results and determine which states correspond to the peaks in the photoelectron spectrum.

Beside the low lying states of these longer chains, there have been a handful of neutral and anion states of SiC examined, and the results of my calculation can be seen in Tables 5 through 10 along with the experimental data. These numbers give a good idea of just how accurate we can expect other calculations to be. The only major discrepencies are with the singlet states and the B $^3\Sigma^-$ state. The singlet states are hampered by a single real determinant as previously mentioned in other molecules, and the B $^3\Sigma^-$ state has actually been problematic for a variety of high level ab-initio calculations. However, in most other situations the DFT/TDDFT energies are within .2 eV of experimental values or better.

Table 7 Results for B $^3\Sigma^-$ SiC

Source	ΔE (eV)	Bond Length ($\mathring{A}$)	Frequency (cm^{-1})
B3LYP/aug-cc-pVDZ	2.116	1.8743	1178.91
B3LYP/aug-cc-pVTZ	2.145	1.8658	1169.52
Larsson (CASSCF)	2.35	1.669	913
Grutter (Neon)	1.44	N/A	1178

Table 8 Results for C $^3\Pi$ SiC

Source	ΔE (eV)	Bond Length ($\mathring{A}$)	Frequency (cm^{-1})
B3LYP/aug-cc-pVDZ	2.585	1.9040	880.50
B3LYP/aug-cc-pVTZ	2.632	1.8900	892.16
Grutter (Neon)	2.84	N/A	600
Butenhoff (LIF)	2.83	1.919	615.7

Table 9 Results for a $^1\Sigma$ SiC

Source	Bond Length ($\mathring{A}$)	Frequency (cm^{-1})
B3LYP/aug-cc-pVDZ	1.6601	1055.78
B3LYP/aug-cc-pVTZ	1.6463	1075.96
Larsson (CASSCF)	1.677	955

Table 10 Results for b $^1\Pi$ SiC

Source	Bond Length $\mathring{A}$	Frequency (cm^{-1})
B3LYP/aug-cc-pVDZ	1.7518	1022.33
B3LYP/aug-cc-pVTZ	1.7405	1067.39
Bernath FTIR	1.731	N/A

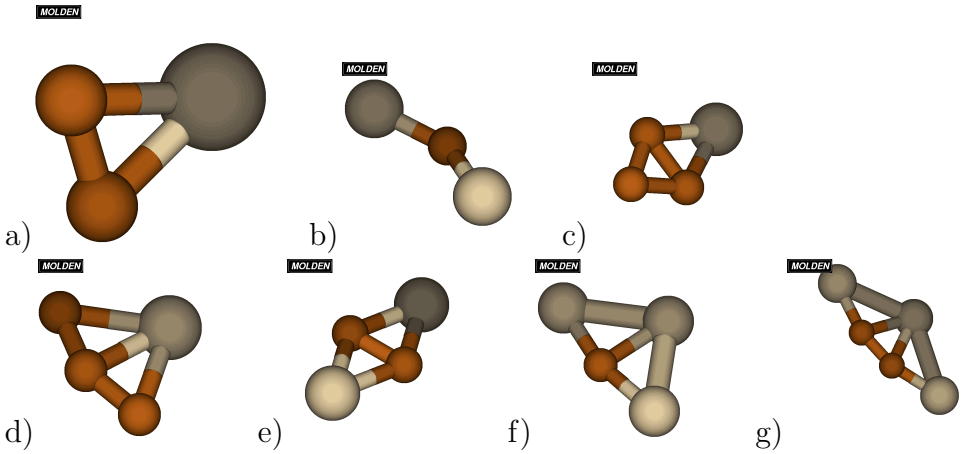

Figure 29 Geometries of Planar Molecules
Geometries of a) SiC_2, b) Si_2C, c) SiC_3, d) SiC_3, e) Si_2C_2, f) Si_3C, and g) Si_2C_3.

4.2 Planar Molecules

While standard density functional methods have problems with some of the excited states mentioned in the previous section, the difficulties that lead to the failures are no longer a factor in the planar molecules, where the π degeneracies disappear. Because each neutral ground state is of a closed shell $^1A_1$ character a single real determinant can be expected to adequately describe each of these molecular systems because there are no open shells.

The orbitals of each cluster can be qualitatively understood by valence bond methods and symmetry orbitals.The orbitals of bent Si_2C are just like those of the linear counterpart, only distorted to match the bent symmetry. The orbitals of SiC_2 can be best described from symmetry arguments keeping in mind that the C_2 fragment maintains its orbital structure and the Si atom simply attaches where symmetry allows. These two clusters have been studied in depth in other work,[43, 61] so I refer the interested reader to that work for more information. Instead, I intend to focus in depth on some of the larger clusters where we can start to learn more lessons about how silicon and carbon interact in more complicated structures.

Occupied:

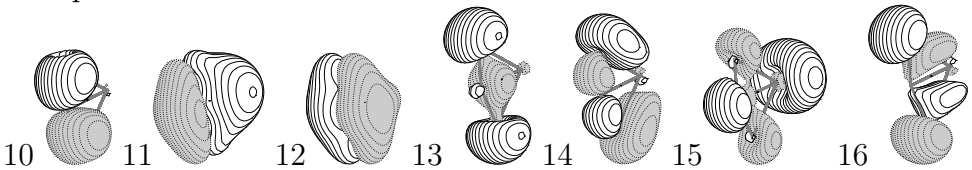

Virtual:

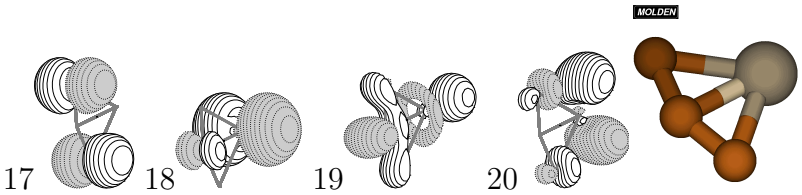

Figure 30 Valence Orbitals for Si-C Bonded Rhomboidal X $^1A_1$ SiC_3

Occupied:

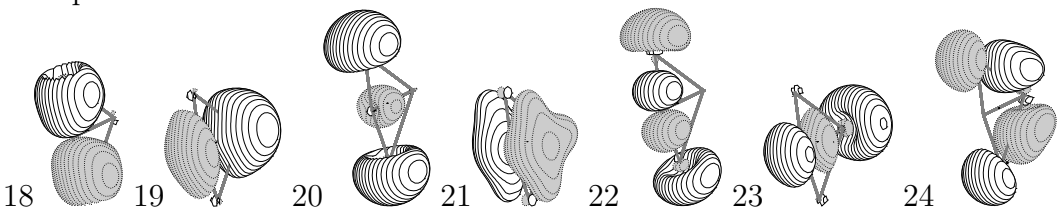

Virtual:

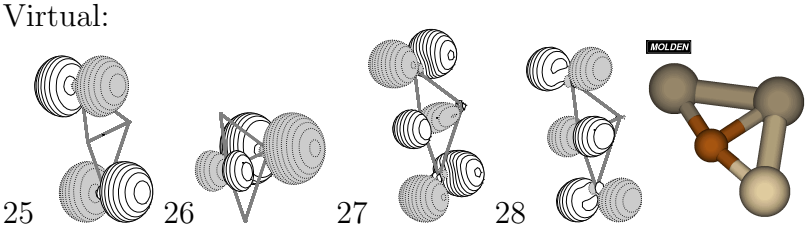

Figure 31 Valence Orbitals for Rhomboidal X $^1A_1$ Si_3C

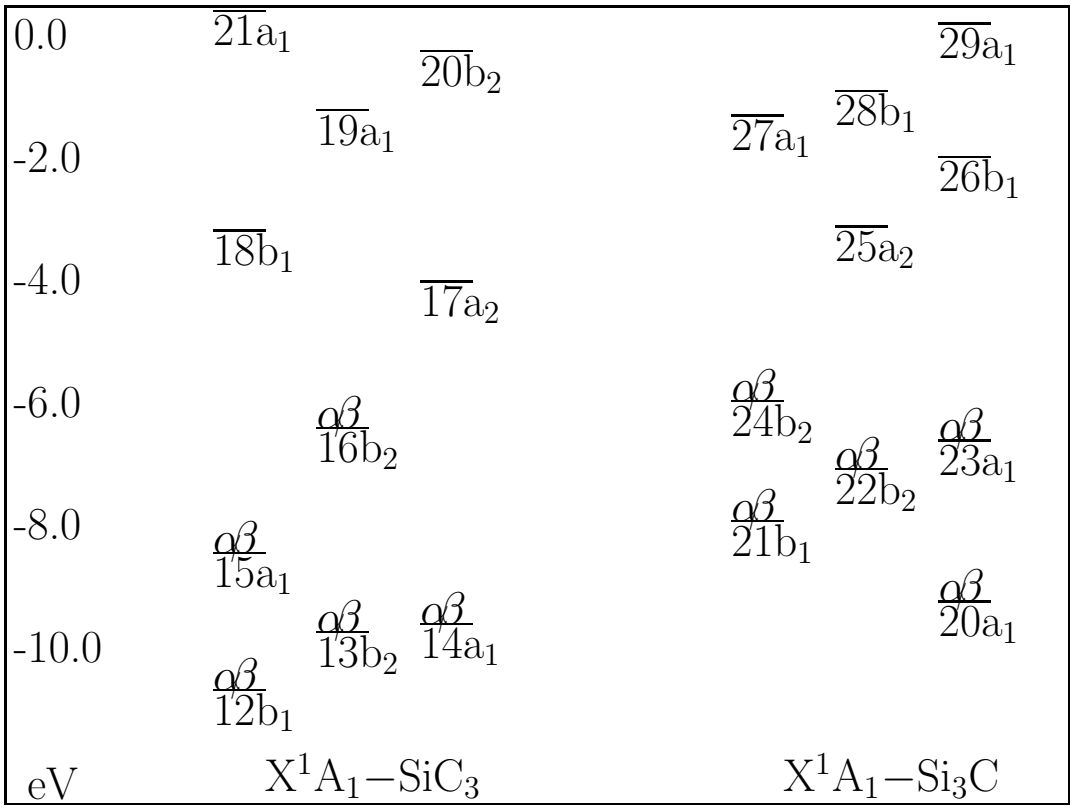

Figure 32 Orbital Energy Comparison of Si-C Bonded Rhomboidal Isomers Here we can see how the orbital energy spacing of the carbon dominated structure, SiC_3, is much larger than it's silicon rich counterpart, Si_3C. In many of the silicon rich structures, multiple orbitals are near the HOMO, possibly leading to a more involved optical spectrum.

I performed calculations on four rhomboidal clusters, and the comparison of the bonding in these clusters can offer more insight into how silicon and carbon interact with one another. These can be subdivided by the type of central bond, either Si-C or C-C, and the results of such a division are quite informative. Once this division is made, we are able to see the effect of replacing carbon atoms with silicon atoms at locations other than the ends of a chain.

For example, let if we begin with the Si-C bonded rhomboidal isomer of SiC_3 and replace the two carbon atoms on either side of the central Si-C bond with silicon atoms, we get Si_3C. The orbitals of these two structures, particularly the HOMO

and LUMO, have the same symmetry and basic shape, but a closer look shows some important differencs. For instance, the HOMO (orbital 16) of this isomer of SiC_3 has more participation from the central carbon atom than the HOMO (orbital 24) of Si_3C. In fact, the silicon atoms in this particular orbital of Si_3C could be seen as a bonding orbital in a bent Si_3 chain.

A similar case can be seen in the orbitals 14 and 22 of SiC_3 and Si_3C, respectively. In these two orbitals, the bonding goes through the central carbon atom instead of the central silicon atom. In this orbital, Si_3C excludes the silicon atom, while SiC_3 allows it a great deal more participation. What this shows is that, for this particular structure, replacing carbon atoms with silicon atoms seems to weaken existing bonds between silicon and carbon atoms. In this case, the bond distance increases from 1.905 $\mathring{A}$ to 1.971 $\mathring{A}$. Furthermore, the comparison of these two structures suggests that if more carbon is in the structure there will be multicenter bonding orbitals, and the orbital energies will be further apart.

A scan over the other orbitals in this structure tells a similar story (only orbitals 12 and 13 of SiC_3 need be transposed to match orbitals 20 and 21 for a comparisons to be made). In general, the carbon rich structure has more participation from other atoms in a given orbital. This can be rationalized from the tendency of carbon to form double bonds and the silicon tendancy to form single bonds. For instance, orbital 15 of SiC_3 and 23 of Si_3C are analogous to one another. However, there is a great deal more carbon s participation in this orbital of SiC_3 than in Si_3C, where the carbon atoms are excluded.

A question we can ask is, "can the lessons of these two clusters can be quickly extended to the C-C bonded rhomboidal clusters, Si_2C_2 and SiC_3?" It is easy to spot the tight multicenter bonding in this isomer of SiC_3, but linear combinations of orbitals 18 and 20 of Si_2C_2 can give the same result, suggesting that the only thing keeping multicenter bonding from occuring is the symmetry of the cluster.

Occupied:

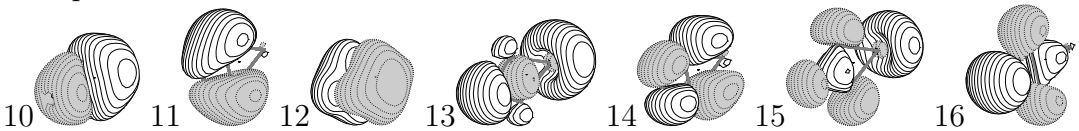

Virtual:

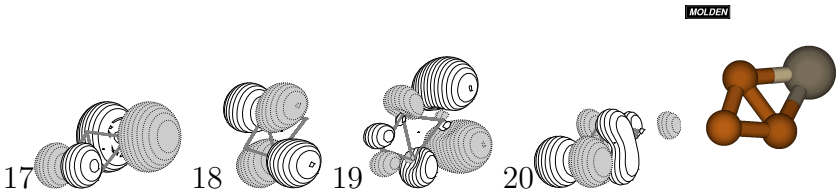

Figure 33 Valence Orbitals for C-C Bonded Rhomboidal X $^1A_1$ SiC_3

Occupied:

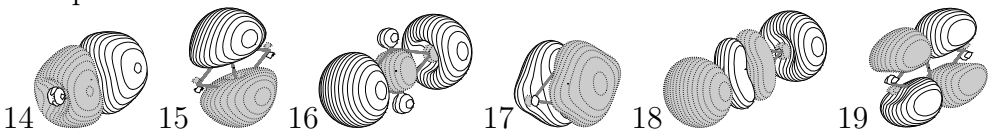

Virtual:

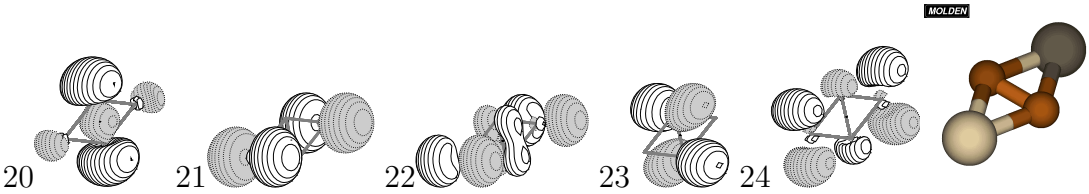

Figure 34 Valence Orbitals for Rhomboidal X $^1A_1$ Si_2C_2

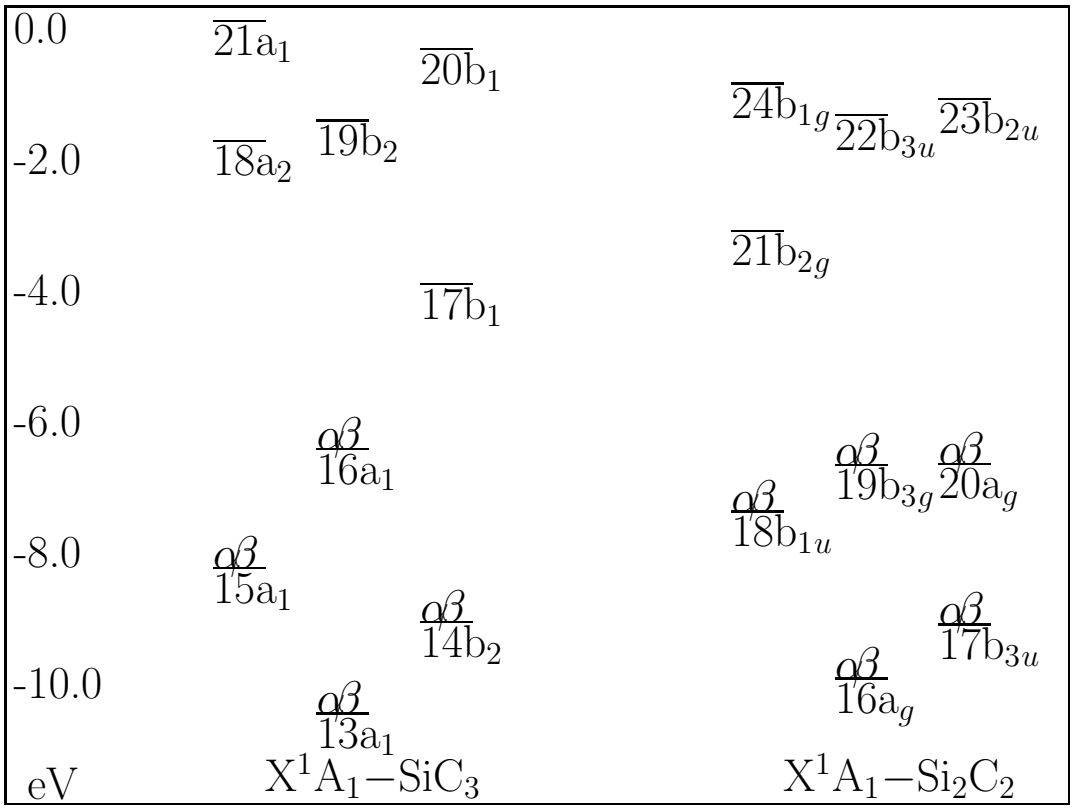

Figure 35 Orbital Energy Comparison of C-C Bonded of Rhomboidal Isomers

Furthermore, this isomer of Si_2C_2 is very much unlike Si_3C in that all of the atoms participate in the orbitals.Essentially, while the Si-C bond may be weakened by additional silicon atoms, the C-C bond does not seem to be. In fact, the C-C bond length decreases from 1.486 to 1.441, indicating an even tighter bond. The tighter bond can be rationalized from the fact that the extra carbon atom in SiC_3 pulls some of the electron density away from the central C-C bond, a problem that is removed in Si_2C_2.

We can also compare the bonding of Si_3C with Si_3C_2 to see how the C_2 cluster differs from atomic carbon in bonding with other silicon atoms. In this case, orbitals analogous to Si3C orbitals that mostly excluded the carbon atomic orbitals receive greater participation from the C_2 submolecule. In fact, many of these orbitals can

Occupied:

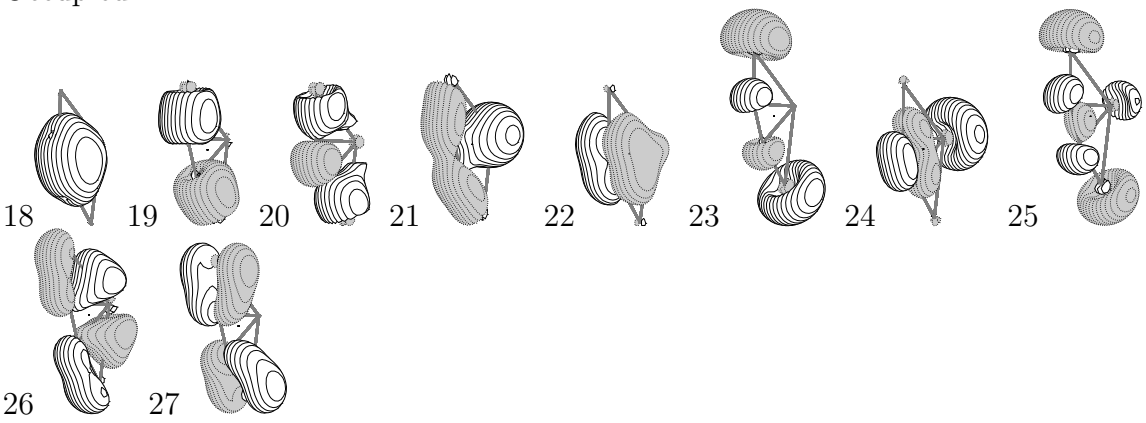

Virtual:

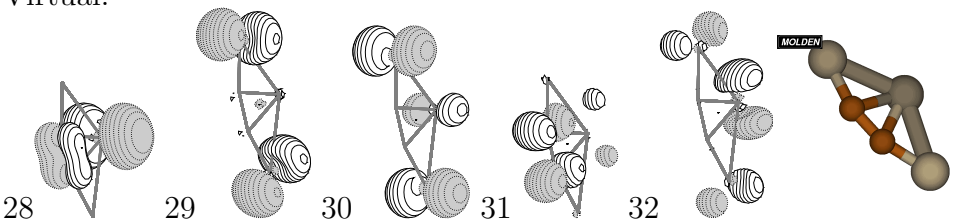

Figure 36 Valence Orbitals for Planar X $^1A_1$ Si_3C_2

be created by adding Si atomic orbital functions of the appropriate symmetry to orbitals of SiC_2. This indicates that the C_2 molecule is able to bond with silicon more readily than a single carbon atom.

Now that we have an understanding of the bonding in these planar clusters, we can turn our attention to the virtual orbitals and the excitations that involve them. The first few virtual Kohn Sham orbitals almost always have dominant silicon p_x orbital components. This can be rationalized from the fact that the silicon p orbitals have a poor overlap with the carbon p orbitals, so they participate less in the lower bonding orbitals. These bonding orbitals and the corresponding antibonding orbitals do not not split as much, leaving silicon p orbitals near the HOMO and LUMO. This means that the lowest singlet excited states of planar SiC clusters, usually in the range of 1-2 eV, almost always return electron density to p_x orbitals of silicon atoms at the edges of the structure. A look at the shifts in bond lengths also confirms that

Table 11 SiC_2 Theoretical and Experimental Results

State	ΔE	ν_1	ν_2	ν_3	R_{SiC}	R_{CC}	f
X-$^1A_1$	0.000	1835.9	789.2	95.6	1.852	1.260	0.0000
	0.000	1746.0	840.6	196.4	1.812	1.250	0.0000
A-$^1B_2$	2.559	1456.1	507.8	491.5	1.874	1.329	0.0163
	2.497	1462	487	462	1.881	1.304	N/A

This table shows the calculated (above) and experimental (below)values for the A^1B_2-X^1A_1 transition of SiC_2, from B3LYP/aug-cc-pVTZ calculations and experimental values from the original work done by Michalopoulos et. al. [43] and other data from the NIST webbook.[47] The major component of this transition is an excitation from orbital 13 to orbital 14 in Figure 37.

Occupied:

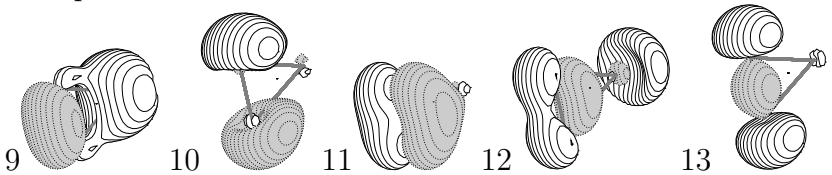

Virtual:

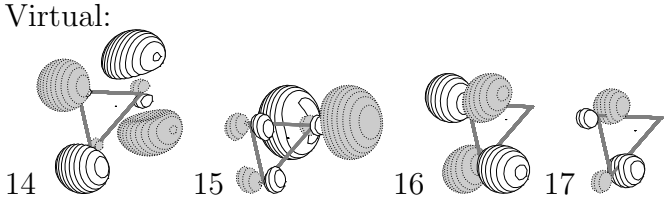

Figure 37 Valence Orbitals for Triangular X $^1\Sigma$ SiC_2

the silicon atoms relax away from the structure in the low lying excited states that I calculated.

The only experimental data available for the excited states of these clusters is the long known A^1B_2-X^1A_1 transition of SiC_2. This transition was used by Michalopoulos et. al. [43] to prove that SiC_2 was a triangular molecule. In the Si_mC_n mapping paper, Dr. Duan found that the triangular ground state was not a stable geometry at the B3LYP/aug-cc-pVDZ level of theory, so Table compares the B3LYP/aug-cc-pVTZ level of theory with the values calculated by Michalopoulos et. al.

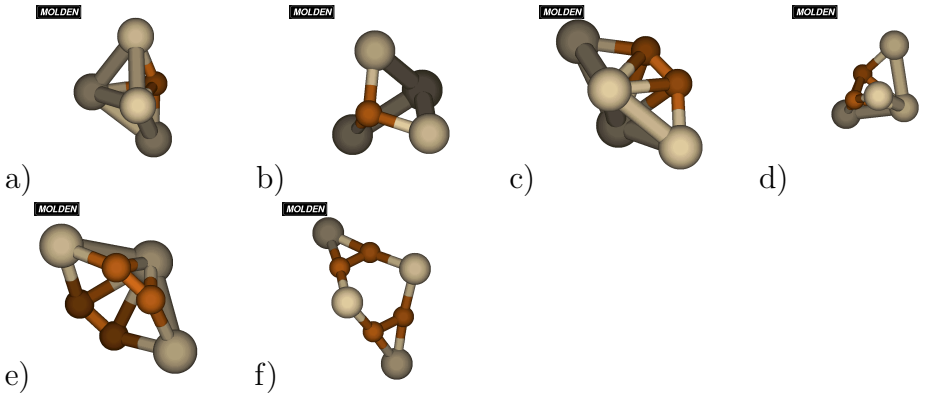

Figure 38 Geometries of Cage Molecules

Although there is no experimental data for excited states of the planar clusters other than SiC_2, a recent work by Rintelman and Gordon gave the first triplet excited states of three of the rhomboidal isomers. A comparison of my calculated values and their MCQDPT/6-31G(d) results can be seen in Table 12. The agreement of these calculations continues to affirm that the B3LYP functional is effective at describing excited states of these clusters. The rest of the singlet states calculated can be found in the appendix.

4.3 Three - Dimensional Structures

Finally, there are the cage structures. In these clusters, the HOMO LUMO gap were expectedly too large for low lying states to cause any of the problems observed in linear clusters. Calculations confirm that the ground states of these clusters are again all of closed shell $^1A_1$ character.

While the previous structures had fairly predictable and well behaved molecular orbitals, I want to examine each of these clusters in depth. There are three reasons for this. First, they were by far the most expensive calculations, but only rarely was I able to get fully converged geometric data for the exited states. Thus the orbital information, coupled with geometric shifts, may be the only thing said about these excited states for some time. Second, it is in the excited states of these clusters that

Table 12 Ab-Initio vs. B3LYP results for Rhomboidal Clusters

State	ΔE	ν_1	ν_2	ν_3	ν_4	ν_5	ν_6
C-C Bonded SiC_3							
$^1A_1$	0.0	1405.7	1026.1	982.5	660.9	388.5	239.2
	0.0	1504	1120	984	720	509	316
$^3B_1$	0.854	1557.5	979.1	834.1	524.9	389.8	143.0
	0.945	1651	1255	747	502	395	271
Si-C Bonded SiC_3							
$^1A_1$	0.0	1595.3	1148.2	764.2	488.8	378.8	200.2
	0.0	1603	1254	852	538	420	279
$^3B_1$	0.315	1366.0	1193.6	696.4	576.6	485.3	228.3
	0.256	1380	1234	755	674	479	363
Si_2C_2							
^1A_g	0.0	1114.1	956.8	934.5	492.8	342.9	193.4
	0.0	1066	1026	1013	543	424	224
$^3B_{2g}$	2.265	1486.6	1239.9	576.8	459.5	353.6	245.3
	2.229	2689	1150	623	474	411	269

State	ΔE	R_1	R_2	R_3	R_4
C-C Bonded SiC_3					
$^1A_1$	0.292	1.862	2.944	1.486	1.442
		1.83		1.50	1.43
$^3B_1$	1.100	1.955	2.937	1.520	1.367
		1.95		1.53	1.35
Si-C Bonded SiC_3					
$^1A_1$	0.477	2.071	1.924	2.619	1.348
		2.06	1.89		1.32
$^3B_1$	0.792	1.978	1.989	2.531	1.349
		1.94	1.96		1.34
Si_2C_2					
^1A_g	0.000	3.422	1.856	1.441	
	0.000	3.33	1.82	1.48	
$^3B_{2g}$	2.265	3.492	1.884	1.417	
	2.229	3.43	1.84	1.41	

In this table, B3LYP/aug-cc-pVDZ (above) calculations for some of the rhomboidal clusters are compared with MCQDPT/6-31G(d)//FORS(12,10/11)/6-31G(d) (below) calculations completed by Rintelmand and Gordon. [53] There is generally excellent agreement. Only one major discrepency appears, in the largest vibrational mode of Si_2C_2. The B3LYP hessian for this cluster was calculated analytically, so I suspect there may be a mistake in the Rintelman and Gordon paper.

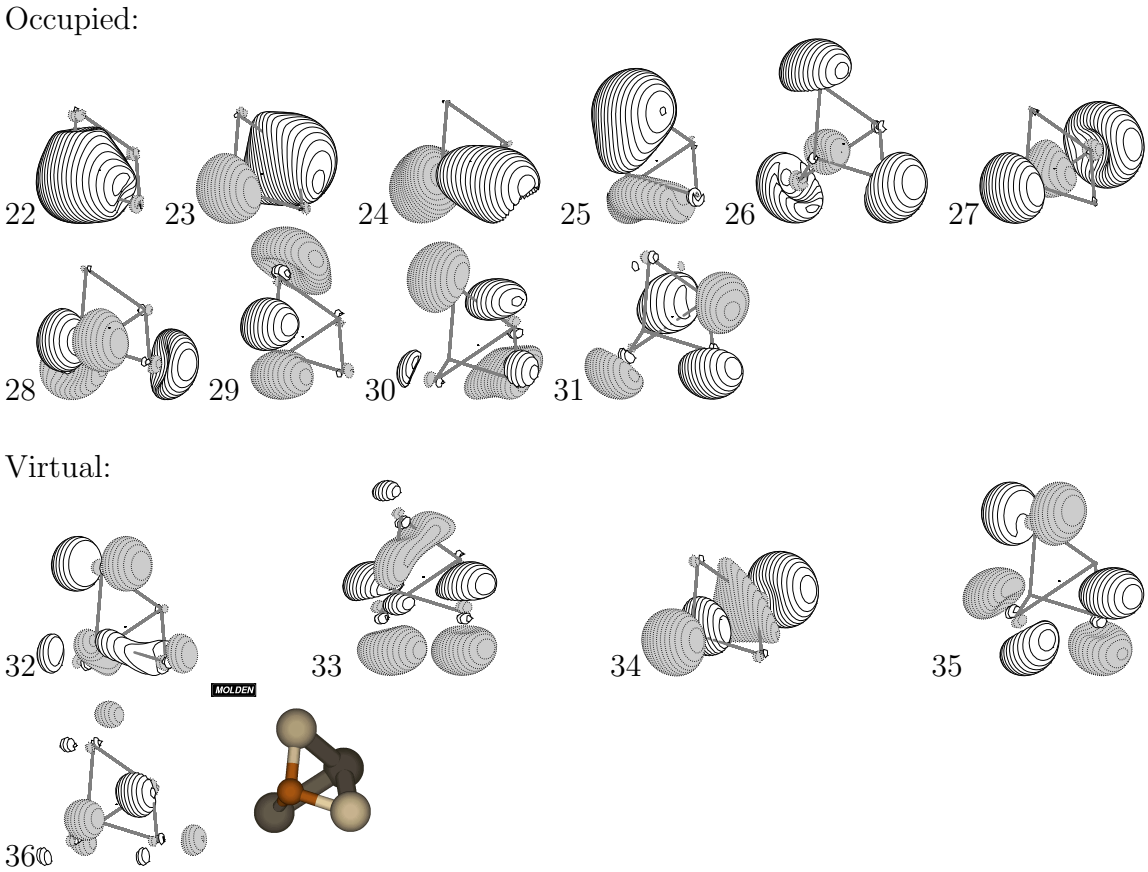

Figure 39 Valence Orbitals for C_{3v} $^1A_1$ Si_4C

we may start to see some of the behaviors of the SiC surface or defects. Finally, there are some orbital structures that are either unexpected or give more insight into the interaction between silicon and carbon. I will start with Si_4C.

Having the highest stoichiometric ratio of silicon to carbon in these clusters, Si_4C is also the smallest 3-D structure. This is not a coincidence, because it is the tendency of silicon to maximize the number of single bonds that stabilizes these clusters. I actually examined two isomers, one being the ground state of the anion (C_{2v}, letter "a" in Figure 38) and the other of the neutral (C_{3v}, letter "b"). Just like the similar Si_5 cluster[51], both are trigonal bipyramidal, but they differ in where the carbon atom is placed within the structure. Thus, this cluster can also teach some useful lessons about the replacement of silicon atoms with carbon in the context of

Occupied:

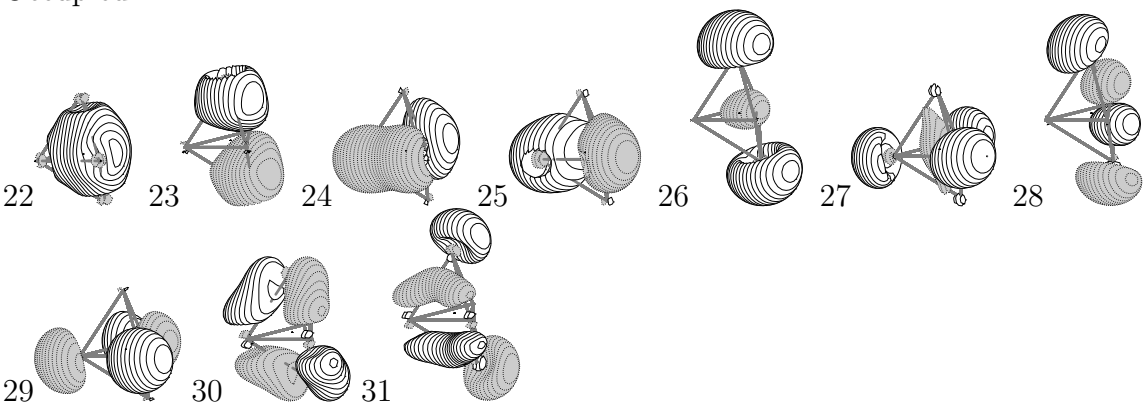

Virtual:

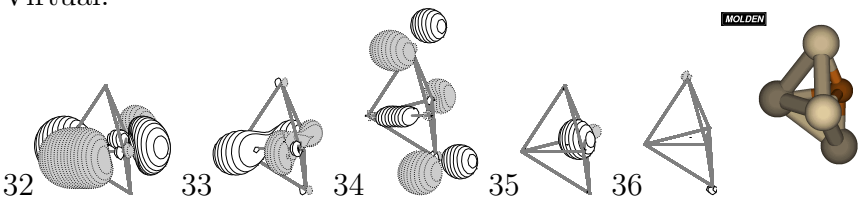

Figure 40 Valence Orbitals for C_{2v} $^1A_1$ Si_4C

a three dimensional structure. Furthermore, the C_{3v} and C_{2v} forms are the neutral and anion ground states, respectively.

The relative orbital energies of the two structures are dominated by contributions from the carbon atom. Recognizing that 24 and 25 are degenerate in the C_{3v} form, the first four valence orbitals for both structures, 22 through 25, are carbon bonding orbitals. Each of these four orbitals bond the carbon to the silicon atoms in accordance with symmetry. However, the next four orbitals, 26 through 29 are anti-bonding orbitals between the carbon and the silicon atom s functions, following the energy ordering of the carbon atomic orbitals. Thus, in bonding with the rest of the structure, the carbon-based orbitals split into bonding and anti-bonding regimes that do not overlap. Finally, orbitals 30 and 31 for both clusters involve p orbital bonding between the silicon atoms. Similar to the most of the previous clusters we have looked at, the virtual orbitals have more silicon p character than anything else, and many of the same conclusions can be drawn.

Occupied:

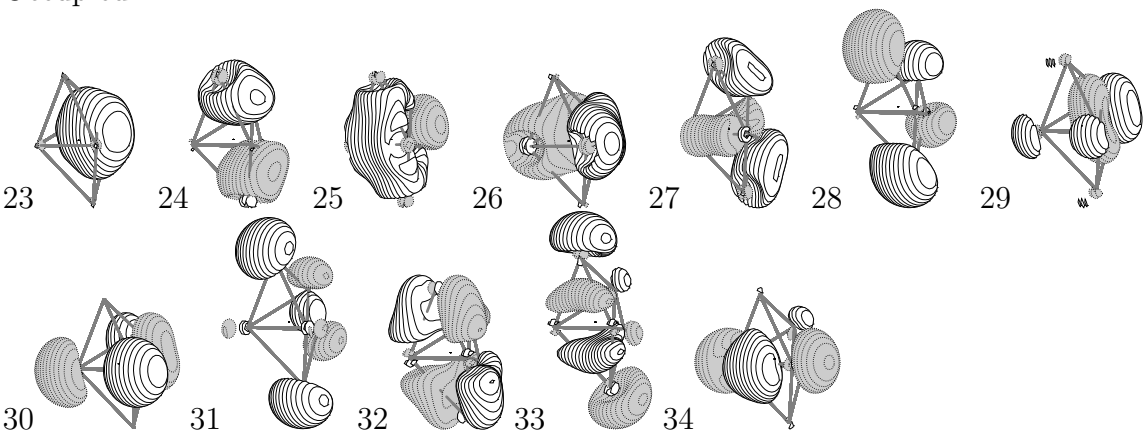

Virtual:

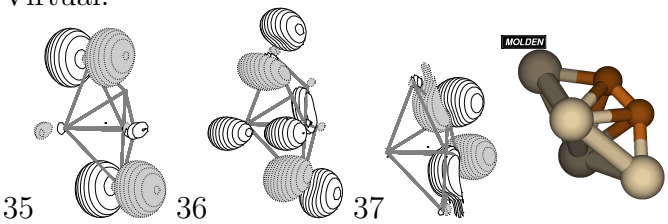

Figure 41 Valence Orbitals for C_{2v} $^1A_1$ Si_4C_2

As seen previously, excited states will return density to the silicon atoms, lengthening their bonds as they move away from the center of the cluster. In the C_{3v} form, the first few excited singlet states that I was able to partially optimize "breathe out," expanding mostly along the A_1 mode, and a few have significant oscillator strengths. Thus there may be future experimental detection of a transition in the neighborhood of 2 eV in accordance with my calculations. Because the C_{2v} form is actually the most stable anion isomer, it is worth noting that there is at least one low lying anion excited states that may further complicate the anion photoelectron spectra beyond just the large changes to the C_{3v} form. The interested reader may consult the appendix for specific constants of interest.

Comparing the C_{2v} forms of Si_4C_2 and Si_4C allows us the opportunity to again see what happens when a C_2 fragment replaces a carbon atom, but this time in a three dimensional structure. The same result as with Si_3C_2 appear. The C_2

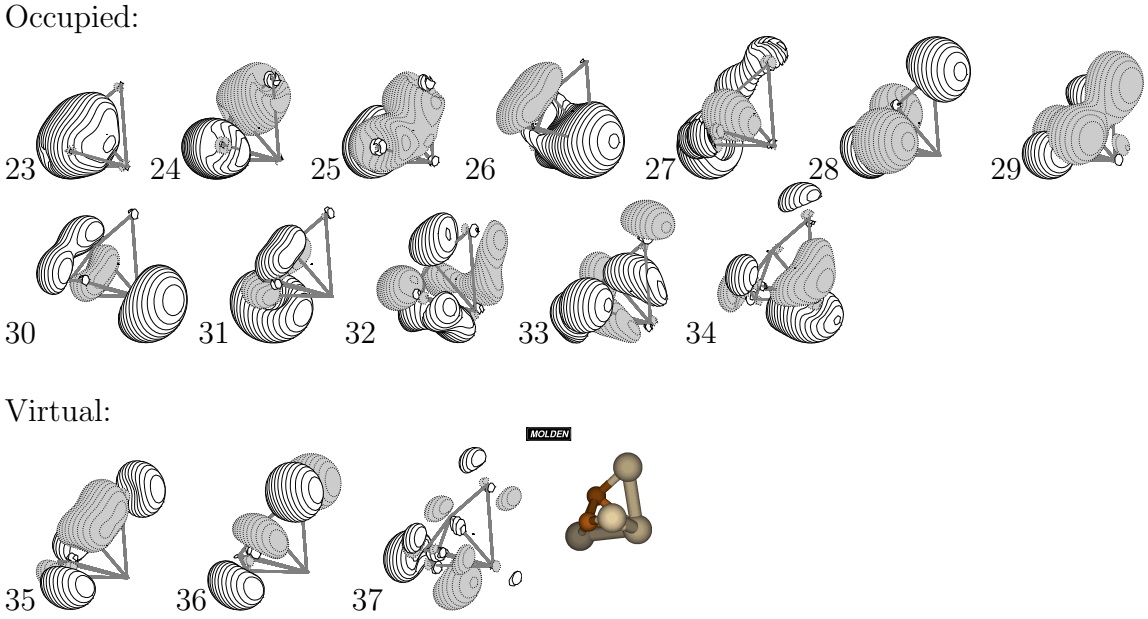

Figure 42 Valence Orbitals for Distorted C_{1v} $^1A_1$ Si_4C_2

fragment participates in more bonding with the silicon atoms, and makes even less of an appearance in the virtual orbitals.

This trend in the virtual orbitals, where a prominent contribution from silicon p orbitals appears frequently, can also be seen in the other isomer of Si_4C_2, where the LUMO(orbital 35) and the orbital 36 are made from terminal silicon p orbitals, and similar things can be said about these excited states as in previous clusters. There are exceptions to this however, particularly in the case of Si_3C_4. This cluster has a higher content of carbon than the previous cages, so that there are more bonding orbitals that can be formed from carbon atomic orbitals. As a result, the first virtual orbital (34) is actually an alternative bonding between the carbon atoms. Later orbitals do exhibit the strong silicon p character, but a trend may likely appear in larger clusters with a higher carbon content. The possible carbon bonds will tend to take precedence energetically over the atomic orbitals of silicon. This would seem obvious from the data seen previously, but it may be useful to see that as the relative amount of carbon increases, there are more possible routes of bonding between those carbon

Occupied:

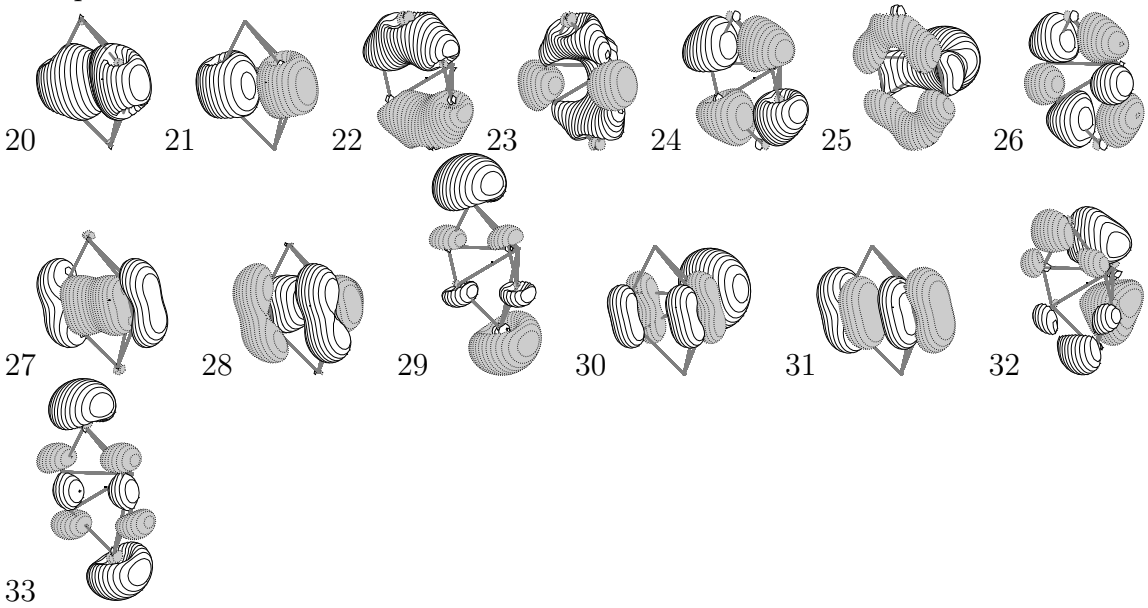

Virtual:

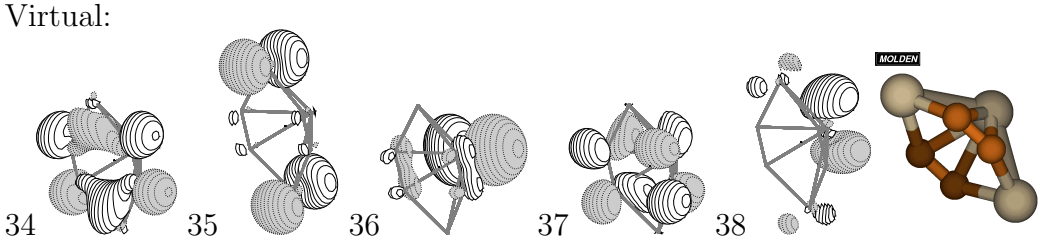

Figure 43 Valence Orbitals for C_{2v} $^1A_1$ Si_3C_4

atoms that are not included in the electronic ground state. This may lead to some insight on the differences between carbon and silicon terminated surfaces, as the reader can likely envision different ways for the carbon atoms on a surface to bond. Those other routes to bonding, if they comprised the low lying states of a carbon terminated surface, would be dramatically different from the atomic excitations of silicon. However, more calculations with larger clusters would be needed to begin to tell how these differences map into the electronic structures of materials.

Si_4C_4 lends itself readily to some functional group analysis, because it is essentially two SiC_2 molecules hinged together by a silicon dimer. The orbitals can be seen in Figure 44. Taking into account that orbitals 12 and 13 of the SiC_2 cluster can

Occupied:

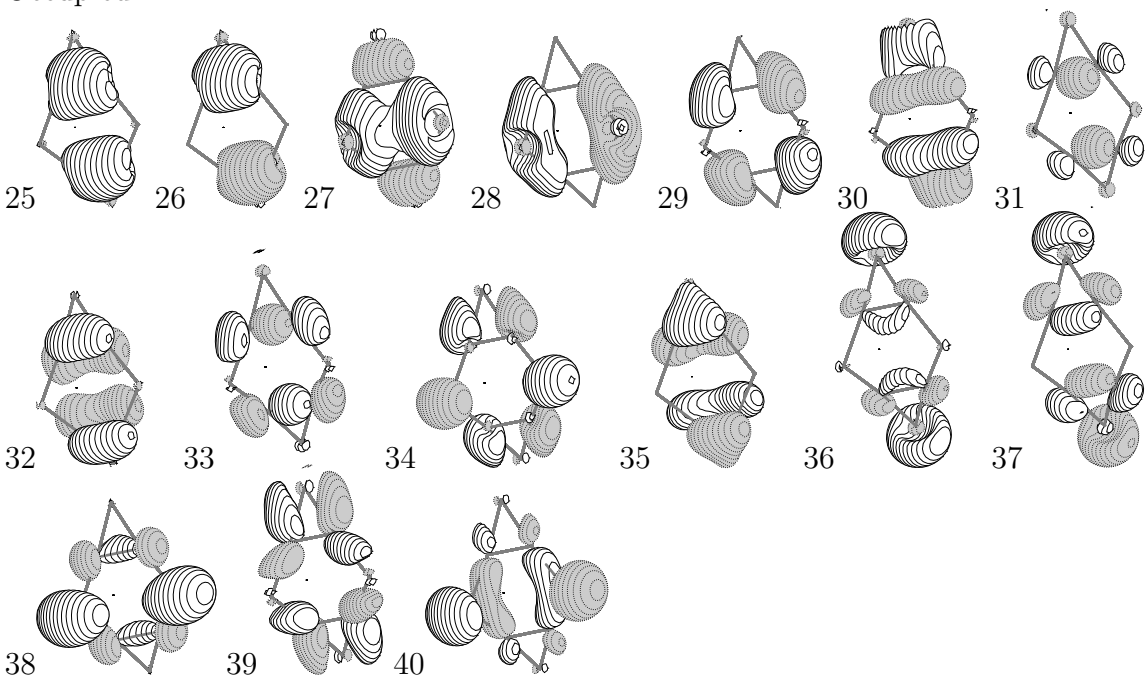

Virtual:

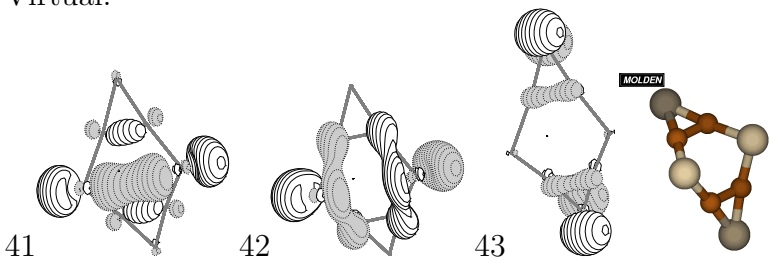

Figure 44 Valence Orbitals for C_{2v} $^1A_1$ Si_4C_4

mix to generate the banana type CC bonds in Si_4C_4 orbital 36, only a few orbitals need to be explained as anything more than SiC_2 orbitals with some leaching from the dimer. Orbitals 27, 28, 34, and 38 are derived from the hinge atoms' s functions with a small amount of mixing from the appropriate p functions to improve bonding. Finally, in orbital 39 there is a significant contribution from silicon p functions.

The interesting symmetry of this molecule also gives some insight. One can see that, with a relatively small amount of distortion, the structure of this molecule can reverse the respective roles that the terminal or hinge silicon atoms play. The

Table 13 Excitation Energies and Oscillator Strengths of Cage Structures

Molecule	Symmetry	ΔE	f
Si_4C_4	C_{2v}	1.671	0.0051
Si_3C_4	C_{2v}	1.984	0.0104
Si_4C_2	C_{1v}	1.321	0.0001
Si_4C_2	C_{2v}	2.034	0.0005
Si_4C	C_{2v}	1.177	0.0017
Si_4C	C_{3v}	2.040	0.0002

only difference between the two pairs is the bonding of the carbon atoms nearby, and yet their corresponding symmetry orbitals appear at radically different points in the orbital energies.

Where an alternative bonding configuration between carbon atoms exists, the LUMO tends to favor this electron structure over the silicon p structures. However, this alternative CC bonding only takes precedence energetically over the Si p orbitals, which always start to appear within the first two virtual orbitals.

As for assessing the accuracy of the calculations on these larger clusters, there are few options. Photoluminescence spectroscopy performed by Dr. Brillson et. al. of bulk SiC has detected surface based electronic transitions with transitions in the neighborhood of 1 to 2 eV. Table 13 shows that nearly all of these clusters have a first singlet excited state within this range. Furthermore, my calculations place the first singlet excited state of Si_4C_4 at 1.671 eV, and one of the more important photoluminescence peaks was detected at 1.65 eV for both C and Si faced 6H SiC.[64] The calculated transition is allowed, and this is made more interesting since the stoichiometric ratio of this cluster is the same as bulk silicon carbide. While, this is certainly not conclusive, it does suggest the possibility that some of these clusters may bond to the silicon carbide surface in ways that allow them to maintain their electronic characteristics.

5. Conclusions and Recommendations

5.1 Chapter Overview

Now that the results have been presented, I will discuss these results with respect to experimental detection and future computational work. In particular, I want to revisit the questions presented in the very first chapter.

5.2 Conclusions of Research

The first question was "Can we expect many more excited states of these clusters in Photoelectron spectra?" The answer is that it depends. If Dr. Lineberger is able to produce some of the longer carbon rich Si_mC_n chains, then the even membered chains will have some low lying excited states. However, based on the 3 eV laser used in previous photoelectron spectrum, the silicon rich clusters will not produce excited electronic states unless they are made to. There may be some possible ways of doing this. If a UV lamp was used to excite the anions before they are photodetached, it would increase the range of electronic states that the 3 eV could leave the molecule in. The calculations I have done on the anion states should help this possibility. Another, probably cleaner, solution would be to just use a higher frequency laser, operating at 4-6 eV, to access these states.

The second question was "What will the spectrum look like of these excited states?" If excited states are accessed the photoelecton spectrum may be similar to the ground state's spectrum. Most of the excited states have similar vibrational frequencies as the ground states. The major difference between the spectra would be from the geometrical differences. As mentioned, most of the excited states cause the silicon atoms to relax away from the rest of the structure, so the normal modes involving this motion would be excited in a transition between the ground and excited states. Although an excited state photoelectron spectrum bypasses the ground state,

we can assume that the differences between the excited state and the ground state photoelecton spectrum would involve the same normal modes.

The third question was "Can any inferences be made about the excited states of larger clusters?" The answer to this is yes. In terms of the linear clusters, there was a clear trend in orbital energies that can be exploited. As the length of the chain increases, the carbon atoms will dominate more and more until the spectrum starts to approach that of long carbon chains. In larger three-dimensional structures, it is likely that the excited states will continue to consist of non bonding silicon p orbitals. Furthermore, based on the trends in the data I have calculated, the larger cage structures will likely excite to non bonding orbitals of atomic silicon, unless those structures are carbon rich.

The fourth question was "How accurate is DFT/TDDFT with respect to experimental results for excitation energies?" The answer, based on the available experimental data, is that the energies come within .1 eV or better. Frequencies are typically within 20 cm^{-1}. Finally, geometries at the aug-cc-pVDZ level are usually within .01 $\mathring{A}$ or better. This of course is excluding the known problems with multiconfigurational states, which I will now address.

5.3 Recommendations for Action

The fifth and final question had two parts, specifically: "Are there any major shortfalls of TDDFT?" and "Can these shortfalls be corrected?" In answer to the first half of the question, I have shown that DFT fails with the singlet states of the even membered chains because of the multiconfigurational character of the states. As for the second part of the question, the answer is yes. Although it was not rigorous, I have shown that a single determinant, if orbitals are allowed to be complex, will likely capture the non-dynamic correlation experienced in some of the linear molecules. If this is indeed the case universally, SB-UKS should be considered as a cheaper and less empirically derived alternative to Multi-Reference DFT. I would imagine that a

normal Kohn Sham SCF procedure could be used to approach the correct complex orbitals, after which a post-SCF SB-UKS scheme could be used to find the final, complex orbitals and corresponding energy. This might be a significant step because of the added difficulty in getting a complex determinant to converge. Such a scheme would not slow down the calculation of systems that do not require complex orbitals, but would automatically correct the systems that do.

Another question that remains to be seen is if there are any similar hurdles for implementing TDDFT within a complex orbital framework, because this would be the only way to capture the non-dynamic correlation of an excited state. It seems that this may be the only way to get accurate results for longer and longer SiC_n and C_n chains, but I am unaware of any formal theoretical development of this, and it is a question that should be looked into.

5.4 Recommendations for Future Research

The obvious next step is to use TDDFT with larger and larger clusters to eventually approach the electronic behavoir of bulk SiC around defects and the surface. Predictions from such calculations would allow us to know, based on the electronic spectrum, exactly what types of bonds were forming on the surface, or what defects were prominent. Furthermore, such calculations could lead to a better understanding of dopants and the types of electron/hole traps they may form.

Another intersting area of research would be to see how the electronic spectrum of these clusters would change upon bonding to the SiC surface, to see if the surface anomalies of SiC can be described with something simpler than full SIMOMM treatment. That would also be the quickest way to determine if any of these clusters are in fact native to the SiC surface.

I believe that this research and the work that can now follow it will one day give us a full understanding of how the surface of SiC behaves. That understanding

will one day allow us to effectively create SiC devices that can be used in aerospace applications.

Appendix A. Numerical Results

This appendix contains the numerical results of the calculations I completed at the B3LYP/aug-cc-pVDZ level of theory. It is ordered in a similar manner to the organization of the results chapter, starting with linear chains and ending with the cage structures. A comparison of the ground states of each spin manifold is given first, followed by the excited states of each spin manifold. The tables list the electronic state where it was determined by Gaussian 03, the relative energies (ΔE, eV), the vibrational frequencies (ν_n, cm^{-1}), geometric parameters (r_n, $\AA$), and oscillator strengths (f, dimensionless). Because of the large number of calculations, this data has been extracted directly from the Gaussian output files. Negative vibrational frequencies correspond to transition states, and in certain cases very large values for vibrational frequencies correspond to failed numerical Hessians.

Table 14 Ground States of Linear SiC_2 Spin Manifolds

Vibrational Summary

State	ΔE	ν_1	ν_2	ν_3	ν_4
$^1\Sigma$	0.000	1914.8	782.8	-47.2	-47.2
^{3}–?	2.007	1859.9	619.5	253.9	139.2

Geometric Summary

State	ΔE	R_1	R_2	R_3
$^1\Sigma$	0.000	1.710	3.002	1.292
^{3}–?	2.007	1.810	3.063	1.253

Optical Summary

State	ΔE	f
$^1\Sigma$	0.000	0.0000
^{3}–?	2.007	0.0000

Table 15 Singlet States of Linear SiC_2

Vibrational Summary

State	ΔE	ν_1	ν_2	ν_3	ν_4
$^1\Sigma$	0.000	1914.8	782.8	-47.2	-47.2
^{1}-?	2.573	1970.9	632.9	267.3	83.1
^{1}-?	2.573	1971.2	632.0	263.1	67.7
^{1}-?	2.799	1405.4	1072.1	562.9	441.0
^{1}-?	3.014	1667.4	600.7	256.0	256.0
^{1}-?	3.014	N/A	N/A	N/A	N/A

Geometric Summary

State	ΔE	R_1	R_2	R_3
$^1\Sigma$	0.000	1.710	3.002	1.292
^{1}-?	2.573	1.831	3.061	1.230
^{1}-?	2.573	1.831	3.061	1.230
^{1}-?	2.799	1.861	3.179	1.317
^{1}-?	3.014	1.859	3.176	1.317
^{1}-?	3.014	1.855	3.172	1.317

Optical Summary

State	ΔE	f
$^1\Sigma$	0.000	0.0000
^{1}-?	2.573	0.0139
^{1}-?	2.573	0.0140
^{1}-?	2.799	0.0108
^{1}-?	3.014	0.0000
^{1}-?	3.014	0.0000

Table 16 Triplet States of Linear SiC_2

Vibrational Summary

State	ΔE	ν_1	ν_2	ν_3	ν_4
^{3}–?	0.000	1859.9	619.5	253.9	139.2
^{3}-?	0.009	1860.9	628.9	620.1	-581.4
^{3}-?	0.551	1629.6	552.4	194.6	115.8
^{3}-?	0.737	41073.2	40175.8	40152.2	32309.5
^{3}-?	1.747	N/A	N/A	N/A	N/A
^{3}-?	1.747	1841.2	794.2	295.5	234.8
^{3}-?	2.873	1986.2	675.9	251.5	241.0

Geometric Summary

State	ΔE	R_1	R_2	R_3
^{3}–?	0.000	1.810	3.063	1.253
^{3}-?	0.009	1.809	3.063	1.253
^{3}-?	0.551	1.857	3.174	1.317
^{3}-?	0.737	1.874	3.189	1.315
^{3}-?	1.747	1.697	2.966	1.268
^{3}-?	1.747	1.697	2.965	1.268
^{3}-?	2.873	1.777	3.013	1.236

Optical Summary

State	ΔE	f
^{3}–?	0.000	0.0000
^{3}-?	0.009	0.0000
^{3}-?	0.551	0.0005
^{3}-?	0.737	0.0012
^{3}-?	1.747	0.0314
^{3}-?	1.747	0.0314
^{3}-?	2.873	0.0009

Table 17 Ground States of Linear Si_2C Spin Manifolds

Vibrational Summary

State	ΔE	ν_1	ν_2	ν_3	ν_4
^{2}–?	0.000	1132.3	541.4	215.4	125.0
$^1\Sigma_g$	1.162	1370.2	574.2	27.6	27.6
^{3}–?	3.690	1085.2	540.1	205.0	94.7
$^2\Sigma_u$	10.390	1206.5	556.9	42.5	42.5

Geometric Summary

State	ΔE	R_1	R_2
^{2}–?	0.000	3.464	1.732
$^1\Sigma_g$	1.162	3.414	1.707
^{3}–?	3.690	3.439	1.720
$^2\Sigma_u$	10.390	3.409	1.704

Optical Summary

State	ΔE	f
^{2}–?	0.000	0.0000
$^1\Sigma_g$	1.162	0.0000
^{3}–?	3.690	0.0000
$^2\Sigma_u$	10.390	0.0000

Table 18 Singlet States of Linear Si_2C

Vibrational Summary

State	ΔE	ν_1	ν_2	ν_3	ν_4
$^1\Sigma_g$	0.000	1370.2	574.2	27.6	27.6
^{1}-?	2.555	961.3	498.2	195.4	195.3
^{1}-?	2.555	961.3	498.2	195.2	195.0
^{1}-?	2.702	975.7	500.3	189.1	188.9
^{1}-?	2.702	976.0	500.3	190.9	190.6
^{1}-?	2.702	975.6	500.1	189.4	189.3
^{1}-?	3.171	948.6	535.0	182.8	159.4

Geometric Summary

State	ΔE	R_1	R_2
$^1\Sigma_g$	0.000	3.414	1.707
^{1}-?	2.555	3.574	1.787
^{1}-?	2.555	3.574	1.787
^{1}-?	2.702	3.572	1.786
^{1}-?	2.702	3.572	1.786
^{1}-?	2.702	3.572	1.786
^{1}-?	3.171	3.447	1.723

Optical Summary

State	ΔE	f
$^1\Sigma_g$	0.000	0.0000
^{1}-?	2.555	0.0000
^{1}-?	2.555	0.0000
^{1}-?	2.702	0.0000
^{1}-?	2.702	0.0000
^{1}-?	2.702	0.0000
^{1}-?	3.171	0.0419

Table 19 Triplet States of Linear Si_2C

Vibrational Summary

State	ΔE	ν_1	ν_2	ν_3	ν_4
^{3}-?	0.000	921.7	505.2	210.4	107.9
^{3}-?	0.173	912.0	518.9	204.4	124.2
^{3}–?	0.310	1085.2	540.1	205.0	94.7
^{3}-?	0.317	1087.3	540.8	532.8	-504.2
^{3}-?	1.731	1337.2	585.5	182.3	176.7

Geometric Summary

State	ΔE	R_1	R_2
^{3}-?	0.000	3.566	1.783
^{3}-?	0.173	3.583	1.792
^{3}–?	0.310	3.439	1.720
^{3}-?	0.317	3.438	1.719
^{3}-?	1.731	3.391	1.695

Optical Summary

State	ΔE	f
^{3}-?	0.000	0.0000
^{3}-?	0.173	0.0000
^{3}–?	0.310	0.0000
^{3}-?	0.317	0.0000
^{3}-?	1.731	0.0161

Table 20 Anion States of Linear Si_2C

Vibrational Summary

State	ΔE	ν_1	ν_2	ν_3	ν_4
^{2}–?	0.000	1132.3	541.4	215.4	125.0
^{2}-?	0.007	1133.8	542.2	495.8	-444.9
^{2}-?	1.750	1393.5	534.2	75.5	-204.2
^{2}-?	1.754	1385.8	555.5	74.2	-178.6
^{2}-?	1.918	1056.9	412.2	280.6	154.5

Geometric Summary

State	ΔE	R_1	R_2
^{2}–?	0.000	3.464	1.732
^{2}-?	0.007	3.463	1.732
^{2}-?	1.750	3.431	1.716
^{2}-?	1.754	3.422	1.711
^{2}-?	1.918	3.627	1.813

Optical Summary

State	ΔE	f
^{2}–?	0.000	0.0000
^{2}-?	0.007	0.0000
^{2}-?	1.750	0.0000
^{2}-?	1.754	0.0998
^{2}-?	1.918	0.0811

Table 21 Cation States of Linear Si_2C

Vibrational Summary

State	ΔE	ν_1	ν_2	ν_3	ν_4
^{2}-?	0.000	1153.9	507.2	68.2	-36.3
^{2}-?	0.000	1155.2	505.8	104.2	92.4
$^2\Sigma_u$	0.324	1206.5	556.9	42.5	42.5
^{2}-?	2.201	1182.4	242.7	242.6	-73.4
^{2}-?	2.554	1081.8	722.7	175.5	174.9

Geometric Summary

State	ΔE	R_1	R_2
^{2}-?	0.000	3.559	1.780
^{2}-?	0.000	3.560	1.780
$^2\Sigma_u$	0.324	3.409	1.704
^{2}-?	2.201	3.505	1.752
^{2}-?	2.554	3.505	1.752

Optical Summary

State	ΔE	f
^{2}-?	0.000	0.0000
^{2}-?	0.000	0.0000
$^2\Sigma_u$	0.324	0.0000
^{2}-?	2.201	0.0288
^{2}-?	2.554	0.0202

Table 22 Ground States of Linear SiC_3 Spin Manifolds

Vibrational Summary

State	ΔE	ν_1 ν_7	ν_2	ν_3	ν_4	ν_5	ν_6
^{2}–?	0.000	1945.8 165.1	1368.0	633.7	455.8	391.7	186.0
$^3\Sigma$	2.649	1984.4 138.8	1323.7	611.6	351.4	351.4	138.8
?–?	3.306	2003.2 105.6	1326.5	605.7	430.6	251.4	164.5
^{2}–?	11.713	2055.1 82.1	1197.6	541.8	308.1	203.8	121.2

Geometric Summary

State	ΔE	R_1	R_2	R_3	R_4	R_5
^{2}–?	0.000	1.711	3.045	1.334	2.624	1.290
$^3\Sigma$	2.649	1.745	3.042	1.296	2.613	1.316
?–?	3.306	1.752	3.051	1.299	2.614	1.315
^{2}–?	11.713	1.830	3.097	1.267	2.622	1.355

Optical Summary

State	ΔE	f
^{2}–?	0.000	0.0000
$^3\Sigma$	2.649	0.0000
?–?	3.306	0.0000
^{2}–?	11.713	0.0000

Table 23 Singlet States of Linear SiC_3

Vibrational Summary

State	ΔE	ν_1 ν_7	ν_2	ν_3	ν_4	ν_5	ν_6
^{1}-?	0.000	2193.3 -1318.0	1471.2	1192.7	675.7	367.2	-424.6
?–?	0.171	2003.2 105.6	1326.5	605.7	430.6	251.4	164.5
^{1}-?	2.368	1836.2 209.0	1092.8	590.5	530.0	421.5	225.5
^{1}-?	3.057	N/A N/A	N/A	N/A	N/A	N/A	N/A
^{1}-?	3.149	1803.0 228.1	1173.4	661.4	521.7	382.9	321.9

Geometric Summary

State	ΔE	R_1	R_2	R_3	R_4	R_5
^{1}-?	0.000	1.686	3.009	1.323	2.574	1.251
?–?	0.171	1.752	3.051	1.299	2.614	1.315
^{1}-?	2.368	1.900	3.169	1.269	2.621	1.352
^{1}-?	3.057	1.625	2.960	1.335	2.624	1.288
^{1}-?	3.149	1.770	3.135	1.365	2.687	1.321

Optical Summary

State	ΔE	f
^{1}-?	0.000	0.0000
?–?	0.171	0.0000
^{1}-?	2.368	0.0017
^{1}-?	3.057	0.0136
^{1}-?	3.149	0.0136

Table 24 Triplet States of Linear SiC_3

Vibrational Summary

State	ΔE	ν_1 ν_7	ν_2	ν_3	ν_4	ν_5	ν_6
$^3\Sigma$	0.000	1984.4 138.8	1323.7	611.6	351.4	351.4	138.8
^{3}-?	1.524	1986.2 -111.8	1479.0	646.7	567.3	462.9	257.4
^{3}-?	1.524	1987.4 152.4	1480.0	647.1	575.5	451.0	174.2
^{3}-?	1.905	1828.5 157.6	1093.9	536.0	506.6	313.4	250.9
^{3}-?	1.907	N/A N/A	N/A	N/A	N/A	N/A	N/A

Geometric Summary

State	ΔE	R_1	R_2	R_3	R_4	R_5
$^3\Sigma$	0.000	1.745	3.042	1.296	2.613	1.316
^{3}-?	1.524	1.704	3.040	1.336	2.580	1.244
^{3}-?	1.524	1.704	3.039	1.336	2.579	1.244
^{3}-?	1.905	1.943	3.199	1.256	2.627	1.370
^{3}-?	1.907	1.934	3.193	1.260	2.634	1.374

Optical Summary

State	ΔE	f
$^3\Sigma$	0.000	0.0000
^{3}-?	1.524	0.0014
^{3}-?	1.524	0.0012
^{3}-?	1.905	0.0013
^{3}-?	1.907	0.0000

Table 25 Anionic States of Linear SiC_3

Vibrational Summary

State	ΔE	ν_1 ν_7	ν_2	ν_3	ν_4	ν_5	ν_6
^{2}–?	0.000	1945.8 165.1	1368.0	633.7	455.8	391.7	186.0
^{2}-?	0.003	1944.4 -772.8	1368.2	892.1	634.2	359.1	-199.9
^{2}-?	1.032	3860.1 -152.1	1119.9	442.3	368.5	365.6	101.2
^{2}-?	1.571	1984.2 56.1	1234.4	510.2	387.7	334.2	148.2
^{2}-?	1.649	2033.3 -375.3	1433.3	631.1	376.1	213.9	-364.6

Geometric Summary

State	ΔE	R_1	R_2	R_3	R_4	R_5
^{2}–?	0.000	1.711	3.045	1.334	2.624	1.290
^{2}-?	0.003	1.710	3.045	1.334	2.625	1.290
^{2}-?	1.032	1.884	3.173	1.290	2.616	1.326
^{2}-?	1.571	1.844	3.134	1.290	2.621	1.331
^{2}-?	1.649	1.665	3.044	1.379	2.616	1.237

Optical Summary

State	ΔE	f
^{2}–?	0.000	0.0000
^{2}-?	0.003	0.0000
^{2}-?	1.032	0.0002
^{2}-?	1.571	0.0000
^{2}-?	1.649	0.0011

Table 26 Cationic States of Linear SiC_3

Vibrational Summary

State	ΔE	ν_1 ν_7	ν_2	ν_3	ν_4	ν_5	ν_6
^{2}-?	0.000	2171.6 -1117.1	1387.0	958.1	605.6	249.1	-274.2
^{2}-?	0.000	2788.6 129.8	1463.0	639.0	506.5	330.7	137.8
^{2}–?	0.401	2055.1 82.1	1197.6	541.8	308.1	203.8	121.2
^{2}-?	2.080	1979.6 132.7	1451.2	582.4	575.1	502.6	162.0
^{2}-?	2.176	N/A N/A	N/A	N/A	N/A	N/A	N/A

Geometric Summary

State	ΔE	R_1	R_2	R_3	R_4	R_5
^{2}-?	0.000	1.776	3.053	1.277	2.571	1.294
^{2}-?	0.000	1.775	3.052	1.277	2.571	1.294
^{2}–?	0.401	1.830	3.097	1.267	2.622	1.355
^{2}-?	2.080	1.785	3.106	1.321	2.558	1.237
^{2}-?	2.176	2.275	3.646	1.371	2.850	1.479

Optical Summary

State	ΔE	f
^{2}-?	0.000	0.0000
^{2}-?	0.000	0.0000
^{2}–?	0.401	0.0000
^{2}-?	2.080	0.0015
^{2}-?	2.176	0.0013

Table 27 Ground States of Linear Si_2C_2 Spin Manifolds

Vibrational Summary

State	ΔE	ν_1 ν_7	ν_2	ν_3	ν_4	ν_5	ν_6
^{2}–?	0.000	1704.2 136.2	955.5	484.6	442.4	383.4	154.5
$^3\Sigma_g$	1.930	1840.5 122.2	883.2	469.9	354.3	354.3	122.2
?–?	2.478	1839.6 97.8	889.4	471.8	421.2	269.3	142.8
^{2}–?	9.450	1978.0 92.9	762.2	440.6	322.2	235.7	114.6

Geometric Summary

State	ΔE	R_1	R_2	R_3
^{2}–?	0.000	1.729	3.040	1.311
$^3\Sigma_g$	1.930	1.754	3.039	1.284
?–?	2.478	1.756	3.042	1.286
^{2}–?	9.450	1.807	3.068	1.261

Optical Summary

State	ΔE	f
^{2}–?	0.000	0.0000
$^3\Sigma_g$	1.930	0.0000
?–?	2.478	0.0000
^{2}–?	9.450	0.0000

Table 28 Singlet States of Linear Si_2C_2

Vibrational Summary

State	ΔE	ν_1 ν_7	ν_2	ν_3	ν_4	ν_5	ν_6
?–?	0.000	1839.6 97.8	889.4	471.8	421.2	269.3	142.8
^{1}-?	0.010	1839.9 -793.6	898.9	890.7	472.3	299.7	-238.3
^{1}-?	1.456	1998.0 73.0	702.8	417.5	343.2	202.6	105.1
^{1}-?	2.672	1786.1 93.9	767.7	420.4	256.7	247.9	97.0
^{1}-?	2.812	1723.1 -233.9	1064.9	524.7	305.0	-107.6	-230.6
^{1}-?	2.949	1366.2 235.1	775.3	520.8	498.6	422.2	272.9
^{1}-?	3.552	1771.2 159.5	1167.0	614.0	592.4	536.6	169.5

Geometric Summary

State	ΔE	R_1	R_2	R_3
?–?	0.000	1.756	3.042	1.286
^{1}-?	0.010	1.755	3.042	1.286
^{1}-?	1.456	1.839	3.095	1.256
^{1}-?	2.672	1.823	3.103	1.280
^{1}-?	2.812	1.694	3.015	1.321
^{1}-?	2.949	1.756	3.131	1.375
^{1}-?	3.552	1.679	2.982	1.303

Optical Summary

State	ΔE	f
?–?	0.000	0.0000
^{1}-?	0.010	0.0000
^{1}-?	1.456	0.0000
^{1}-?	2.672	0.2670
^{1}-?	2.812	0.1962
^{1}-?	2.949	0.0004
^{1}-?	3.552	0.0318

Table 29 Triplet States of Linear Si_2C_2

Vibrational Summary

State	ΔE	ν_1 ν_7	ν_2	ν_3	ν_4	ν_5	ν_6
$^3\Sigma_g$	0.000	1840.5 122.2	883.2	469.9	354.3	354.3	122.2
^{3}-?	1.191	1983.6 92.7	640.5	370.4	270.3	269.3	93.7
^{3}-?	1.191	1983.6 91.4	640.4	370.4	269.2	269.0	91.8
^{3}-?	1.337	2020.0 92.2	643.3	387.7	268.8	268.4	92.3
^{3}-?	2.550	N/A N/A	N/A	N/A	N/A	N/A	N/A
^{3}-?	2.765	1728.0 -190.3	1042.0	525.4	-136.0	-136.1	-187.3
^{3}-?	2.765	1710.1 -70.7	935.1	502.2	462.9	404.3	177.2

Geometric Summary

State	ΔE	R_1	R_2	R_3
$^3\Sigma_g$	0.000	1.754	3.039	1.284
^{3}-?	1.191	1.873	3.118	1.245
^{3}-?	1.191	1.873	3.118	1.245
^{3}-?	1.337	1.867	3.113	1.246
^{3}-?	2.550	1.835	3.126	1.290
^{3}-?	2.765	1.703	3.011	1.308
^{3}-?	2.765	1.703	3.012	1.309

Optical Summary

State	ΔE	f
$^3\Sigma_g$	0.000	0.0000
^{3}-?	1.191	0.0000
^{3}-?	1.191	0.0000
^{3}-?	1.337	0.0000
^{3}-?	2.550	0.3037
^{3}-?	2.765	0.1954
^{3}-?	2.765	0.0000

Table 30 Anionic States of Linear Si_2C_2

Vibrational Summary

State	ΔE	ν_1 ν_7	ν_2	ν_3	ν_4	ν_5	ν_6
^{2}-?	0.000	N/A N/A	N/A	N/A	N/A	N/A	N/A
^{2}–?	0.330	1704.2 136.2	955.5	484.6	442.4	383.4	154.5
^{2}-?	0.333	936.3 -284.8	919.8	453.8	341.3	-211.6	-220.3
^{2}-?	1.103	1759.5 110.9	712.9	349.5	345.6	306.6	114.2
^{2}-?	1.588	N/A N/A	N/A	N/A	N/A	N/A	N/A
^{2}-?	1.732	1828.5 104.8	772.2	410.3	371.0	309.0	124.4
^{2}-?	2.026	1880.1 102.0	795.7	435.6	375.2	305.2	127.7

Geometric Summary

State	ΔE	R_1	R_2	R_3
^{2}-?	0.000	1.868	3.164	1.296
^{2}–?	0.330	1.729	3.040	1.311
^{2}-?	0.333	1.729	3.040	1.311
^{2}-?	1.103	1.837	3.099	1.262
^{2}-?	1.588	1.812	3.083	1.270
^{2}-?	1.732	1.808	3.080	1.272
^{2}-?	2.026	1.799	3.074	1.275

Optical Summary

State	ΔE	f
^{2}-?	0.000	0.0000
^{2}–?	0.330	0.0000
^{2}-?	0.333	0.0001
^{2}-?	1.103	0.0000
^{2}-?	1.588	0.0006
^{2}-?	1.732	0.0000
^{2}-?	2.026	0.0000

Table 31 Cationic States of Linear Si_2C_2

Vibrational Summary

State	ΔE	ν_1 ν_7	ν_2	ν_3	ν_4	ν_5	ν_6
^{2}–?	0.000	1978.0 92.9	762.2	440.6	322.2	235.7	114.6
^{2}-?	0.005	1978.1 -664.1	763.8	737.5	441.2	239.9	-178.7
^{2}-?	1.613	2116.3 -93.9	614.2	388.3	130.8	90.0	89.6
^{2}-?	1.934	1918.4 239.9	527.1	318.8	310.9	308.9	240.0
^{2}-?	2.090	1844.1 128.8	782.0	474.6	388.7	384.9	131.4
^{2}-?	2.265	1141.9 -206.1	836.8	476.8	442.1	411.6	-203.6
^{2}-?	2.520	1919.1 -182.2	1021.3	475.1	372.1	138.3	137.9

Geometric Summary

State	ΔE	R_1	R_2	R_3
^{2}–?	0.000	1.807	3.068	1.261
^{2}-?	0.005	1.807	3.068	1.261
^{2}-?	1.613	1.907	3.145	1.238
^{2}-?	1.934	1.900	3.148	1.248
^{2}-?	2.090	1.741	3.019	1.278
^{2}-?	2.265	1.786	3.184	1.398
^{2}-?	2.520	1.741	3.003	1.263

Optical Summary

State	ΔE	f
^{2}–?	0.000	0.0000
^{2}-?	0.005	0.0000
^{2}-?	1.613	0.1421
^{2}-?	1.934	0.1413
^{2}-?	2.090	0.0000
^{2}-?	2.265	0.0912
^{2}-?	2.520	0.0007

Table 32 Singlet States of Linear SiC_4

Vibrational Summary

State	ΔE	ν_1	ν_2	ν_3	ν_4	ν_5	ν_6
		ν_7	ν_8	ν_9	ν_{10}		
$^1\Sigma$	0.000	2180.7	1886.1	1175.4	571.8	429.1	429.1
		149.9	149.9	83.9	83.9		
^{1}-?	2.092	1927.2	1789.7	1026.6	491.9	317.3	317.1
		200.8	199.8	95.7	93.9		
^{1}-?	2.235	1929.2	1794.7	1028.8	495.5	318.9	318.9
		191.9	191.7	95.7	87.8		
^{1}-?	2.235	1929.4	1794.9	1028.4	495.1	319.0	318.9
		190.7	190.2	94.8	94.2		
^{1}-?	2.558	N/A	N/A	N/A	N/A	N/A	N/A
		N/A	N/A	N/A	N/A		

Geometric Summary

State	ΔE	R_1	R_2	R_3	R_4	R_5	R_6
		R_7	R_8				
$^1\Sigma$	0.000	1.711	2.991	1.280	2.587	3.874	1.307
		2.594	1.287				
^{1}-?	2.092	1.808	3.078	1.269	2.594	3.898	1.324
		2.629	1.304				
^{1}-?	2.235	1.807	3.076	1.269	2.594	3.898	1.325
		2.629	1.304				
^{1}-?	2.235	1.807	3.076	1.269	2.595	3.898	1.325
		2.629	1.304				
^{1}-?	2.558	1.795	3.035	1.240	2.621	3.825	1.381
		2.585	1.204				

Optical Summary

State	ΔE	f
$^1\Sigma$	0.000	0.0000
^{1}-?	2.092	0.0000
^{1}-?	2.235	0.0000
^{1}-?	2.235	0.0000
^{1}-?	2.558	0.0020

Table 33 Ground States of Linear Si_2C_3 Spin Manifolds

Vibrational Summary

State	ΔE	ν_1	ν_2	ν_3	ν_4	ν_5	ν_6
		ν_7	ν_8	ν_9	ν_{10}		
^{2}–?	0.000	1747.9	1498.8	798.5	544.9	475.7	448.4
		272.7	220.4	97.3	87.2		
$^1\Sigma_g$	1.765	2043.8	1574.4	902.0	535.9	535.9	463.8
		199.8	199.8	81.6	81.6		
^{3}–?	3.258	1738.5	1481.8	691.6	511.6	429.8	371.3
		260.4	194.3	79.5	77.5		

Geometric Summary

State	ΔE	R_1	R_2	R_3	R_4
^{2}–?	0.000	1.718	3.022	1.303	2.607
$^1\Sigma_g$	1.765	1.702	2.998	1.297	2.593
^{3}–?	3.258	1.761	3.057	1.296	2.591

Optical Summary

State	ΔE	f
^{2}–?	0.000	0.0000
$^1\Sigma_g$	1.765	0.0000
^{3}–?	3.258	0.0000

Table 34 Singlet States of Linear Si_2C_3

Vibrational Summary

State	ΔE	ν_1	ν_2	ν_3	ν_4	ν_5	ν_6
		ν_7	ν_8	ν_9	ν_{10}		
$^1\Sigma_g$	0.000	2043.8	1574.4	902.0	535.9	535.9	463.8
		199.8	199.8	81.6	81.6		
^{1}-?	1.835	1738.3	1483.4	711.9	451.5	451.3	433.5
		232.5	231.8	85.6	84.2		
^{1}-?	1.974	1740.5	1486.9	721.4	454.9	454.8	433.5
		228.1	227.9	85.7	84.2		
^{1}-?	1.974	N/A	N/A	N/A	N/A	N/A	N/A
		N/A	N/A	N/A	N/A		
^{1}-?	3.683	2129.7	1485.2	771.5	449.0	448.6	416.3
		46.9	18.1	-67.4	-71.9		

Geometric Summary

State	ΔE	R_1	R_2	R_3	R_4
$^1\Sigma_g$	0.000	1.702	2.998	1.297	2.593
^{1}-?	1.835	1.758	3.055	1.296	2.592
^{1}-?	1.974	1.757	3.054	1.297	2.593
^{1}-?	1.974	1.757	3.054	1.297	2.595
^{1}-?	3.683	1.795	3.090	1.296	2.591

Optical Summary

State	ΔE	f
$^1\Sigma_g$	0.000	0.0000
^{1}-?	1.835	0.0000
^{1}-?	1.974	0.0000
^{1}-?	1.974	0.0000
^{1}-?	3.683	0.0000

Table 35 Triplet States of Linear Si_2C_3

Vibrational Summary

State	ΔE	ν_1	ν_2	ν_3	ν_4	ν_5	ν_6
		ν_7	ν_8	ν_9	ν_{10}		
^{3}–?	0.000	1738.5	1481.8	691.6	511.6	429.8	371.3
		260.4	194.3	79.5	77.5		
^{3}-?	0.003	1739.5	1480.1	1234.0	718.5	692.0	428.8
		320.9	-214.0	-516.7	-1445.3		
^{3}-?	0.326	1635.6	1469.8	664.2	436.1	434.8	427.0
		224.1	222.8	83.1	83.0		
^{3}-?	1.615	N/A	N/A	N/A	N/A	N/A	N/A
		N/A	N/A	N/A	N/A		
^{3}-?	1.616	N/A	N/A	N/A	N/A	N/A	N/A
		N/A	N/A	N/A	N/A		

Geometric Summary

State	ΔE	R_1	R_2	R_3	R_4
^{3}–?	0.000	1.761	3.057	1.296	2.591
^{3}-?	0.003	1.761	3.057	1.296	2.592
^{3}-?	0.326	1.764	3.060	1.297	2.593
^{3}-?	1.615	1.836	3.130	1.294	2.589
^{3}-?	1.616	1.832	3.123	1.291	2.582

Optical Summary

State	ΔE	f
^{3}–?	0.000	0.0000
^{3}-?	0.003	0.0000
^{3}-?	0.326	0.0000
^{3}-?	1.615	0.0547
^{3}-?	1.616	0.0367

Table 36 Anionic States of Linear Si_2C_3

Vibrational Summary

State	ΔE	ν_1	ν_2	ν_3	ν_4	ν_5	ν_6
		ν_7	ν_8	ν_9	ν_{10}		
^{2}–?	0.000	1747.9	1498.8	798.5	544.9	475.7	448.4
		272.7	220.4	97.3	87.2		
^{2}-?	0.005	1749.5	1498.8	946.0	799.3	567.2	448.4
		256.7	-154.7	-419.4	-739.5		
^{2}-?	1.324	N/A	N/A	N/A	N/A	N/A	N/A
		N/A	N/A	N/A	N/A		
^{2}-?	1.517	1866.6	1447.7	727.1	464.2	432.3	415.0
		258.6	211.6	86.6	86.3		
^{2}-?	1.782	1964.6	1523.8	827.1	542.5	470.6	439.1
		215.2	84.6	47.4	-74.7		

Geometric Summary

State	ΔE	R_1	R_2	R_3	R_4
^{2}–?	0.000	1.718	3.022	1.303	2.607
^{2}-?	0.005	1.718	3.022	1.303	2.607
^{2}-?	1.324	1.780	3.079	1.299	2.598
^{2}-?	1.517	1.766	3.067	1.301	2.602
^{2}-?	1.782	1.735	3.035	1.301	2.601

Optical Summary

State	ΔE	f
^{2}–?	0.000	0.0000
^{2}-?	0.005	0.0000
^{2}-?	1.324	0.0015
^{2}-?	1.517	0.0000
^{2}-?	1.782	0.0476

Table 37 Ground States of Triangular SiC_2 Spin Manifolds

Vibrational Summary

State	ΔE	ν_1	ν_2	ν_3	ν_4	ν_5	ν_6
$^2B_1$	0.000	1401.6	988.5	832.1	599.1	359.4	323.6
$^1A_1$	2.024	1405.7	1026.1	982.5	660.9	388.5	239.2
$^3B_1$	2.831	1557.5	979.1	834.1	524.9	389.8	143.0
$^2A_1$	10.701	1616.2	1281.0	820.1	551.7	400.2	289.9

Geometric Summary

State	ΔE	R_1	R_2	R_3	R_4
$^2B_1$	0.000	1.909	2.991	1.473	1.433
$^1A_1$	2.024	1.862	2.944	1.486	1.442
$^3B_1$	2.831	1.955	2.937	1.520	1.367
$^2A_1$	10.701	1.959	2.923	1.540	1.360

Optical Summary

State	ΔE	f
$^2B_1$	0.000	0.0000
$^1A_1$	2.024	0.0000
$^3B_1$	2.831	0.0000
$^2A_1$	10.701	0.0000

Table 38 Singlet Excited States of Triangular SiC_2

Vibrational Summary

State	ΔE	ν_1	ν_2	ν_3
$^1A_1$	0.000	1835.9	789.2	95.6
$^1B_1$	2.527	1906.0	590.3	-298.5
$^1B_2$	2.559	1456.1	507.8	491.5
$^1A_2$	3.656	1468.4	470.4	229.2
$^1B_2$	4.071	N/A	N/A	N/A

Geometric Summary

State	ΔE	R_1	R_2
$^1A_1$	0.000	1.852	1.260
$^1B_1$	2.527	2.007	1.248
$^1B_2$	2.559	1.874	1.329
$^1A_2$	3.656	2.061	1.342
$^1B_2$	4.071	1.931	1.340

Optical Summary

State	ΔE	f
$^1A_1$	0.000	0.0000
$^1B_1$	2.527	0.0031
$^1B_2$	2.559	0.0163
$^1A_2$	3.656	0.0000
$^1B_2$	4.071	0.0143

Table 39 Triplet Excited States of Triangular SiC_2

Vibrational Summary

State	ΔE	ν_1	ν_2	ν_3
$^3B_2$	0.000	1560.3	656.5	588.7
$^3A_1$	1.062	1358.1	725.7	487.6
$^3A_2$	1.069	1928.9	323.7	-490.0
$^3B_1$	1.635	1434.1	448.4	289.5
$^3B_1$	3.000	1340.3	671.3	654.6

Geometric Summary

State	ΔE	R_1	R_2
$^3B_2$	0.000	1.891	1.309
$^3A_1$	1.062	1.863	1.358
$^3A_2$	1.069	2.078	1.248
$^3B_1$	1.635	2.038	1.354
$^3B_1$	3.000	1.853	1.373

Optical Summary

State	ΔE	f
$^3B_2$	0.000	0.0000
$^3A_1$	1.062	0.0142
$^3A_2$	1.069	0.0063
$^3B_1$	1.635	0.0029
$^3B_1$	3.000	0.0006

Table 40 Ground States of Bent Si_2C Spin Manifolds

Vibrational Summary

State	ΔE	ν_1	ν_2	ν_3	ν_4	ν_5	ν_6
$^2B_1$	0.000	1401.6	988.5	832.1	599.1	359.4	323.6
$^1A_1$	2.024	1405.7	1026.1	982.5	660.9	388.5	239.2
$^3B_1$	2.831	1557.5	979.1	834.1	524.9	389.8	143.0
$^2A_1$	10.701	1616.2	1281.0	820.1	551.7	400.2	289.9

Geometric Summary

State	ΔE	R_1	R_2	R_3	R_4
$^2B_1$	0.000	1.909	2.991	1.473	1.433
$^1A_1$	2.024	1.862	2.944	1.486	1.442
$^3B_1$	2.831	1.955	2.937	1.520	1.367
$^2A_1$	10.701	1.959	2.923	1.540	1.360

Optical Summary

State	ΔE	f
$^2B_1$	0.000	0.0000
$^1A_1$	2.024	0.0000
$^3B_1$	2.831	0.0000
$^2A_1$	10.701	0.0000

Table 41 Singlet Excited States of Bent Si_2C

Vibrational Summary

State	ΔE	ν_1	ν_2	ν_3
$^1A_1$	0.000	1291.4	728.1	65.5
$^1A_2$	2.558	961.4	498.2	195.1
$^1A_2$	2.705	734.7	453.0	298.1
$^1B_2$	2.705	977.5	501.1	188.0
$^1B_1$	2.801	1176.9	580.8	-133.0
$^1A_1$	3.176	N/A	N/A	N/A

Geometric Summary

State	ΔE	R_1	R_2
$^1A_1$	0.000	3.157	1.709
$^1A_2$	2.558	3.574	1.787
$^1A_2$	2.705	3.572	1.786
$^1B_2$	2.705	3.571	1.785
$^1B_1$	2.801	3.446	1.723
$^1A_1$	3.176	3.421	1.716

Optical Summary

State	ΔE	f
$^1A_1$	0.000	0.0000
$^1A_2$	2.558	0.0000
$^1A_2$	2.705	0.0315
$^1B_2$	2.705	0.0004
$^1B_1$	2.801	0.0356
$^1A_1$	3.176	0.0355

Table 42 Triplet Excited States of Bent Si_2C

Vibrational Summary

State	ΔE	ν_1	ν_2	ν_3
$^3B_2$	0.000	N/A	N/A	N/A
$^3B_1$	0.137	1085.3	540.1	94.6
$^3B_1$	0.143	1085.6	540.0	532.4

Geometric Summary

State	ΔE	R_1	R_2
$^3B_2$	0.000	3.584	1.792
$^3B_1$	0.137	3.439	1.719
$^3B_1$	0.143	3.439	1.720

Optical Summary

State	ΔE	f
$^3B_2$	0.000	0.0008
$^3B_1$	0.137	0.0000
$^3B_1$	0.143	0.0001

Table 43 Ground States of C-C Bonded Rhomboidal SiC_3 Spin Manifolds

Vibrational Summary

State	ΔE	ν_1	ν_2	ν_3	ν_4	ν_5	ν_6
$^2B_1$	0.000	1401.6	988.5	832.1	599.1	359.4	323.6
$^1A_1$	2.024	1405.7	1026.1	982.5	660.9	388.5	239.2
$^3B_1$	2.831	1557.5	979.1	834.1	524.9	389.8	143.0
$^2A_1$	10.701	1616.2	1281.0	820.1	551.7	400.2	289.9

Geometric Summary

State	ΔE	R_1	R_2	R_3	R_4
$^2B_1$	0.000	1.909	2.991	1.473	1.433
$^1A_1$	2.024	1.862	2.944	1.486	1.442
$^3B_1$	2.831	1.955	2.937	1.520	1.367
$^2A_1$	10.701	1.959	2.923	1.540	1.360

Optical Summary

State	ΔE	f
$^2B_1$	0.000	0.0000
$^1A_1$	2.024	0.0000
$^3B_1$	2.831	0.0000
$^2A_1$	10.701	0.0000

Table 44 Singlet States of C-C Bonded Rhomboidal SiC_3

Vibrational Summary

State	ΔE	ν_1	ν_2	ν_3	ν_4	ν_5	ν_6
$^1A_1$	0.000	1405.7	1026.1	982.5	660.9	388.5	239.2
$^1B_1$	0.870	1547.8	1153.3	1054.8	901.8	556.3	348.9
$^1A_2$	1.751	2511.5	1400.7	870.1	827.5	636.3	142.5
$^1A_2$	1.799	2382.0	1061.9	884.2	554.7	527.9	258.3
$^1B_2$	2.988	N/A	N/A	N/A	N/A	N/A	N/A
$^1A_2$	2.994	1559.1	838.5	776.5	475.0	279.4	-530.7
$^1B_1$	4.890	1378.3	1290.5	1040.1	543.3	402.6	-488.5

Geometric Summary

State	ΔE	R_1	R_2	R_3	R_4
$^1A_1$	0.000	1.862	2.944	1.486	1.442
$^1B_1$	0.870	1.982	2.953	1.504	1.349
$^1A_2$	1.751	1.897	2.593	1.959	1.377
$^1A_2$	1.799	1.820	2.775	1.766	1.476
$^1B_2$	2.988	2.144	3.094	1.576	1.353
$^1A_2$	2.994	2.049	3.242	1.363	1.476
$^1B_1$	4.890	1.928	3.066	1.423	1.459

Optical Summary

State	ΔE	f
$^1A_1$	0.000	0.0000
$^1B_1$	0.870	0.0024
$^1A_2$	1.751	0.0011
$^1A_2$	1.799	0.0003
$^1B_2$	2.988	0.0002
$^1A_2$	2.994	0.0022
$^1B_1$	4.890	0.0104

Table 45 Triplet States of C-C Bonded Rhomboidal SiC_3

Vibrational Summary

State	ΔE	ν_1	ν_2	ν_3	ν_4	ν_5	ν_6
$^3B_1$	0.000	1557.5	979.1	834.1	524.9	389.8	143.0
$^3B_2$	0.838	N/A	N/A	N/A	N/A	N/A	N/A
$^3A_2$	1.930	1673.7	1580.8	725.0	-36.1	-194.8	-237.2
$^3B_2$	1.933	6002.3	-7212.7	-9944.9	-10020.4	-16509.3	N/A
$^3A_1$	1.957	1324.2	1033.5	579.6	464.5	365.4	-478.9

Geometric Summary

State	ΔE	R_1	R_2	R_3	R_4
$^3B_1$	0.000	1.955	2.937	1.520	1.367
$^3B_2$	0.838	1.923	2.638	1.920	1.367
$^3A_2$	1.930	2.205	3.160	1.583	1.357
$^3B_2$	1.933	2.052	3.249	1.359	1.478
$^3A_1$	1.957	1.853	2.951	1.466	1.448

Optical Summary

State	ΔE	f
$^3B_1$	0.000	0.0000
$^3B_2$	0.838	0.0012
$^3A_2$	1.930	0.0003
$^3B_2$	1.933	0.0040
$^3A_1$	1.957	0.0000

Table 46 Doublet States of C-C Bonded Rhomboidal SiC_3

Vibrational Summary

State	ΔE	ν_1	ν_2	ν_3	ν_4	ν_5	ν_6
$^2B_1$	0.000	1401.6	988.5	832.1	599.1	359.4	323.6
$^2B_2$	1.605	N/A	N/A	N/A	N/A	N/A	N/A
$^2B_1$	1.834	1530.4	887.8	647.5	526.5	459.0	-799.9
$^2A_2$	2.017	1400.7	959.7	859.9	479.4	113.8	-384.1
$^2B_1$	2.557	1423.8	1001.6	1000.0	592.8	380.9	-190.7

Geometric Summary

State	ΔE	R_1	R_2	R_3	R_4
$^2B_1$	0.000	1.909	2.991	1.473	1.433
$^2B_2$	1.605	1.855	2.825	1.717	1.460
$^2B_1$	1.834	1.966	2.966	1.502	1.374
$^2A_2$	2.017	1.977	3.050	1.503	1.434
$^2B_1$	2.557	1.901	2.987	1.473	1.437

Optical Summary

State	ΔE	f
$^2B_1$	0.000	0.0000
$^2B_2$	1.605	0.0032
$^2B_1$	1.834	0.0057
$^2A_2$	2.017	0.0000
$^2B_1$	2.557	0.0210

Table 47 Doublet States of C-C Bonded Rhomboidal SiC_3

Vibrational Summary

State	ΔE	ν_1	ν_2	ν_3	ν_4	ν_5	ν_6
$^2A_1$	0.000	1616.2	1281.0	820.1	551.7	400.2	289.9
$^2B_1$	1.857	1652.1	1549.6	632.6	353.9	348.5	-627.9
$^2A_1$	1.983	1391.1	1108.5	1015.0	676.9	477.1	259.8
$^2B_2$	2.486	N/A	N/A	N/A	N/A	N/A	N/A
$^2B_1$	2.712	1802.4	1507.3	1000.7	581.3	485.7	-331.9

Geometric Summary

State	ΔE	R_1	R_2	R_3	R_4
$^2A_1$	0.000	1.959	2.923	1.540	1.360
$^2B_1$	1.857	2.178	2.990	1.710	1.306
$^2A_1$	1.983	1.801	2.915	1.478	1.472
$^2B_2$	2.486	2.003	3.235	1.380	1.520
$^2B_1$	2.712	1.918	2.881	1.506	1.347

Optical Summary

State	ΔE	f
$^2A_1$	0.000	0.0000
$^2B_1$	1.857	0.0022
$^2A_1$	1.983	0.0243
$^2B_2$	2.486	0.0031
$^2B_1$	2.712	0.0034

Table 48 Ground States of Si-C Bonded Rhomboidal SiC_3 Spin Manifolds

Vibrational Summary

State	ΔE	ν_1	ν_2	ν_3	ν_4	ν_5	ν_6
$^2A_2$	0.000	1352.3	1097.5	845.9	499.8	429.0	-107.3
$^1A_1$	2.167	1595.3	1148.2	764.2	488.8	378.8	200.2
$^3B_1$	2.482	1366.0	1193.6	696.4	576.6	485.3	228.3
$^2B_2$	11.185	1626.5	1248.4	581.1	493.9	296.9	165.6

Geometric Summary

State	ΔE	R_1	R_2	R_3	R_4
$^2A_2$	0.000	2.023	1.861	2.650	1.366
$^1A_1$	2.167	2.071	1.924	2.619	1.348
$^3B_1$	2.482	1.978	1.989	2.531	1.349
$^2B_2$	11.185	2.074	2.141	2.490	1.335

Optical Summary

State	ΔE	f
$^2A_2$	0.000	0.0000
$^1A_1$	2.167	0.0000
$^3B_1$	2.482	0.0000
$^2B_2$	11.185	0.0000

Table 49 Singlet States of Si-C Bonded Rhomboidal SiC_3

Vibrational Summary

State	ΔE	ν_1	ν_2	ν_3	ν_4	ν_5	ν_6
$^1A_1$	0.000	1595.3	1148.2	764.2	488.8	378.8	200.2
$^1B_1$	1.133	1297.9	1203.0	675.4	560.4	523.5	-353.9
$^1A_2$	1.302	1737.1	1031.6	509.7	244.3	-767.1	-3026.5
$^1A_2$	1.702	2462.2	1292.6	798.5	610.1	437.1	125.2
$^1B_2$	2.489	N/A	N/A	N/A	N/A	N/A	N/A
$^1B_1$	3.462	1348.8	1084.2	911.2	496.6	474.4	321.8
$^1A_2$	4.510	3280.9	2582.6	1994.4	1392.5	1249.1	-1545.6

Geometric Summary

State	ΔE	R_1	R_2	R_3	R_4
$^1A_1$	0.000	2.071	1.924	2.619	1.348
$^1B_1$	1.133	1.978	2.003	2.522	1.348
$^1A_2$	1.302	2.116	2.418	2.315	1.326
$^1A_2$	1.702	2.115	2.236	2.449	1.327
$^1B_2$	2.489	1.917	2.331	2.344	1.427
$^1B_1$	3.462	2.176	1.864	2.697	1.357
$^1A_2$	4.510	2.131	1.997	2.589	1.330

Optical Summary

State	ΔE	f
$^1A_1$	0.000	0.0000
$^1B_1$	1.133	0.0021
$^1A_2$	1.302	0.0000
$^1A_2$	1.702	0.0001
$^1B_2$	2.489	0.0084
$^1B_1$	3.462	0.0119
$^1A_2$	4.510	0.0251

Table 50 Triplet States of Si-C Bonded Rhomboidal SiC_3

Vibrational Summary

State	ΔE	ν_1	ν_2	ν_3	ν_4	ν_5	ν_6
$^3B_1$	0.000	1366.0	1193.6	696.4	576.6	485.3	228.3
$^3B_2$	1.293	N/A	N/A	N/A	N/A	N/A	N/A
$^3A_2$	1.955	1469.3	1448.5	895.3	498.7	304.1	265.1
$^3B_2$	2.486	1282.6	1101.3	532.5	376.6	247.9	152.9
$^3B_2$	2.759	1034.4	992.6	729.7	487.6	363.8	-1165.5

Geometric Summary

State	ΔE	R_1	R_2	R_3	R_4
$^3B_1$	0.000	1.978	1.989	2.531	1.349
$^3B_2$	1.293	2.163	2.247	2.472	1.323
$^3A_2$	1.955	2.096	2.438	2.276	1.325
$^3B_2$	2.486	2.022	1.938	2.644	1.384
$^3B_2$	2.759	2.022	1.938	2.644	1.384

Optical Summary

State	ΔE	f
$^3B_1$	0.000	0.0000
$^3B_2$	1.293	0.0028
$^3A_2$	1.955	0.0000
$^3B_2$	2.486	0.0432
$^3B_2$	2.759	0.0682

Table 51 Doublet States of Si-C Bonded Rhomboidal SiC_3

Vibrational Summary

State	ΔE	ν_1	ν_2	ν_3	ν_4	ν_5	ν_6
$^2A_2$	0.000	1352.3	1097.5	845.9	499.8	429.0	-107.3
$^2B_2$	0.807	1622.9	1191.9	706.2	453.1	150.7	-169.0
$^2A_2$	1.093	4368.3	1230.5	763.1	504.6	415.6	313.2
$^2A_2$	1.443	1222.3	1161.8	643.7	481.2	467.9	-939.1
$^2B_1$	1.585	1523.7	1137.8	796.1	613.9	601.8	470.2

Geometric Summary

State	ΔE	R_1	R_2	R_3	R_4
$^2A_2$	0.000	2.023	1.861	2.650	1.366
$^2B_2$	0.807	2.145	2.027	2.591	1.334
$^2A_2$	1.093	2.095	2.133	2.516	1.338
$^2A_2$	1.443	2.072	2.107	2.516	1.339
$^2B_1$	1.585	1.938	1.912	2.574	1.368

Optical Summary

State	ΔE	f
$^2A_2$	0.000	0.0000
$^2B_2$	0.807	0.0002
$^2A_2$	1.093	0.0000
$^2A_2$	1.443	0.0000
$^2B_1$	1.585	0.0059

Table 52 Doublet States of Si-C Bonded Rhomboidal SiC_3

Vibrational Summary

State	ΔE	ν_1	ν_2	ν_3	ν_4	ν_5	ν_6
$^2B_2$	0.000	1626.5	1248.4	581.1	493.9	296.9	165.6
$^2A_1$	0.896	1390.1	1109.0	1014.4	677.2	477.1	261.0
$^2A_2$	1.911	1482.7	1331.8	772.2	630.1	467.4	342.8
$^2B_2$	2.003	N/A	N/A	N/A	N/A	N/A	N/A
$^2A_2$	2.436	2007.6	1202.8	772.4	711.1	514.5	425.9

Geometric Summary

State	ΔE	R_1	R_2	R_3	R_4
$^2B_2$	0.000	2.074	2.141	2.490	1.335
$^2A_1$	0.896	1.801	2.915	1.478	1.472
$^2A_2$	1.911	1.881	1.921	2.473	1.335
$^2B_2$	2.003	1.960	1.828	2.627	1.365
$^2A_2$	2.436	1.879	1.888	2.518	1.353

Optical Summary

State	ΔE	f
$^2B_2$	0.000	0.0000
$^2A_1$	0.896	0.0016
$^2A_2$	1.911	0.0007
$^2B_2$	2.003	0.0112
$^2A_2$	2.436	0.0000

Table 53 Ground States of Rhomboidal Si_2C_2 Spin Manifolds

Vibrational Summary

State	ΔE	ν_1	ν_2	ν_3	ν_4	ν_5	ν_6
^1A_g	0.000	1114.1	956.8	934.5	492.8	342.9	193.4
$^3B_{2g}$	2.265	1486.6	1239.9	576.8	459.5	353.6	245.3
^2A_g	8.957	1204.8	658.9	462.6	344.4	192.3	-2058.1

Geometric Summary

State	ΔE	R_1	R_2	R_3
^1A_g	0.000	3.422	1.856	1.441
$^3B_{2g}$	2.265	3.492	1.884	1.417
^2A_g	8.957	3.500	1.890	1.427

Optical Summary

State	ΔE	f
^1A_g	0.000	0.0000
$^3B_{2g}$	2.265	0.0000
^2A_g	8.957	0.0000

Table 54 Singlet States of Rhomboidal Si_2C_2

Vibrational Summary

State	ΔE	ν_1	ν_2	ν_3	ν_4	ν_5	ν_6
^1A_g	0.000	1114.1	956.8	934.5	492.8	342.9	193.4
$^1B_{1g}$	2.049	1545.8	1268.7	552.1	384.8	297.3	281.4
$^1B_{2g}$	2.308	2945.1	2914.2	516.5	308.6	-3316.5	-3817.7
$^1B_{2g}$	2.317	3929.7	3684.6	881.9	481.7	-2900.5	-2920.8
$^1B_{3u}$	3.306	967.5	849.0	570.3	491.2	472.9	304.5
^1A_u	3.452	1634.2	1107.1	753.7	330.8	233.8	-77.3

Geometric Summary

State	ΔE	R_1	R_2	R_3
^1A_g	0.000	3.422	1.856	1.441
$^1B_{1g}$	2.049	3.679	1.957	1.335
$^1B_{2g}$	2.308	3.501	1.891	1.431
$^1B_{2g}$	2.317	3.501	1.891	1.431
$^1B_{3u}$	3.306	3.340	1.842	1.554
^1A_u	3.452	3.808	2.014	1.309

Optical Summary

State	ΔE	f
^1A_g	0.000	0.0000
$^1B_{1g}$	2.049	0.0000
$^1B_{2g}$	2.308	0.0000
$^1B_{2g}$	2.317	0.0000
$^1B_{3u}$	3.306	0.0502
^1A_u	3.452	0.0069

Table 55 Triplet States of Rhomboidal Si_2C_2

Vibrational Summary

State	ΔE	ν_1	ν_2	ν_3	ν_4	ν_5	ν_6
$^3B_{2g}$	0.000	1486.6	1239.9	576.8	459.5	353.6	245.3
$^3B_{3g}$	0.706	10801.9	8010.8	7994.6	7197.7	5107.7	4316.8
^3A_u	1.504	8913.0	7067.1	6308.6	378.9	-7356.3	-7369.0

Geometric Summary

State	ΔE	R_1	R_2	R_3
$^3B_{2g}$	0.000	3.492	1.884	1.417
$^3B_{3g}$	0.706	2.927	1.830	2.197
^3A_u	1.504	3.664	1.964	1.415

Optical Summary

State	ΔE	f
$^3B_{2g}$	0.000	0.0000
$^3B_{3g}$	0.706	0.0119
^3A_u	1.504	0.1005

Table 56 Ground States of Rhomboidal Si_3C Spin Manifolds

Vibrational Summary

State	ΔE	ν_1	ν_2	ν_3	ν_4	ν_5	ν_6
$^2A_2$	0.000	923.6	654.9	480.0	285.5	258.2	220.3
$^1A_1$	1.536	1082.0	624.8	495.2	329.4	290.2	178.7
$^3B_1$	2.857	806.5	711.8	473.3	248.6	193.8	-149.6

Geometric Summary

State	ΔE	R_1	R_2	R_3	R_4
$^2A_2$	0.000	1.937	2.444	1.804	3.568
$^1A_1$	1.536	1.971	2.468	1.778	3.522
$^3B_1$	2.857	1.846	2.663	1.806	3.605

Optical Summary

State	ΔE	f
$^2A_2$	0.000	0.0000
$^1A_1$	1.536	0.0000
$^3B_1$	2.857	0.0000

Table 57 Singlet States of Rhomboidal Si_3C

Vibrational Summary

State	ΔE	ν_1	ν_2	ν_3	ν_4	ν_5	ν_6
$^1A_1$	0.000	1082.0	624.8	495.2	329.4	290.2	178.7
$^1B_1$	1.627	842.3	708.4	479.9	253.8	199.7	-187.6
$^1A_2$	2.322	1292.4	766.2	454.4	316.9	308.6	248.9
$^1A_2$	2.792	965.0	613.6	421.5	405.2	107.0	-113.2
$^1B_1$	3.066	N/A	N/A	N/A	N/A	N/A	N/A

Geometric Summary

State	ΔE	R_1	R_2	R_3	R_4
$^1A_1$	0.000	1.971	2.468	1.778	3.522
$^1B_1$	1.627	1.853	2.668	1.802	3.596
$^1A_2$	2.322	1.857	2.383	1.864	3.667
$^1A_2$	2.792	1.964	2.454	1.800	3.559
$^1B_1$	3.066	1.930	2.444	1.804	3.570

Optical Summary

State	ΔE	f
$^1A_1$	0.000	0.0000
$^1B_1$	1.627	0.0003
$^1A_2$	2.322	0.0000
$^1A_2$	2.792	0.0000
$^1B_1$	3.066	0.0269

Table 58 Triplet States of Rhomboidal Si_3C

Vibrational Summary

State	ΔE	ν_1	ν_2	ν_3	ν_4	ν_5	ν_6
$^3B_1$	0.000	806.5	711.8	473.3	248.6	193.8	-149.6
$^3B_2$	0.546	N/A	N/A	N/A	N/A	N/A	N/A
$^3B_2$	1.278	1290.9	943.8	546.8	462.9	335.1	90.5
$^3B_1$	1.280	2067.8	2062.2	474.5	226.4	215.2	-311.3
$^3A_1$	1.346	864.8	698.3	505.5	429.5	276.8	276.1

Geometric Summary

State	ΔE	R_1	R_2	R_3	R_4
$^3B_1$	0.000	1.846	2.663	1.806	3.605
$^3B_2$	0.546	2.158	2.801	1.728	3.455
$^3B_2$	1.278	1.927	2.475	1.807	3.587
$^3B_1$	1.280	1.815	3.144	1.816	3.145
$^3A_1$	1.346	1.855	2.387	1.856	3.656

Optical Summary

State	ΔE	f
$^3B_1$	0.000	0.0000
$^3B_2$	0.546	0.0000
$^3B_2$	1.278	0.0001
$^3B_1$	1.280	0.0022
$^3A_1$	1.346	0.0028

Table 59 Doublet States of Rhomboidal Si_3C^-

Vibrational Summary

State	ΔE	ν_1	ν_2	ν_3	ν_4	ν_5	ν_6
$^2A_2$	0.000	923.6	654.9	480.0	285.5	258.2	220.3
$^2B_2$	0.701	N/A	N/A	N/A	N/A	N/A	N/A
$^2A_2$	1.473	1014.4	700.6	499.6	450.4	191.4	-89.7
$^2B_2$	1.829	N/A	N/A	N/A	N/A	N/A	N/A
$^2B_2$	1.829	1069.0	678.1	474.4	333.4	287.1	-113.4

Geometric Summary

State	ΔE	R_1	R_2	R_3	R_4
$^2A_2$	0.000	1.937	2.444	1.804	3.568
$^2B_2$	0.701	2.220	2.502	1.754	3.418
$^2A_2$	1.473	1.867	2.613	1.812	3.624
$^2B_2$	1.829	1.910	2.486	1.805	3.590
$^2B_2$	1.829	1.912	2.483	1.806	3.591

Optical Summary

State	ΔE	f
$^2A_2$	0.000	0.0000
$^2B_2$	0.701	0.0001
$^2A_2$	1.473	0.0000
$^2B_2$	1.829	0.0878
$^2B_2$	1.829	0.0827

Table 60 Doublet States of Rhomboidal Si_3C^+

Vibrational Summary

State	ΔE	ν_1	ν_2	ν_3	ν_4	ν_5	ν_6
$^2B_2$	0.000	N/A	N/A	N/A	N/A	N/A	N/A
$^2A_1$	0.414	N/A	N/A	N/A	N/A	N/A	N/A
$^2B_1$	0.495	N/A	N/A	N/A	N/A	N/A	N/A
$^2A_2$	1.015	916.3	531.2	396.5	247.1	234.3	155.3

Geometric Summary

State	ΔE	R_1	R_2	R_3	R_4
$^2B_2$	0.000	1.888	2.433	1.833	3.627
$^2A_1$	0.414	1.982	2.550	1.762	3.514
$^2B_1$	0.495	1.927	3.390	1.990	3.454
$^2A_2$	1.015	2.112	2.621	1.857	3.681

Optical Summary

State	ΔE	f
$^2B_2$	0.000	0.0004
$^2A_1$	0.414	0.0043
$^2B_1$	0.495	0.0008
$^2A_2$	1.015	0.0000

Table 61 Ground States of C_{3v} Si_4C Spin Manifolds

Vibrational Summary

State	ΔE	ν_1	ν_2	ν_3	ν_4	ν_5	ν_6
		ν_7	ν_8	ν_9			
^{2}–?	0.000	N/A	N/A	N/A	N/A	N/A	N/A
		N/A	N/A	N/A			
$^1A_1$	1.371	701.8	701.8	648.4	386.1	318.0	285.0
		285.0	238.9	238.9			
^{3}–?	3.323	N/A	N/A	N/A	N/A	N/A	N/A
		N/A	N/A	N/A			

Geometric Summary

State	ΔE	R_1	R_2	R_3	R_4
^{2}–?	0.000	1.896	2.370	3.076	2.463
$^1A_1$	1.371	1.864	2.533	2.920	2.421
^{3}–?	3.323	1.825	2.429	2.889	2.373

Optical Summary

State	ΔE	f
^{2}–?	0.000	0.0000
$^1A_1$	1.371	0.0000
^{3}–?	3.323	0.0000

Table 62 Singlet Excited States of C_{3v} Si_4C

Vibrational Summary

State	ΔE	ν_1	ν_2	ν_3	ν_4	ν_5	ν_6
		ν_7	ν_8	ν_9			
$^1A_1$	0.000	701.8	701.8	648.4	386.1	318.0	285.0
		285.0	238.9	238.9			
^{1}-?	2.040	519.2	418.4	404.7	274.1	181.4	101.3
		61.8	-1164.7	-1165.7			
^{1}-?	2.257	N/A	N/A	N/A	N/A	N/A	N/A
		N/A	N/A	N/A			
^{1}-?	2.258	N/A	N/A	N/A	N/A	N/A	N/A
		N/A	N/A	N/A			
^{1}-?	2.522	N/A	N/A	N/A	N/A	N/A	N/A
		N/A	N/A	N/A			

Geometric Summary

State	ΔE	R_1	R_2	R_3	R_4
$^1A_1$	0.000	1.864	2.533	2.920	2.421
^{1}-?	2.040	1.859	2.266	3.126	2.563
^{1}-?	2.257	1.988	2.298	3.268	2.521
^{1}-?	2.258	1.849	2.296	3.132	2.631
^{1}-?	2.522	1.888	2.545	2.980	2.466

Optical Summary

State	ΔE	f
$^1A_1$	0.000	0.0000
^{1}-?	2.040	0.0002
^{1}-?	2.257	0.0031
^{1}-?	2.258	0.0196
^{1}-?	2.522	0.0245

Table 63 Doublet Excited States of C_{3v} Si_4C^-

Vibrational Summary

State	ΔE
^{2}-?	0.000
^{2}–?	0.047
^{2}-E	0.102
^{2}-?	1.294
^{2}-?	1.359

Geometric Summary

State	ΔE	R_1	R_2	R_3	R_4
^{2}-?	0.000	1.871	2.375	3.023	2.437
^{2}–?	0.047	1.896	2.370	3.076	2.463
^{2}-E	0.102	1.913	2.150	3.179	2.442
^{2}-?	1.294	1.870	2.057	3.180	2.502
^{2}-?	1.359	1.874	2.113	3.171	2.507

Optical Summary

State	ΔE	f
^{2}-?	0.000	0.0008
^{2}–?	0.047	0.0000
^{2}-E	0.102	0.0011
^{2}-?	1.294	0.0042
^{2}-?	1.359	0.0078

Table 64 Ground States of C_{2v} Si_4C Spin Manifolds

Vibrational Summary

State	ΔE	ν_1	ν_2	ν_3	ν_4	ν_5	ν_6
		ν_7	ν_8	ν_9			
$^2A_1$	0.000	921.9	587.0	442.5	410.1	313.2	265.4
		244.3	185.5	177.8			
$^3B_1$	2.981	934.3	597.7	386.8	317.5	270.7	264.3
		260.0	258.9	146.4			

Geometric Summary

State	ΔE	R_1	R_2	R_3	R_4	R_5
$^2A_1$	0.000	2.083	1.823	2.649	2.510	3.546
$^3B_1$	2.981	2.126	1.819	2.976	2.469	3.454

Optical Summary

State	ΔE	f
$^2A_1$	0.000	0.0000
$^3B_1$	2.981	0.0000

Table 65 Singlet Excited States of C_{2v} Si_4C

Vibrational Summary

State	ΔE
$^1B_1$	0.000
$^1B_2$	1.177
$^1B_1$	1.381
$^1B_2$	1.404

Geometric Summary

State	ΔE	R_1	R_2	R_3	R_4	R_5
$^1B_1$	0.000	2.150	1.789	2.966	2.432	3.361
$^1B_2$	1.177	2.090	1.791	2.405	2.953	3.520
$^1B_1$	1.381	2.070	1.833	2.651	2.546	3.592
$^1B_2$	1.404	2.093	1.911	2.486	2.484	3.659

Optical Summary

State	ΔE	f
$^1B_1$	0.000	0.0003
$^1B_2$	1.177	0.0017
$^1B_1$	1.381	0.0002
$^1B_2$	1.404	0.0019

Table 66 Triplet Excited States of C_{2v} Si_4C

Vibrational Summary

State	ΔE	ν_1	ν_2	ν_3	ν_4	ν_5	ν_6
		ν_7	ν_8	ν_9			
$^3B_1$	0.000	934.3	597.7	386.8	317.5	270.7	264.3
		260.0	258.9	146.4			
$^3B_2$	0.036	N/A	N/A	N/A	N/A	N/A	N/A
		N/A	N/A	N/A			
$^3A_2$	1.019	N/A	N/A	N/A	N/A	N/A	N/A
		N/A	N/A	N/A			
$^3B_1$	1.383	N/A	N/A	N/A	N/A	N/A	N/A
		N/A	N/A	N/A			
$^3B_2$	1.394	N/A	N/A	N/A	N/A	N/A	N/A
		N/A	N/A	N/A			

Geometric Summary

State	ΔE	R_1	R_2	R_3	R_4	R_5
$^3B_1$	0.000	2.126	1.819	2.976	2.469	3.454
$^3B_2$	0.036	2.199	1.817	3.068	2.579	3.508
$^3A_2$	1.019	2.073	1.893	2.470	2.467	3.630
$^3B_1$	1.383	2.080	1.876	2.574	2.476	3.603
$^3B_2$	1.394	2.198	1.833	2.268	2.627	3.601

Optical Summary

State	ΔE	f
$^3B_1$	0.000	0.0000
$^3B_2$	0.036	0.0001
$^3A_2$	1.019	0.0000
$^3B_1$	1.383	0.0012
$^3B_2$	1.394	0.0045

Table 67 Doublet Excited States of C_{2v} Si_4C^-

Vibrational Summary

State	ΔE	ν_1	ν_2	ν_3	ν_4	ν_5	ν_6
		ν_7	ν_8	ν_9			
$^2A_1$	0.000	921.9	587.0	442.5	410.1	313.2	265.4
		244.3	185.5	177.8			
$^2A_2$	0.420	N/A	N/A	N/A	N/A	N/A	N/A
		N/A	N/A	N/A			
$^2B_1$	0.781	N/A	N/A	N/A	N/A	N/A	N/A
		N/A	N/A	N/A			
$^2B_2$	1.522	N/A	N/A	N/A	N/A	N/A	N/A
		N/A	N/A	N/A			
$^2A_1$	2.087	N/A	N/A	N/A	N/A	N/A	N/A
		N/A	N/A	N/A			

Geometric Summary

State	ΔE	R_1	R_2	R_3	R_4	R_5
$^2A_1$	0.000	2.083	1.823	2.649	2.510	3.546
$^2A_2$	0.420	2.268	1.775	2.325	2.674	3.501
$^2B_1$	0.781	2.400	1.818	2.695	2.419	3.257
$^2B_2$	1.522	2.173	1.876	2.372	2.473	3.566
$^2A_1$	2.087	2.143	1.861	2.486	2.480	3.559

Optical Summary

State	ΔE	f
$^2A_1$	0.000	0.0000
$^2A_2$	0.420	0.0004
$^2B_1$	0.781	0.0000
$^2B_2$	1.522	0.0039
$^2A_1$	2.087	0.0006

Table 68 Ground States of C_{2v} Si_4C_2 Spin Manifolds

Vibrational Summary

State	ΔE	ν_1	ν_2	ν_3	ν_4	ν_5	ν_6
		ν_7	ν_8	ν_9	ν_{10}	ν_{11}	
$^2B_1$	0.000	1605.4	654.9	540.9	468.1	364.9	331.7
		308.2	188.2	176.8	169.9	138.2	
$^1A_1$	1.008	1645.4	759.0	575.7	458.1	381.3	370.1
		337.5	335.9	285.9	168.6	130.6	
$^3B_1$	2.820	1493.2	697.9	573.6	407.2	394.8	302.0
		251.4	245.6	215.9	215.9	142.7	

Geometric Summary

State	ΔE	R_1	R_2	R_3	R_4	R_5	R_6
$^2B_1$	0.000	2.537	2.599	2.192	1.873	3.047	1.317
$^1A_1$	1.008	2.531	2.514	2.226	1.852	2.988	1.309
$^3B_1$	2.820	3.098	2.602	2.152	1.845	3.001	1.343

Optical Summary

State	ΔE	f
$^2B_1$	0.000	0.0000
$^1A_1$	1.008	0.0000
$^3B_1$	2.820	0.0000

Table 69 Singlet States of C_{2v} Si_4C_2

Vibrational Summary

State	ΔE	ν_1	ν_2	ν_3	ν_4	ν_5	ν_6
		ν_7	ν_8	ν_9	ν_{10}	ν_{11}	
$^1A_1$	0.000	1645.4	759.0	575.7	458.1	381.3	370.1
		337.5	335.9	285.9	168.6	130.6	
$^1B_1$	2.034	N/A	N/A	N/A	N/A	N/A	N/A
		N/A	N/A	N/A	N/A	N/A	
$^1A_2$	2.328	N/A	N/A	N/A	N/A	N/A	N/A
		N/A	N/A	N/A	N/A	N/A	
$^1A_1$	2.585	N/A	N/A	N/A	N/A	N/A	N/A
		N/A	N/A	N/A	N/A	N/A	
$^1B_2$	3.196	N/A	N/A	N/A	N/A	N/A	N/A
		N/A	N/A	N/A	N/A	N/A	

Geometric Summary

State	ΔE	R_1	R_2	R_3	R_4	R_5	R_6
		R_7					
$^1A_1$	0.000	2.531	2.514	2.226	1.852	2.988	1.309
		N/A					
$^1B_1$	2.034	2.615	2.707	2.134	1.840	3.075	1.333
		N/A					
$^1A_2$	2.328	3.323	2.423	2.305	3.507	1.986	2.913
		1.294					
$^1A_1$	2.585	2.227	2.548	2.088	1.739	3.135	1.541
		N/A					
$^1B_2$	3.196	2.425	2.531	2.244	1.869	3.086	1.403
		N/A					

Optical Summary

State	ΔE	f
$^1A_1$	0.000	0.0000
$^1B_1$	2.034	0.0005
$^1A_2$	2.328	0.0000
$^1A_1$	2.585	0.0004
$^1B_2$	3.196	0.0003

Table 70 Triplet States of C_{2v} Si_4C_2

Vibrational Summary

State	ΔE	ν_1	ν_2	ν_3	ν_4	ν_5	ν_6
		ν_7	ν_8	ν_9	ν_{10}	ν_{11}	
$^3B_1$	0.000	1493.2	697.9	573.6	407.2	394.8	302.0
		251.4	245.6	215.9	215.9	142.7	
$^3B_2$	1.045	N/A	N/A	N/A	N/A	N/A	N/A
		N/A	N/A	N/A	N/A	N/A	
$^3B_2$	1.045	N/A	N/A	N/A	N/A	N/A	N/A
		N/A	N/A	N/A	N/A	N/A	
$^3A_2$	1.244	N/A	N/A	N/A	N/A	N/A	N/A
		N/A	N/A	N/A	N/A	N/A	
$^3B_2$	1.624	N/A	N/A	N/A	N/A	N/A	N/A
		N/A	N/A	N/A	N/A	N/A	

Geometric Summary

State	ΔE	R_1	R_2	R_3	R_4	R_5	R_6
$^3B_1$	0.000	3.098	2.602	2.152	1.845	3.001	1.343
$^3B_2$	1.045	2.632	2.511	2.387	1.904	2.978	1.278
$^3B_2$	1.045	2.652	2.562	2.304	1.919	3.013	1.273
$^3A_2$	1.244	2.568	2.612	2.195	1.831	3.102	1.423
$^3B_2$	1.624	2.475	3.013	2.296	1.821	3.112	1.321

Optical Summary

State	ΔE	f
$^3B_1$	0.000	0.0000
$^3B_2$	1.045	0.0008
$^3B_2$	1.045	0.0017
$^3A_2$	1.244	0.0000
$^3B_2$	1.624	0.0001

Table 71 Doublet States of C_{2v} $Si_4C_2^-$

Vibrational Summary

State	ΔE	ν_1	ν_2	ν_3	ν_4	ν_5	ν_6
		ν_7	ν_8	ν_9	ν_{10}	ν_{11}	
$^2B_1$	0.000	1605.4	654.9	540.9	468.1	364.9	331.7
		308.2	188.2	176.8	169.9	138.2	
$^2B_1$	0.236	N/A	N/A	N/A	N/A	N/A	N/A
		N/A	N/A	N/A	N/A	N/A	
$^2B_1$	0.682	N/A	N/A	N/A	N/A	N/A	N/A
		N/A	N/A	N/A	N/A	N/A	
$^2B_1$	0.981	N/A	N/A	N/A	N/A	N/A	N/A
		N/A	N/A	N/A	N/A	N/A	
$^2A_1$	1.569	N/A	N/A	N/A	N/A	N/A	N/A
		N/A	N/A	N/A	N/A	N/A	

Geometric Summary

State	ΔE	R_1	R_2	R_3	R_4	R_5	R_6
		R_7					
$^2B_1$	0.000	2.537	2.599	2.192	1.873	3.047	1.317
		N/A					
$^2B_1$	0.236	2.265	2.900	2.190	1.899	3.248	1.409
		N/A					
$^2B_1$	0.682	2.720	2.406	2.487	3.832	1.940	2.945
		1.281					
$^2B_1$	0.981	2.458	2.519	2.255	1.852	2.995	1.314
		N/A					
$^2A_1$	1.569	2.567	2.577	2.356	1.834	2.998	1.331
		N/A					

Optical Summary

State	ΔE	f
$^2B_1$	0.000	0.0000
$^2B_1$	0.236	0.0002
$^2B_1$	0.682	0.0010
$^2B_1$	0.981	0.0034
$^2A_1$	1.569	0.0022

Table 72 Ground States of Distorted Si_4C_2 Spin Manifolds

Vibrational Summary

State	ΔE	ν_1	ν_2	ν_3	ν_4	ν_5	ν_6
		ν_7	ν_8	ν_9	ν_{10}	ν_{11}	
^{2}-A'	0.000	1043.2	828.2	774.3	494.2	426.0	320.0
		301.9	226.1	222.0	170.0	154.8	
^{1}-A'	2.072	1055.3	855.7	732.7	529.9	418.3	317.8
		274.6	237.2	204.8	65.0	-276.1	
^{3}-A'	3.096	1066.5	773.5	764.8	470.1	363.8	289.2
		255.1	226.7	210.6	144.6	119.9	

Geometric Summary

State	ΔE	R_1	R_2	R_3	R_4	R_5	R_6
		R_7	R_8	R_9			
^{2}-A'	0.000	2.691	2.523	3.654	1.844	2.733	2.586
		2.154	1.887	1.512			
^{1}-A'	2.072	3.038	2.558	3.586	1.790	2.810	2.553
		2.180	1.885	1.544			
^{3}-A'	3.096	2.981	2.492	3.726	1.856	2.818	3.115
		2.133	1.870	1.509			

Optical Summary

State	ΔE	f
^{2}-A'	0.000	0.0000
^{1}-A'	2.072	0.0000
^{3}-A'	3.096	0.0000

Table 73 Singlet Excited States of Distorted Si_4C_2

Vibrational Summary

State	ΔE	ν_1	ν_2	ν_3	ν_4	ν_5	ν_6
		ν_7	ν_8	ν_9	ν_{10}	ν_{11}	
^{1}-A'	0.000	1055.3	855.7	732.7	529.9	418.3	317.8
		274.6	237.2	204.8	65.0	-276.1	
^{1}-A'	1.321	N/A	N/A	N/A	N/A	N/A	N/A
		N/A	N/A	N/A	N/A	N/A	
^{1}-A"	1.552	N/A	N/A	N/A	N/A	N/A	N/A
		N/A	N/A	N/A	N/A	N/A	
^{1}-A"	2.010	N/A	N/A	N/A	N/A	N/A	N/A
		N/A	N/A	N/A	N/A	N/A	
^{1}-A'	2.716	N/A	N/A	N/A	N/A	N/A	N/A
		N/A	N/A	N/A	N/A	N/A	

Geometric Summary

State	ΔE	R_1	R_2	R_3	R_4	R_5	R_6
		R_7	R_8	R_9			
^{1}-A'	0.000	3.038	2.558	3.586	1.790	2.810	2.553
		2.180	1.885	1.544			
^{1}-A'	1.321	2.932	2.514	3.724	1.851	2.800	2.888
		2.087	1.882	1.505			
^{1}-A"	1.552	2.522	2.668	3.754	1.895	2.700	2.705
		2.184	1.895	1.466			
^{1}-A"	2.010	2.642	2.606	3.796	1.876	2.698	2.744
		2.138	1.956	1.422			
^{1}-A'	2.716	2.685	2.541	3.718	1.830	2.790	2.577
		2.023	1.926	1.651			

Optical Summary

State	ΔE	f
^{1}-A'	0.000	0.0000
^{1}-A'	1.321	0.0001
^{1}-A"	1.552	0.0000
^{1}-A"	2.010	0.0114
^{1}-A'	2.716	0.0016

Table 74 Triplet Excited States of Distorted Si_4C_2

Vibrational Summary

State	ΔE	ν_1	ν_2	ν_3	ν_4	ν_5	ν_6
		ν_7	ν_8	ν_9	ν_{10}	ν_{11}	
^{3}-A'	0.000	1066.5	773.5	764.8	470.1	363.8	289.2
		255.1	226.7	210.6	144.6	119.9	
^{3}-A"	0.450	N/A	N/A	N/A	N/A	N/A	N/A
		N/A	N/A	N/A	N/A	N/A	
^{3}-A'	0.524	N/A	N/A	N/A	N/A	N/A	N/A
		N/A	N/A	N/A	N/A	N/A	
^{3}-A'	1.283	N/A	N/A	N/A	N/A	N/A	N/A
		N/A	N/A	N/A	N/A	N/A	
^{3}-A'	1.472	N/A	N/A	N/A	N/A	N/A	N/A
		N/A	N/A	N/A	N/A	N/A	

Geometric Summary

State	ΔE	R_1	R_2	R_3	R_4	R_5	R_6
		R_7	R_8	R_9			
^{3}-A'	0.000	2.981	2.492	3.726	1.856	2.818	3.115
		2.133	1.870	1.509			
^{3}-A"	0.450	2.622	2.622	3.779	1.981	2.838	2.739
		2.173	1.837	1.575			
^{3}-A'	0.524	2.525	2.579	3.739	1.883	2.683	2.694
		2.157	1.903	1.445			
^{3}-A'	1.283	2.502	2.614	3.579	1.939	2.779	2.501
		2.133	1.701	1.585			
^{3}-A'	1.472	2.583	2.593	3.603	1.845	2.771	2.379
		2.022	1.815	1.656			

Optical Summary

State	ΔE	f
^{3}-A'	0.000	0.0000
^{3}-A"	0.450	0.0000
^{3}-A'	0.524	0.0002
^{3}-A'	1.283	0.0012
^{3}-A'	1.472	0.0013

Table 75 Doublet Excited States of Distorted $Si_4C_2^-$

Vibrational Summary

State	ΔE	ν_1	ν_2	ν_3	ν_4	ν_5	ν_6
		ν_7	ν_8	ν_9	ν_{10}	ν_{11}	
^{2}-A'	0.000	1043.2	828.2	774.3	494.2	426.0	320.0
		301.9	226.1	222.0	170.0	154.8	
^{2}-A'	1.575	N/A	N/A	N/A	N/A	N/A	N/A
		N/A	N/A	N/A	N/A	N/A	
^{2}-A"	1.779	N/A	N/A	N/A	N/A	N/A	N/A
		N/A	N/A	N/A	N/A	N/A	
^{2}-A'	1.842	N/A	N/A	N/A	N/A	N/A	N/A
		N/A	N/A	N/A	N/A	N/A	
^{2}-A'	1.975	N/A	N/A	N/A	N/A	N/A	N/A
		N/A	N/A	N/A	N/A	N/A	

Geometric Summary

State	ΔE	R_1	R_2	R_3	R_4	R_5	R_6
		R_7	R_8	R_9			
^{2}-A'	0.000	2.691	2.523	3.654	1.844	2.733	2.586
		2.154	1.887	1.512			
^{2}-A'	1.575	2.763	2.464	3.760	1.897	2.773	2.855
		2.109	1.890	1.481			
^{2}-A"	1.779	2.630	2.661	3.876	1.932	2.716	2.784
		2.141	1.973	1.387			
^{2}-A'	1.842	2.853	2.576	3.764	1.876	2.838	2.846
		2.137	1.906	1.591			
^{2}-A'	1.975	2.515	2.624	3.853	1.979	2.735	2.712
		2.095	1.906	1.417			

Optical Summary

State	ΔE	f
^{2}-A'	0.000	0.0000
^{2}-A'	1.575	0.0005
^{2}-A"	1.779	0.0090
^{2}-A'	1.842	0.0041
^{2}-A'	1.975	0.0002

Table 76 Ground States of C_{2v} Si_4C_4 Spin Manifolds

Vibrational Summary

State	ΔE	ν_1	ν_2	ν_3	ν_4	ν_5	ν_6
		ν_7	ν_8	ν_9	ν_{10}	ν_{11}	
$^2B_2$	0.000	1353.5	1270.9	910.8	850.9	311.9	268.7
		206.6	203.7	168.0	151.2	48.3	
$^1A_1$	2.253	1322.9	1250.0	893.6	871.5	312.8	309.2
		217.7	179.1	128.1	99.9	77.2	
$^3A_1$	3.498	1387.5	1130.4	949.0	877.0	254.5	226.3
		193.5	168.4	138.6	86.3	44.5	

Geometric Summary

State	ΔE	R_1	R_2	R_3	R_4	R_5	R_6
		R_7	R_8				
$^2B_2$	0.000	3.705	3.866	1.900	3.003	1.854	2.740
		1.398	3.076				
$^1A_1$	2.253	3.737	3.141	1.897	2.832	1.844	2.723
		1.406	3.065				
$^3A_1$	3.498	3.727	3.702	1.905	2.955	1.864	2.895
		1.379	3.207				

Optical Summary

State	ΔE	f
$^2B_2$	0.000	0.0000
$^1A_1$	2.253	0.0000
$^3A_1$	3.498	0.0000

Table 77 Singlet Excited States of C_{2v} Si_4C_4

Vibrational Summary

State	ΔE	ν_1	ν_2	ν_3	ν_4	ν_5	ν_6
		ν_7	ν_8	ν_9	ν_{10}	ν_{11}	
$^1A_1$	0.000	1322.9	1250.0	893.6	871.5	312.8	309.2
		217.7	179.1	128.1	99.9	77.2	
$^1B_2$	1.671	N/A	N/A	N/A	N/A	N/A	N/A
		N/A	N/A	N/A	N/A	N/A	
$^1B_1$	1.712	N/A	N/A	N/A	N/A	N/A	N/A
		N/A	N/A	N/A	N/A	N/A	
$^1A_1$	1.744	N/A	N/A	N/A	N/A	N/A	N/A
		N/A	N/A	N/A	N/A	N/A	
$^1A_2$	2.058	N/A	N/A	N/A	N/A	N/A	N/A
		N/A	N/A	N/A	N/A	N/A	

Geometric Summary

State	ΔE	R_1	R_2	R_3	R_4	R_5	R_6
		R_7	R_8				
$^1A_1$	0.000	3.737	3.141	1.897	2.832	1.844	2.723
		1.406	3.065				
$^1B_2$	1.671	3.630	3.541	1.836	2.904	1.828	2.710
		1.429	3.064				
$^1B_1$	1.712	3.720	3.597	1.904	2.914	1.849	2.614
		1.352	2.942				
$^1A_1$	1.744	3.730	3.533	1.904	2.925	1.866	2.796
		1.395	3.125				
$^1A_2$	2.058	3.828	3.612	1.963	2.944	1.898	2.630
		1.332	2.948				

Optical Summary

State	ΔE	f
$^1A_1$	0.000	0.0000
$^1B_2$	1.671	0.0051
$^1B_1$	1.712	0.0004
$^1A_1$	1.744	0.0015
$^1A_2$	2.058	0.0000

Table 78 Triplet Excited States of C_{2v} Si_4C_4

Vibrational Summary

State	ΔE	ν_1	ν_2	ν_3	ν_4	ν_5	ν_6
		ν_7	ν_8	ν_9	ν_{10}	ν_{11}	
$^3B_2$	0.000	N/A	N/A	N/A	N/A	N/A	N/A
		N/A	N/A	N/A	N/A	N/A	
$^3A_1$	0.154	1387.5	1130.4	949.0	877.0	254.5	226.3
		193.5	168.4	138.6	86.3	44.5	
$^3B_2$	1.135	N/A	N/A	N/A	N/A	N/A	N/A
		N/A	N/A	N/A	N/A	N/A	
$^3B_2$	1.232	N/A	N/A	N/A	N/A	N/A	N/A
		N/A	N/A	N/A	N/A	N/A	
$^3A_2$	1.278	N/A	N/A	N/A	N/A	N/A	N/A
		N/A	N/A	N/A	N/A	N/A	

Geometric Summary

State	ΔE	R_1	R_2	R_3	R_4	R_5	R_6
		R_7	R_8				
$^3B_2$	0.000	3.755	3.581	1.933	2.938	1.857	2.885
		1.367	3.193				
$^3A_1$	0.154	3.727	3.702	1.905	2.955	1.864	2.895
		1.379	3.207				
$^3B_2$	1.135	3.831	3.369	1.937	2.899	1.908	2.885
		1.381	3.199				
$^3B_2$	1.232	3.777	3.554	1.937	2.949	1.868	2.811
		1.392	3.137				
$^3A_2$	1.278	3.730	3.607	2.005	3.075	1.731	2.890
		1.508	3.260				

Optical Summary

State	ΔE	f
$^3B_2$	0.000	0.0000
$^3A_1$	0.154	0.0000
$^3B_2$	1.135	0.0133
$^3B_2$	1.232	0.0182
$^3A_2$	1.278	0.0065

Table 79 Doublet Excited States of C_{2v} $Si_4C_4^-$

Vibrational Summary

State	ΔE	ν_1	ν_2	ν_3	ν_4	ν_5	ν_6
		ν_7	ν_8	ν_9	ν_{10}	ν_{11}	
$^2B_2$	0.000	1353.5	1270.9	910.8	850.9	311.9	268.7
		206.6	203.7	168.0	151.2	48.3	
$^2B_2$	0.694	N/A	N/A	N/A	N/A	N/A	N/A
		N/A	N/A	N/A	N/A	N/A	
$^2B_1$	1.425	N/A	N/A	N/A	N/A	N/A	N/A
		N/A	N/A	N/A	N/A	N/A	
$^2B_2$	1.597	N/A	N/A	N/A	N/A	N/A	N/A
		N/A	N/A	N/A	N/A	N/A	
$^2A_2$	1.777	N/A	N/A	N/A	N/A	N/A	N/A
		N/A	N/A	N/A	N/A	N/A	

Geometric Summary

State	ΔE	R_1	R_2	R_3	R_4	R_5	R_6
		R_7	R_8				
$^2B_2$	0.000	3.705	3.866	1.900	3.003	1.854	2.740
		1.398	3.076				
$^2B_2$	0.694	3.775	3.307	1.959	2.891	1.824	2.775
		1.367	3.093				
$^2B_1$	1.425	3.733	3.855	1.884	2.972	1.944	2.723
		1.371	3.049				
$^2B_2$	1.597	3.776	3.208	1.913	2.849	1.883	2.842
		1.390	3.164				
$^2A_2$	1.777	3.772	3.347	1.905	2.871	1.884	2.741
		1.379	3.068				

Optical Summary

State	ΔE	f
$^2B_2$	0.000	0.0000
$^2B_2$	0.694	0.0038
$^2B_1$	1.425	0.0000
$^2B_2$	1.597	0.0056
$^2A_2$	1.777	0.0000

Bibliography

1. Information about the Aeronautical Systems Center Mean Shared Resource Center can be found online at: http://www.asc.hpc.mil/
2. S. Alberty, Principles of Physical Chemistry.
3. J. Anglada et. al. "Low-lying Electronci States of CSi^- and Electron Affinity of CSi According to Ab-Initio MRD-CI Calculation." J. Phys. B.: At. Mol. Phys. 16:2469, 1983.
4. A.J. Apponi et. al. "Astronomical Detection of Rhomboidal SiC_3." Astrophys. J., 516:L103, 1999.
5. K. Balasubramian. "Relativistic Effects in Chemistry Part A." John Wiley and Sons, New York, 1997.
6. V. Barone. "Recent Advances in Density Functional Methods." World Scientific, New Jersey, 2002.
7. R. Bauernschmidtt, R. Ahlrichs. "Treatment of electronic excitations within the adiabatic approximation of time dependant density functional theory." Chem. Phys. L. 256:454.
8. P.F. Bernath et. al. "Theoretical Prediction and Experimental Deteaction of the SiC Molecule." Physical Review Letters 60:197 (1988)
9. A.D. Boese, N.L. Doltsinis, N.C. Handy, and M. Sprik. "New generalized gradient approximation functionals." J. Chem. Phys. 112:1670.
10. C.R. Brazier et al. "The A 3Σ-X 3Π transition of the SiC radical." J. Chem. Phys. 91:7384 (1989).
11. T. J. Butenhoff and E.A. Rohlfing. "The $C^3\Pi$-$X^3\Pi$ band system of the SiC radical." J. Chem. Phys. 95:3939.
12. Z.-L. Cai, J.P. Francois. "Theoretical Study fo the SiC^- Anion." J.Phys.Chem. A 103:1007, 1999.
13. D.M. Ceperly, B.J Alder. "Ground State of the Electron Gas by a Stochastic Method." Phys Rev Lett, 45:566, 1980
14. Chen, Peter. Article in "Unimolecular and Bimolecular Ion-Molecule Reaction Dynamics", Cheuk-Yiu Ng, John Wiley and Sons, New York, 1994.
15. D.P. Chong. "Recent Advances in Density Functional Methods." Singapore, World Scientific.

16. C. Cohen-Tannoudji, D. Diu, F. Laloe. "Quantum Mechanics." John Wiley and Sons, New York, 1977.

17. G.E. Davico, R.L. Schwartz, W.C. Lineberger. "Photoelectron spectroscopy of C_3Si and C_4Si_2 anions." J. Chem. Phys., 115:1789, 2001.

18. A.K. Dhara, S.K. Ghosh. "Density Functional Theory for Time Dependent Systems." Phys Rev A, 35:442, 1987.

19. X. Ding et al. Fourier Transform Infrared Observation of SiC_n Chains, I, The ν_4 Mode of Linear SiC_9. J. Chem. Phys. 110(23):11214, 1999.

20. X. Duan, L. W. Burggraf, D. E. Weeks, G. E. Davico, and R. L. Schwartz. "Photoelectron spectroscopy of $Si_2C_3^-$ and quantum chemistry of the linear Si_2C_3 cluster and its isomers." J. Chem. Phys., 116:3601, 2002.

21. X. Duan. "Mapping Ground State Properties of SimCn (m,n = 1-4) Neutral and Anionic Clusters with Quantum Mechanism Methods." Unpublished.

22. Dunning, Thom H. Jr. Gaussian basis sets for use in correlated molecular calculations. I. The atoms boron through neon and hydrogen, Journal of Chemical Physics. 90: 1007-1023 (15 January 1989).

23. Dunning,Thom. H., Jr., Gaussian Basis Functions for Use in Molecular Calculations. III. Contraction of (10s6p) Atomic Basis Sets for the First- Row Atoms, Journal of Chemical Physics. 55: 716-723 (15 July 1971).

24. K. Ervin, J. Ho, and W.C. Lineberger. "A study of the singlet and triplet states of vinylidene by photoelectron spectroscopy of H2C2, D2C2- and HDC2-. Vinylidine-acetylene isomerization." J. Chem. Phys., 91:5974.

25. F. Furche and R. Ahlrichs. "Adiabatic time dependant density functional methods for excited state properties." J. Chem. Phys., 117:7433, 2002.

26. Gaussian 03, Revision A.1, M. J. Frisch, G. W. Trucks, H. B. Schlegel, G. E. Scuseria, M. A. Robb, J. R. Cheeseman, J. A. Montgomery, Jr., T. Vreven, K. N. Kudin, J. C. Burant, J. M. Millam, S. S. Iyengar, J. Tomasi, V. Barone, B. Mennucci, M. Cossi, G. Scalmani, N. Rega, G. A. Petersson, H. Nakatsuji, M. Hada, M. Ehara, K. Toyota, R. Fukuda, J. Hasegawa, M. Ishida, T. Nakajima, Y. Honda, O. Kitao, H. Nakai, M. Klene, X. Li, J. E. Knox, H. P. Hratchian, J. B. Cross, C. Adamo, J. Jaramillo, R. Gomperts, R. E. Stratmann, O. Yazyev, A. J. Austin, R. Cammi, C. Pomelli, J. W. Ochterski, P. Y. Ayala, K. Morokuma, G. A. Voth, P. Salvador, J. J. Dannenberg, V. G. Zakrzewski, S. Dapprich, A. D. Daniels, M. C. Strain, O. Farkas, D. K. Malick, A. D. Rabuck, K. Raghavachari, J. B. Foresman, J. V. Ortiz, Q. Cui, A. G. Baboul, S. Clifford, J. Cioslowski, B. B. Stefanov, G. Liu, A. Liashenko, P. Piskorz, I. Komaromi, R. L. Martin, D. J. Fox, T. Keith, M. A. Al-Laham, C. Y. Peng, A. Nanayakkara, M. Challacombe,

P. M. W. Gill, B. Johnson, W. Chen, M. W. Wong, C. Gonzalez, and J. A. Pople, Gaussian, Inc., Pittsburgh PA, 2003.

27. V.D. Gordon et. al. Structures of the linear silicon carbides SiC_4 and SiC_6: Isotopic substitution and Ab Initio theory. J. Chem. Phys., 113:5311, 2000.

28. E.K.U. Gross, R.M. Dreizler. "Density Functional Theory." Plenum Press, New York, 1995.

29. M. Grutter, et. al. "Electronic Absorption Spectra of SiC^- and SiC in Neon Matrices." J. Phys. Chem A, 101:275, 1997.

30. H. Heinze, A. Gorling and N. Rosch. "An Efficient Method For Calculating Molecular Excitation Energies by Time Dependent Density Functional Theory." Journ. Chem. Phys. 113:2088, 2000.

31. Henry, Jean W. Use of Quantum Mechanical Calculations to Investigate Small Silicon Carbide Clusters. MS thesis, AFIT/GAP/ENP/01M-04. Graduate School of Engineering and Management, Air Force Institute of Technology (AU), Wright-Patterson AFB OH, March 2001 (AD-A392522).

32. Hohenberg, P. and W. Kohn. Inhomogeneous Electron Gas, Physical Review. 136B: B864-B871 (9 November 1964).

33. S. Hunsicker and R.O. Jones. "Structure and bonding in mixed silicon-carbon clusters and their anions." J. Chem. Phys., 105:5048, 1996.

34. J.D. Jackson. "Classical Electrodynamics: Third Edition." John Wiley and Sons, New York, 1999.

35. Y. Jung, Y. Akinaga, K.D. Jordan, M.S. Gordon. "An ab-initio study of the structure of the two-, three-, and five-dimer silicon clusters: An approach to the Si(100) surface." Theor. Chem. Acc. 109:268.

36. W. Koch, M. Holthausen. "A Chemist's Guide to Density Functional Theory." Wiley-VCH, 2001.

37. W. Kohn, L.J. Sham. "Self Consistent Equations Including Exchange and Correlation Effects." Phys Rev A 140:1133, 1965.

38. M. Larsson. "The X $^3\Pi$, $B^3\Sigma$, and $C^3\Pi$ states of SiC according to ab-initio CASSCF-CCI calculations. J. Phys. B.: At. Mol. Phys, 19:L261, 1986.

39. A. Masunov. "Where Density Functional Theory Goes Wrong and How to Fix it. Spin Balanced UKS Formalism." Los Alamos National Laboratory Archive.

40. "Materials Science Annual Report 1998", www.ifm.liu.se/matephys/AAnew/research/annrep/annrep98/arepsic.htm

41. D. Mearns, W. Kohn. "Frequency-Dependent v-Representability in Density Functional Theory." Phys Rev A, 35:4796, 1987.

42. P.W. Merrill, Publ. Astronom. Soc. Pac. 38 :175 (1926).

43. D.L. Michalopoulos, M.E. Geusic, P.R.R. Langridge-Smith, and R.E. Smalley. "Visible Spectroscopy of jet cooled SiC_2: Geometry and electronic structure." J. Chem. Phys. 80:3556, 1984.

44. M.C. McCarthy et. al. "Laboratory Detection of Five New Linear Silicon Carbides." Astropys. J., 538:766, 2000.

45. A. Nagy. "Density functional theory and applications to atoms and molecules." Institute of Theoretical Physics, Elsevier, 1998. Physics Reports 298:1.

46. A. Nakajima et. al. "Photoelectron Spectroscopy of Silicon-Carbon Cluster Anions." J. Chem. Phys. 103(6):2050 1995.

47. National Institute of Standards and Technology Chemistry WebBook, webbook.nist.gov/chemistry

48. A.V. Orden, T.F. Giesen, R.A. Provencal, H.J. Hwang, and R.J Saykally. "Characterization of silicon-carbon clusters by infrared laser spectroscopy: The v3(sigma sub u) band of linear Si2C3."

49. R.G. Parr, W. Yang. "Density Functional Theory of Atoms and Molecules." Oxford University Press, New York, 1989.

50. L.M. Raff. "Principles of Physical Chemistry." Prentice Hall, Upper Saddle River, New Jersey, 2001.

51. K. Raghavachari. Theoretical study of small silicon clusters: Equilibrium geometries and electronic structures of Si_n (n=2-7, 10), Journal of Chemical Physics. 84: 5672-5686 (15 May 1986).

52. C.M. Rholfing, R.L. Martin. "A Theoretical Study of the Isovalent Diatomics C_2, Si_2, and SiC." J. Phys. Chem. 90:2043, 1986.

53. J. Rintelman, M. Gordon. "Structure and energetics of the silicon carbide clusters SiC3 and Si2C2." J Chem Phys, 115:1795, 2001.

54. Roberts, John. Quantum Mechanical Calculations of Monoxides of Silicon Carbide Molecules.

55. E. Runge, E.K.U. Gross. "Density Functional Theory for Time Dependent Systems." Phys Rev Lett, 52:997, 1984.

56. K.W. Sattlemeyer, H.F. Schaeffer, J.F. Stanton. "The Global Minimum Structure of SiC_3: The Controversy Continues." J.Chem.Phys., 116(21):9151, 2002.

57. G.Schaftenaar and J.H. Noordik, "Molden: a pre- and post-processing program for molecular and electronic structures", J. Comput.-Aided Mol. Design, 14 (2000) 123-134.

58. Second International High Temperature Electronics Conference, Session I, Charlotte, NC, June 5-10, 1994.

59. J.M. Seminario. "Recent Developments and Applications of Modern Density Functional Theory." Elsevier Science B.V.

60. J.R.Shoemaker, L.W.Burggraf, M.S.Gordon. J.Phys.Chem.A 103, 3245-51(1999).

61. A. Spielfiedel et. al. "Theoretical Study of the Electronic States of Si_2C." J. Phys. Chem., 100:10055, 1996.

62. Szabo, Attila and Neil S. Ostlund. Modern Quantum Chemistry: Introduction to Advanced Structure Theory. Mineola NY: 1996.

63. D.J. Wales. "Electronic Structure of Small Silicon Clusters."

64. A.P. Young, J. Jones, and L.J. Brillson. "Low Energy Cathodoluminescence Spectroscopy of Etched 6H-SiC Surfaces." J. Vac. Sic. Technol. A., 17(5):2692, 1999.

65. A Zangwill, P. Soven. "Density Functional Approach to Local Field Effects in Finite Systems." Phys. Rev. A 21:1561, 1980.

66. C. Zhao and K. Balasubramanian. "Geometries and spectroscopic properties of silicon clusters." J. Chem. Phys. 116:3690.

REPORT DOCUMENTATION PAGE

Form Approved
OMB No. 074-0188

1. REPORT DATE *(DD-MM-YYYY)*	**2. REPORT TYPE**	**3. DATES COVERED** *(From – To)*
06/15/03	Master's Thesis	June 2003 - June 2004

4. TITLE AND SUBTITLE
EXCITED STATES OF SILICON CARBIDE CLUSTERS BY TIME DEPENDENT DENSITY FUNCTIONAL THEORY

5a. CONTRACT NUMBER

5b. GRANT NUMBER

5c. PROGRAM ELEMENT NUMBER

6. AUTHOR(S)

Boyd, John E., First Lieutenant, USAF

5d. PROJECT NUMBER

5e. TASK NUMBER

5f. WORK UNIT NUMBER

7. PERFORMING ORGANIZATION NAMES(S) AND ADDRESS(S)
Air Force Institute of Technology
Graduate School of Engineering and Management (AFIT/EN)
2950 Hobson Street, Building 641, WPAFB OH 45433-7765

8. PERFORMING ORGANIZATION REPORT NUMBER
AFIT/GNE/ENP/04-02

9. SPONSORING/MONITORING AGENCY NAME(S) AND ADDRESS(ES)
Air Force Office of Scientific Research
Attn: Dr. Michael R. Berman, AFOSR/NL
801 N. Randolph St., Rm. 732
Arlington VA 22203-1977

10. SPONSOR/MONITOR'S ACRONYM(S)
AFOSR

11. SPONSOR/MONITOR'S REPORT NUMBER(S)

12. DISTRIBUTION/AVAILABILITY STATEMENT
APPROVED FOR PUBLIC RELEASE; DISTRIBUTION UNLIMITED.

13. SUPPLEMENTARY NOTES

14. ABSTRACT Previous AFIT research with density functional theory (DFT) has shown DFT to be accurate for the ground states of small Si_mC_n (m,n < 5) clusters. Evaluating the accuracy of time dependent DFT (TDDFT) to calculate the excited states of these clusters was the focus of this research. It is shown that for the excited states that can be expressed as a single electron configuration, energies calculated are generally within .1 eV or better of experimental differences. A possible scheme for correcting multiconfigurational singlet states, is also presented, which also brings their energies to within .1 eV of experiment. Calculations on larger, cage-like structures show excitation energies consistent with spectroscopic measurements of SiC surface defects, suggesting the possibility that the SiC surface forms similar clusters. Calculations on the equilibrium geometries and vibrational frequencies of yet unobserved states of the smaller clusters can aid in their detection in interstellar atmospheres and the laboratory. Finally, this research offers further insight into how silicon and carbon interact with one another as stoichiometry changes, which may one day lead to better semiconductors for aerospace applications.

15. SUBJECT TERMS
Quantum Mechanics, Silicon Carbide, Density Functional Theory (DFT), Molecular Modeling, Computational Chemistry, Excited States

16. SECURITY CLASSIFICATION OF:			**17. LIMITATION OF ABSTRACT**	**18. NUMBER OF PAGES**	**19a. NAME OF RESPONSIBLE PERSON**
a. REPORT	**b. ABSTRACT**	**c. THIS PAGE**			Dr. Larry W. Burggraf (ENP)
U	**U**	**U**	**UU**	173	**19b. TELEPHONE NUMBER** *(Include area code)* (937) 255-3636 ext 4507; e-mail: Larry.Burggraf@afit.edu

Standard Form 298 (Rev. 8-98)
Prescribed by ANSI Std. Z39-18